Acetylacetonates and their nitrogen derivatives as antenna ligands for lanthanoid ions

M.Sc. thesis
University of Jyväskylä
Department of chemistry
30.07.2023
Oona Auvinen

Abstract

This master's thesis focuses on the luminescence of lanthanoid complexes. Emphasis is on acetylacetonate (AcAc) ligands, and their nitrogen derivatives in particular, namely ketoiminate (NacAc) ligands, that may function as antenna ligands to enhance lanthanoid luminescence which can be utilized to develop luminescent sensors. Ln ions are suitable for various applications and technologies, such as light-emitting diodes (LEDs), solar cells, anti-counterfeiting tags, and fluorescent probes because of their unique electronic configurations and photonic properties, which are introduced the first part of the thesis. Mechanisms that underlie lanthanoid luminescence, including energy transfer and photosensitization, are reviewed after which the focus of the thesis is shifted to the syntheses and photonic properties of AcAc and NacAc ligands followed by the discussion of their lanthanoid complexes. Finally, some sensor applications of lanthanoid AcAc compounds are reviewed.

In the experimental part, NacAc ligands and their yttrium complexes were synthesized with the intention of investigating their luminescence properties. In the end, new crystal structures for (*Z*)-1,1,1,5,5,5-hexafluoro-4-(mesitylamino)pent-3-en-2-one (**29**) and potassium (*Z*)-1,1,1,5,5,5-hexafluoro-4-(mesitylimino)pent-2-en-2-olate (**31**) were obtained. Two new yttrium complexes Tris(4-(mesitylimino)pent-2-en-2-olato)-yttrium (**35**) and Tris(1,1,1,5,5,5-hexafluoro-4-(mesitylimino)pent-2-en-2-olato)-yttrium (**36**) were synthesized but because of the limited time reserved for experimental work and problems related to the moisture sensitive nature of the complexes, which often complicated workups, there was no time to investigate the luminescence properties of the targeted complexes. Synthesized compounds were characterized with IR, EA, NMR and single crystal X-ray crystallography. If the synthesized NacAc compounds turn out to be good antenna ligands for Ln ions then, for example, similar compounds could be used as emitting complexes in the 3D printable molecular sensors.

Tiivistelmä

Tässä pro gradu työssä tutkitaan lantanoidien luminesenssia keskittyen asetyyliasetonaatti (AcAc) johdannaisiin sekä erityisesti niiden typpijohdannaisten, ketoiminaattien (NacAc), käyttöön antenniligandeina lantanoidien luminesenssin tehostamiseksi ja luminoivien sensorien kehittämiseksi. Lantanoidiyhdisteet soveltuvat monenlaisiin teknologisiin käyttökohteisiin kuten LED valoihin, aurinkokennoihin, väärentämistä estäviin tunnisteleimoihin ja fluoresoiviin antureihin ainutlaatuisten fotonisten ja elektronisten ominaisuuksiensa ansiosta, joita esitellään tutkielman alussa. Tutkielmassa käydään läpi myös lantanoidien luminesenssin taustalla olevia mekanismeja, mukaan lukien energian siirtoprosessit ja valoherkistys (*photosensitization*), jonka jälkeen käydään läpi AcAc ja NacAc ligandien sekä niiden lantanoidikompleksien synteesejä ja optisia ominaisuuksia. Lopuksi tutustutaan joihinkin AcAc lantanoidiyhdisteiden sovelluksiin sensoreina.

Kokeellisessa osassa syntetisoitiin NacAc ligandeja sekä niiden yttrium komplekseja, joiden luminesenssi ominaisuuksia oli tarkoitus tutkia. Työn aikana saatiin määritettyä kaksi uutta kiderakennetta syntetisoiduille yhdisteille (*Z*)-1,1,1,5,5,5-heksafluoro-4-(mesityyli-amino)pent-3-en-2-oni (**29**) ja kalium(*Z*)-1,1,1,5,5,5-heksafluoro-4-(mesityyli-imino)pent-2-en-2-olaatti (**31**). Lisäksi syntetisoitiin kaksi uutta yttrium kompleksia: Tris(4-(mesityylimino)pent-2-en-2-olaatti)-yttrium (**35**) ja Tris(1,1,1,5,5,5-heksafluoro-4-(mesityylimino)pent-2-en-2-olaatti)-yttrium (**36**). Kokeelliseen työhön varatun rajallisen ajan ja kompleksien kosteusherkkyydestä johtuvien ongelmien vuoksi kyseisten kompleksien luminesenssi ominaisuuksia ei ehditty tutkimaan. Syntetisoitujen yhdisteiden karakterisoinnissa hyödynnettiin IR- ja NMR spektroskopiaa, alkuaine analyysiä ja yksikide röntgenkristallografiaa. Jos NacAc yhdisteet osoittautuvat hyviksi antenniligandeiksi lantanoideille, niitä voitaisiin käyttää esimerkiksi emittoivina yhdisteinä 3D printattavissa molekyylisensoreissa.

Preface

Experimental work was carried out in summer 2022 and the thesis was written in winter 2022-summer 2023 as part of nano chemistry master program in the Department of the Chemistry at the University of Jyväskylä. The supervisors of the thesis were assistant professor Jani Moilanen and co-supervisors in experimental work were postdoctoral researcher Pasi Salonen and PhD student Essi Barkas. The focuses of the thesis were limited to AcAc type compounds and their nitrogen derivatives as antenna ligands for Ln ions and how the luminescence of these types of complexes can be utilized in sensor applications. In the experimental part ketoiminate (NacAc) ligands and their yttrium complexes were synthesized and characterized. The References were searched through Web of science, Google scholar, Reaxys and ConQuest program of the Cambridge Crystallographic Data Centre.

I would like to express my gratitude to my supervisors Jani Moilanen and Pasi Salonen for guiding the experimental part. Also, thanks to Pasi being there for the last-minute help with the thesis. Additionally, I want to thank Essi Barkas for her assistance in the lab whenever needed. Special thanks to Jani for directing the entire literature part, providing work-life experiences, social contacts, and the opportunity to work on an interesting subject throughout the summer. Thanks also to Mikko Rautiainen for revising this thesis. I am especially grateful to Essi for her emotional support and encouragement during those late-night thesis writing sessions at her place. I also extend my thanks to all my friends who supported me throughout the process and wrote the thesis with me, even on Viilu's terrace when I preferred not to be alone writing while others were having fun. Lastly, thanks to all my colleagues at Weeefiner who showed interest in my progress and encouraged me forward.

30.7.2023
Oona Auvinen

Table of contents

Abbreviations

AcAc	Acetylacetonate
bfa	3-Benzoyl-1,1,1-Trifluoroacetone
biby	2,2'-bipyridine
bpm	2,2-bipyrimidine
CBP	4,4′-Bis(N-carbazolyl)-1,1′-biphenyl
CT	Charge transfer
dbm	Dibenzoylmethane
(*mm'/pp'*)-dbm-Cl_2	(*meta,meta'/para,para'*)dicholodibenzoylmethane
ET	Energy transfer
Et_2O	Diethyl ether
FWHM	Full width at half maximum
hfac	1,1,1,5,5,5-Hexafluoroacetylacetonate
HOMO	Highest occupied molecular orbital
HPBA	N-(2-pyridinyl)benzoylacetamide
ISC	Intersystem crossing
KHMDS	Potassium bis(trimethylsilyl)amide
LCD	Liquid Crystal Display
LED	Light emitting diode
LMCT	Ligand to metal charge transfer
Ln	Lanthanoid
LUMO	Lowest occupied molecular orbital
NacAc	Ketoiminate
NIR	Near-infrared light

NMR	nuclear magnetic resonance
OLED	organic light-emitting diode
phen	1,10-phenanthroline
PL	Photoluminescence
PLA	polylactic acid
PyAm	2-amidinopyridine
SCXRD	Single-crystal X-ray diffraction
SMM	Single molecule magnet
SOC	Spin orbit coupling
tfac	1,1,1-Trifluoroacetylacetonate
TL	Triboluminescence
tmh	2,2,6,6-Tetramethylheptadionate
THF	Tetrahydrofuran
tppo	Triphenylphosphine oxide
tppz	2,3,5,6- tetrakis(2-pyridyl)pyrazine
tta	2-thenoyltrifluoroacetone

1 Introduction

Luminescence properties of Lanthanoids (Ln) have been an interesting research target for decades because they can be utilized in day-to-day applications. The ability of Ln ions to emit light through f-f transitions when Ln ions are excited by an external source makes them useful in applications such as fluorescent probes, phosphors in fluorescent lamps and lightbulbs, optical thermometers, luminescent markers for bio-analytical screening, diagnostic tests, liquid-crystal displays (LCDs) and other light emitting materials. Lanthanoids exhibit also strong magnetic properties and they are widely used in permanent magnets and telecommunication devices.[1–5] The magnetic properties of Ln ions can also be combined with luminescence properties in optomagnetic devices,[4,6] however, the focus of the thesis is on the luminescence properties of Lanthanoids.

Ln ions have very low molar absorption coefficients ($\varepsilon < 10\ M^{-1}\ cm^{-1}$), because of which luminescent Ln complexes typically contain luminescence sensitizers that are called antenna ligands.[7] These light-harvesting ligands can absorb and transfer energy to the Ln ion through several different routes and mechanisms, which is why choosing the right antenna ligand for the right Ln is important.[7,8] Recent developments in Ln antenna ligands have opened up new possibilities for Ln luminescence in various applications.[8] However, there is still a need for longer absorption range antennas to achieve more controlled energy transfer (ET) and luminescence.[9]

Light absorbing antenna ligands are used in everyday life, for example, in fluorescent dyes to increase the efficiency of energy transfer between the dye and its surroundings, in solar cells to help capturing wider range of wavelengths of light, in biomedical research as tools for studying protein-protein interactions, and in biosensors for detecting various biomolecules, including enzymes and nucleic acids. The properties of antenna ligand have an effect on the emission wavelength and quantum yield of the luminescent material.[8]

The luminescence efficiency of Ln ions depends directly on the efficiency of ET or charge transfer (CT) from the ligand to the Ln ion if the excitation is done via a ligand.[9] Acetylacetonate (AcAc) ligands are commonly used antennas for the Ln ions because they are strongly absorbing compounds that can efficiently transfer the absorbed energy to the

Ln ions. Luminescent Ln AcAc complexes can be designed to sensitize various properties, such as pH changes,[10] temperature,[11–13] and certain molecules like Et_2O[14]. The nitrogen derivatives of AcAc ligands, namely ketoiminate (NacAc) ligands, have found application in catalysis.[15–17] However, despite the common use of nitrogen ligands as auxiliaries in AcAc Ln complexes,[18] the luminescent properties of NacAc Ln complexes, have not been studied extensively. AcAc and NacAc ligand structures are given in Scheme 1.

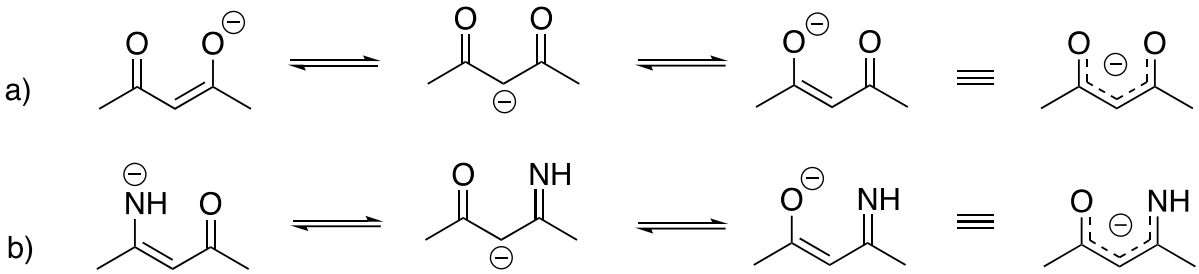

Scheme 1. Generic representation of a) AcAc and b) NacAc ligands, including their tautomers.

In principle, by introducing new substituents into the imino site of NacAc ligand, its chemical and physical properties can be varied more if compared to AcAc ligand, where only the organic backbone can be modified.[19] The modification of the framework of a ligand also changes the electron structure of the complex, which can lead to better antenna properties. However, this aspect has not been studied yet in the case of NacAc ligands. For this reason, the NacAc ligands were chosen for the experimental part.

2 Lanthanoids

Lanthanoids are 15 metallic elements with atomic numbers 57-71 from La to Lu. Ln ions have unique optical, magnetic, chemical, and physical properties due to the presence of their 4f electrons. These properties make them valuable in various applications involving magnetic and optical technologies, including the realm of quantum computing. Moreover, they are soft, malleable and very reactive metals. On the common +3 oxidation state of Ln all their valence electrons are on 4f orbitals, except for La and Lu.[1–4]

All Ln ions have similar chemical properties like complex formation affinities and solubilities and because of this they are difficult to separate from each other.[2] Lanthanoids were named by

the first element in series, lanthanum, which came from Greek word *lanthanein* which means "escaping notice".[4] All Ln ions have been discovered and identified between 1803 and 1907, except for promethium, which was artificially synthesized in a laboratory in 1947.[20] Because of the very similar properties to Ln ions, yttrium and scandium are often included to the series and together these elements are called the rare earth elements even though they are not so rare. The recovery of Ln ions presents certain challenges, entails significant expenses, and has environmental implications. Recovery of Ln ions were first done by fractional crystallization after which also other methods have been used.[2,4]

Lanthanoids are electropositive metals and their Ln^{3+} ions classified as hard Lewis acids. Their 4f valence electrons are shielded by overlying filled 5s and 5p shells because of which 4f orbitals are called core like orbitals. Thus, 4f electrons do not form covalent type bonds like d-electrons of transition metals with ligands and interactions of Ln^{3+} ions with ligands are mainly electrostatics in nature.[2,8,20] Thus, the coordination geometry of the Ln^{3+} complex is difficult to predict and it is mainly determined by the steric properties of the ligands.

Because of the ionic bonding Ln ions form coordination complexes with donor atoms that are hard Lewis bases like oxygen. Because of the oxophilic nature of Ln ions, complexes containing ligands with softer donor atoms, like nitrogen atoms, have not been studied as extensively as complexes containing oxygen donor atoms.[8,14,21] Due to their large ionic radii, Ln ions form complexes with high coordination numbers. However, if the coordinating ligand is bulky enough, complexes with lower coordination number are formed because of steric hindarance.[17,21] The chemistry of trivalent Ln ions depends on their ionic radii, which decrease from La to Lu due to lanthanoid contraction. Lanthanoid contraction is caused by nuclear attraction of poorly shielded f-electrons, resulting in gradual reduction of ionic radii across the Ln series as nuclear charge increases.[22]

Metallic Ln ions are very susceptible to oxidation and have three oxidation states +2, +3 and +4 of which the most stable oxidation state is +3.[2,4,8] Some Ln ions appear also with oxidation state +2 or +4. In particular, the empty, half-filled, or full 4f shell favor the +2 and +4 oxidation states.[4] These Ln ions include Ce^{+4}, Eu^{+2}, Yb^{2+}, and Sm^{2+}. The reason for the prevalence of oxidation state +3 is the fact that the sum of the three first ionization energies for all the Ln ions is low (Figure 1).[5]

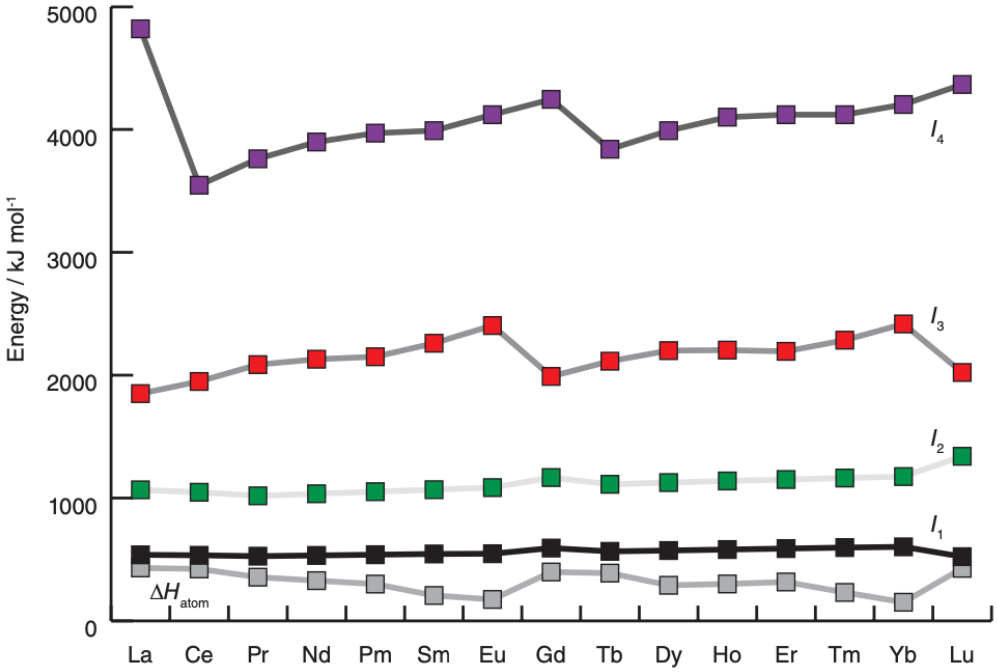

Figure 1. Ionization energies and atomization energies (grey) for Ln ions. Adapted from reference, Duward Shriver, Mark Weller, Tina Overton, Jonathan Rourke, F. A., *Inorganic Chemistry. 6th edition. Oxford university press, 2014. ss. 626-643.*[5]

The valence electron configurations for Ln^{3+} are [Xe]$4f^n$ (n= 0-14) and they are shown in Figure 2 together with the corresponding term symbols. Many Ln^{3+} have unpaired 4f electrons which gives Ln^{3+} their magnetic properties and paramagnetic nature.[4] Ln ions have many electronic levels because of electron-electron repulsion (coulomb interaction), spin orbit coupling (SOC) and ligand field effect each of which split the energy levels. The weakest interaction, ligand field effect splits the SOC states into quantized microstates m_j (Figure 3). These states describe the various ways in which the orbitals of a given configuration can be populated, and they are represented by the term symbols. The term symbol is a label that denotes the multiplicity (2S+1, where S is the total spin), the total angular momentum (J), and the total orbital momentum (L) of the electronic orbital state of the Ln^{3+} ion in the complex[2,20]

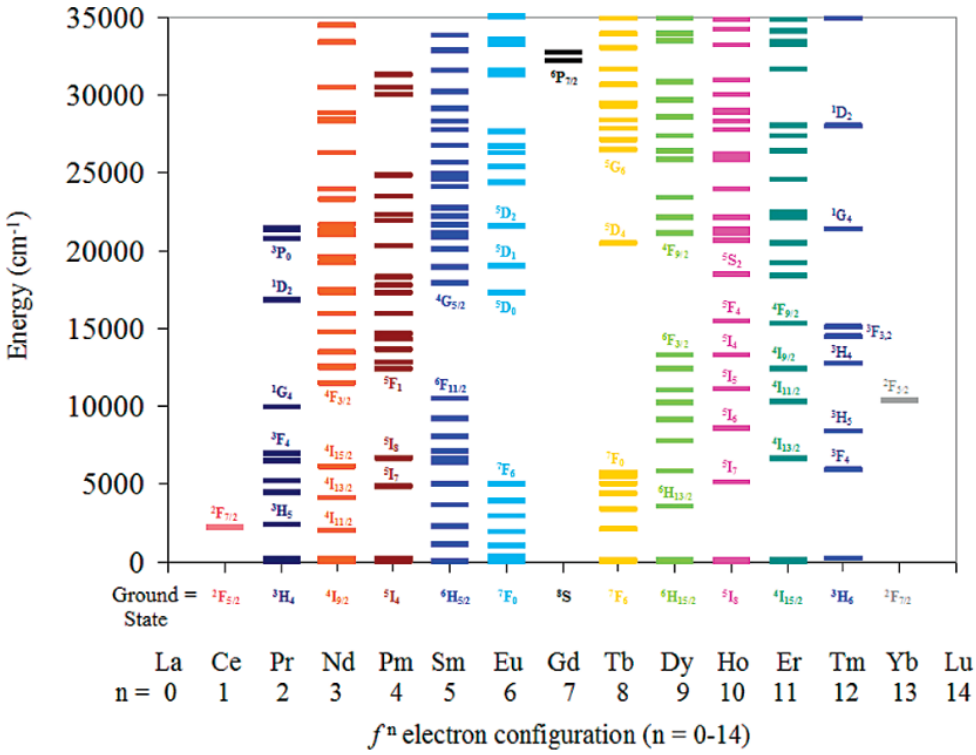

Figure 2. Valence electron configurations, energy levels and term symbols for trivalent Ln ions. Adapted with permission from Moore, E. G.; Samuel, A. P. S. ja Raymond, K. N., From antenna to assay: lessons learned in lanthanide luminescence, *Acc. Chem. Res.*, **2009**, *42*, 542–552. Copyright 2023 American Chemical Society.

Electron-electron repulsion splits Ln^{3+} energy levels by ~10^4 cm^{-1} to degenerate ^{2S+1}L states expressed by orbital quantum numbers S, P, D,… corresponding to L = 0, 1, 2, ... These levels are further split into 2J+1 number of J-levels by SOC and are represented by the term symbol $^{2S+1}L_J$. Ln ions have relatively large spin-orbit coupling ~10^3 cm^{-1} because they are heavy elements. These *free ion levels* originating from SOC are then split into m_j levels by the crystal field (10^2 cm^{-1}) when Ln^{3+} ions reside in a coordination environment.[2,20] An electric field generated by ligands does not lift the degeneracy of m_j levels when a Ln^{3+} ion has odd number of electrons. These kind of degenerate energy levels are called Kramers doublets.[23]

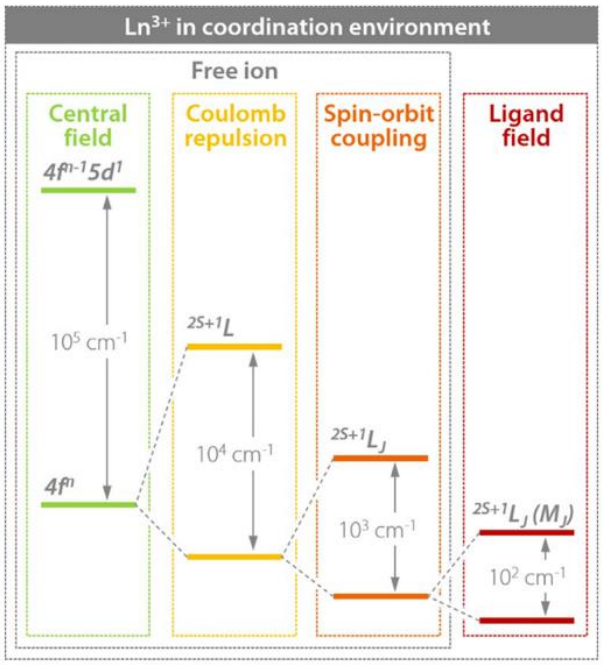

Figure 3. Splitting of lanthanoid energy levels by different interactions. Adapted from *Angew. Chemie - Int. Ed.*, **2021**, *60*, 1728–1746 with permission from John Wiley and Sons.[4]

Kramers doublets are a key factor to many magnetic applications like single molecule magnets (SMM).[23] The degeneracy of Kramers doublets can be further split with an external magnetic field and this phenomenon is called the Zeeman effect.[4,20,23] Splitting of microstates by crystal field is important in terms of magnetism but it also causes the fine structure of the luminescence spectrum, even though the main emission lines are caused by excitations between SOC states and influence of the host lattice is only seen in hyperfine structures.[2,4] The energy levels of 4f orbitals are ladder like,[23] with sharp and easily recognizable emission lines having full width at half maximum (FWHM) < 10 nm which are similar to those of free ions.[2,8,20]

2.1 Lanthanoid luminescence

Luminescence is a light emitting phenomenon, which many elements show, but it is especially intrinsic for Ln ions. Ln ions show luminescence in the ultraviolet (UV), visible and near infrared (NIR) spectral range from 285 nm to 1250 nm.[12,24] Luminescence of Ln^{3+} ions originates from 4f-4f transitions and their complexes usually have stable emission colors with FWHM < 10 nm, *i.e.*, the emitted light is nearly monochromatic, which is why they have

attracted a lot of attention.[8,25] Ln^{3+} complexes can have very high emission quantum yields and they form some of the most efficient luminescent materials known to date.[1] They have long emission lifetimes (length measured in ms), large Stokes shifts, and large number of sharp, characteristic, low intensity emission bands.[3,4,20,23,26] The many microstates of Ln ions enable a huge amount of possible transitions between them and all Ln^{3+} except La^{3+} and Lu^{3+} show luminescence that originates from 4f-4f transitions.[27]

Photoluminescence of Ln^{3+} ions can be an efficient process but still all Ln^{3+} ions have low molar absorption coefficients ($\varepsilon < 10\ M^{-1}\ cm^{-1}$) due to the fact that most of transitions are parity forbidden. Because of this the direct excitation to the emitting level of Ln ion is not efficient and leads to low luminescence efficiency.[4,7] However, the weak light absorption of Ln ion can be enhanced by the antenna effect (or sensitization) wherein an optically active ion is placed in an organic or inorganic matrix that functions as a light harvesting material for the Ln ion.[7] For example, coordination of Ln ions with organic ligands to form complexes is a common and efficient way to enhance the luminescence intensity of Ln ions.[8,24,25] This allows for high quantum yields and more efficient luminescence.

The 4f-4f electric-dipole transitions are Laporte-forbidden due to the selection rule mandating an odd change in the sum of angular momenta of electrons between initial and final states so transitions between orbitals with same parity terms are not allowed (g↔g and u↔u are forbidden).[20] However this parity selection rule can be broken by SOC which makes these transitions become partially allowed by the effect of field perturbations and partial admixture of 4f orbitals with opposite parity wavefunctions like 5d and molecular orbitals.[4,28] Such a partial allowance can be accomplished with asymmetric ligands and/or asymmetric coordination environment. When the Ln^{3+} ion is placed in a non-centrosymmetric matrix, thermal vibrations can induce temporary changes in symmetry and make transitions forbidden by selection rules allowed to occur.[4,24] Ln^{3+} ions without allowed transitions are often weakly colored, and, in contrast to these, Ln^{2+} and Ln^{4+} can have very intense color resulting from the 5d-4f transitions in the visible region of the spectrum. In other words, Ln^{2+} and Ln^{4+} ions can show better luminescence properties than Ln^{3+} ions in some cases.[4,5]

The nature of the luminescence depends on the used Ln. The wavelength of emitted light depends on the energy gap between emitting and ground state and it is well known that many physical and chemical variables like, moisture, temperature, electric field and magnetic fields

have an effect on the luminescence of Ln ions, and for this reason Ln luminescence can be used to monitor all these variables.[4] Ln ions often have emission in visible and near-infrared regions of the electromagnetic spectrum and luminescence can be classified into different subspecies according to the formation of the excited state.[8] Absorption of the energy that leads to the excitations can, for example, originates from light (absorption of photon; photoluminescence)[25], heat (thermoluminescence)[5], mechanical stress (triboluminescence)[29] chemical reaction (chemiluminescence)[7] or electricity (electroluminescence)[30]. Apart from photoluminescence and electroluminescence, other forms of luminescence are quite rare with Ln ions, as they often require special conditions to occur.[9] These five different luminescence types are discussed below.

Triboluminescence (TL) of Ln complexes can be utilized in pressure sensors, where the emission of Ln ion is caused by friction or deformation of the material. This kind of phenomenon is largely seen both in centrosymmetric and non-centrosymmetric crystals for example [Eu(*pp'*-dbm-Cl_2)$_3$(phen)],[31] [Eu(*mm'*-dbm-Cl_2)$_3$(phen)],[31] [Eu(tta)$_3$(bipy)],[31] [Eu(tta)$_3$(phen)],[32] and [Tb(AcAc)$_3$(phen)][29], where *mm'/pp'*-dbm-Cl_2 = *meta,meta'/para,para'*-dichlorodibenzoylmethane, phen = 1,10-phenanthroline, tta = 2-thenoyltrifluoroacetone, and biby = 2,2'-bipyridine. (see section 4.1.1). In non-centrosymmetric crystals the piezoelectric effect often plays a role in exciting the complex and thus they often show more intense TL than symmetric structures.[31] Crystal fracturing along a plane breaks the Van der Waals interaction between molecules and creates a charge to the so-called cleavage surface. The electric field is generated between oppositely charged cleavaged planes, leading to excitation of electrons. However the theory behind TL is not yet fully understood.[29,31] Also electroluminescent compounds can be utilized in pressure sensing but electroluminescent Ln^{3+} complexes are more often used in displays and lightings.[27]

In electroluminescence, the emission occurs upon excitation by an electric current. Luminescent Ln compounds in electroluminescent devices can be excited by impact of electrons or through the recombination of an electron-hole pair (e-h). The e-h pair forms when a current is applied to the anode and cathode, and electrons injected into LUMO by the cathode recombine with holes of HOMO generated by the anode in an emitting layer, resulting in the creation of an excited state.[33] Lanthanoids electroluminescence is commonly used in LEDs and organic light-emitting diodes (OLEDs) to produce light. Tb^{3+} and Eu^{3+} complexes are

frequently used in displays because they exhibit high purity green and red light. Similarly, Nd^{3+}, Er^{3+}, and Yb^{3+} complexes have great potential in night-vision devices due to their NIR emission.[5,27,34] The alternative emission mechanisms in Ln electroluminescence include f-f transitions, d-f transitions, ligand-based transitions, and an exciplex formation.[27] An example of the latter is provided in chapter 4.1.2.[27,34]

Ln chemiluminescence can be utilized for the detection of metal ions, small molecules such as Et_2O, as well as biomolecules like proteins and nucleic acids. In chemiluminescence the emission is fully caused by a chemical reaction such as oxidation-reduction (redox).[7] In addition to chemiluminescence, also photoluminescent Ln complexes can be used to detect all of these. In photoluminescent Ln complex, for example, the conformational change or quenching oscillations induced by binding of the target molecule to the complex can alter the luminescent properties of the material (see section 4.1.4). With this kind of chemical sensing it is possible to determine even the concentration of the target molecule.[14]

Photoluminescent Ln compounds like phosphors emit light when excited with an external energy source.[1] Two common types of photoluminescence (PL) are phosphorescence and fluorescence. Fluorescence is short lived (lifetime in the order of ns) luminescence originating from transitions between states with the same multiplicity ($\Delta S = 0$), usually from singlet-to-singlet state ($S_1 \rightarrow S_0$), while phosphorescence is long lasting ($\geq \mu s$) emission that can be observed even after removing the exciting illumination source. In phosphorescence the transition occurs from an excited triplet state (T_1) to the ground state singlet (S_0) by an intersystem crossing (ISC).[5,7]

PL of Ln ions can be used in many sensor applications for example to detect temperature, pH, molecules, gases, and ions.[14,25,26] PL is usually temperature dependent and temperature can affect various luminescent properties of the Ln complex such as lifetime or intensity (Figure 4.).[1] This is why photoluminescent Ln complexes have huge potential as luminescent thermometers.

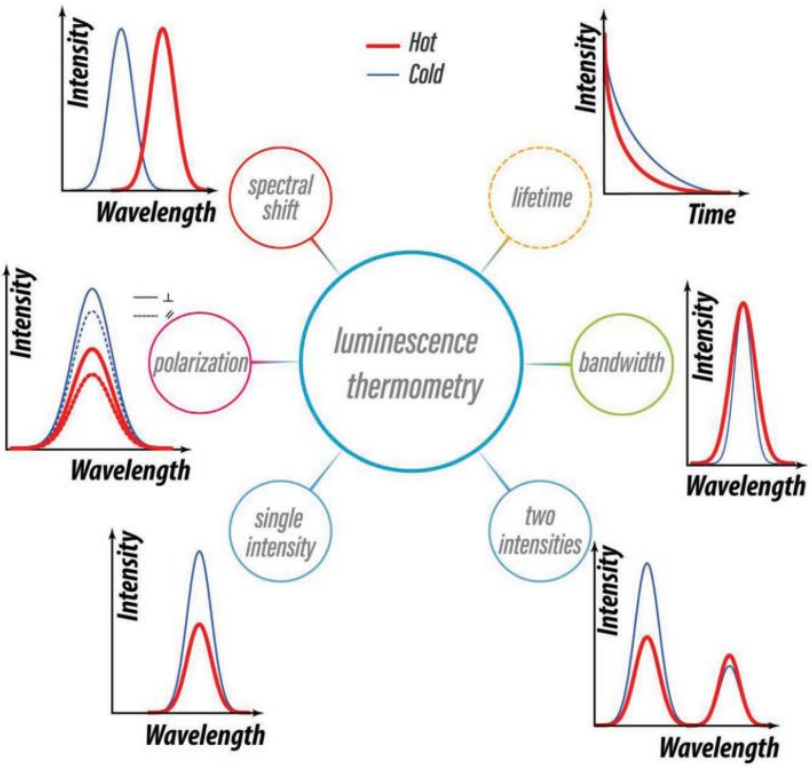

Figure 4. The ways how temperature can change the luminescence properties of lanthanoid materials. Adapted from *Adv. Opt. Mater.*, **2019**, *7*, 1–30 with permission from John Wiley and Sons.[1]

By measuring the changes in luminescence like the intensity ratio between two emission lines of materials, it is possible to derive a calibration curve for the process that can then be used to measure the temperature. Luminescent thermometers exhibit thermal sensitivity, typically around S_r^T > 1% K^{-1}, meaning that the luminescence intensity of the thermometer changes by approximately 1% for every Kelvin (K). In addition, they offer high spatial resolution (< 10 µm) with short acquisition times (< 1 ms). Luminescent thermometers have become more popular because of their huge potential in the fields of nanotechnology and nanomedicine. For now luminescence based non-contact sensors are one of the most promising accurate thermometers because of those properties which enables them to sense small differences in temperature fast and unambiguously. [1,23]

Also, thermoluminescence of Ln compounds can be used in luminescent thermometers but the principles are different. In thermoluminescence the Ln complex is first exposed to ionizing radiation after which the electrons become trapped in localized energy states. When the complex is heated the trapped electrons gain enough energy to overcome the energy barrier

that prevents them from relaxing. Subsequently, light is emitted as a result of electron relaxation.[35]

3 Antenna ligands and antenna effect

An antenna ligand is a compound that can effectively absorb and transfer energy to the emitting Ln center, leading to an increased brightness of Ln luminescence. This is crucial for luminescent Ln complexes because of the low molar absorption coefficients of Ln ions. However, combined with antenna ligands, they can exhibit some of the brightest emissions among all the discovered emitting materials.[8] Thus, to effectively utilize the luminescence of Ln ions, it is necessary to enhance their brightness.[4]

The Antenna effect was first discovered by Weissman,[36] who noticed that Ln complexes with organic ligands can exhibit strong metal-centered luminescence upon excitation in an absorption band of organic ligand. This sensitization process can be modelled with Jablonsky's diagram.[7,36] In contrast to Ln ions, most of organic molecules have better absorption properties and molar extinction coefficients that are generally thousands times larger. In addition to this, organic molecules absorbs much broader spectral range.[4] The light sensitization by the antenna ligand is based on initial excitation through allowed electronic transitions to ligand excited singlet states (S_n). The excited singlet states have short lifetimes and excitation energy can be rapidly relaxed to the lowest lying triplet state T_1 through ISC, from where the energy is transferred either indirectly (via ISC) or directly, to the excited $^{2S+1}L_J$ states of the Ln ion, if the ET process is more favorable than relaxation via ligand centered emission. This results in a broader absorption spectrum for the Ln^{3+} complex and a higher quantum yield of luminescence. [4,37,38]

Every Ln has their own optimal energy range between emitting level and the T_1 level of the ligand which yield the best ET to get the highest quantum yield of photoluminescence.[4] If energy gap between a ligand's T_1 level and Ln ions emitting level are too close to each other, the exited state energy can be back transferred to the ligand via thermally activated processes leading to the quenching of PL.[4,24] This is why the perfect resonance between the emitting state of Ln ion and T_1 state of ligand should be avoided.[4] The rule of thumb is that the sensitizing

exited state of donor must be at least $10k_BT$ (2050 cm^{-1} at the ambient temperature) higher in energy[26] and less than 3500 cm^{-1} compared to the accepting Ln excited state.[20] In addition to this, because sensitization usually occurs via a triplet state, the antenna should have high ISC efficiency (η_{isc}) and energy gap to its own singlet state smaller or equal to 5000 cm^{-1}.[20,21,24] The typical energy transfer processes occurring in Ln ions complexes are presented in Figure 5.

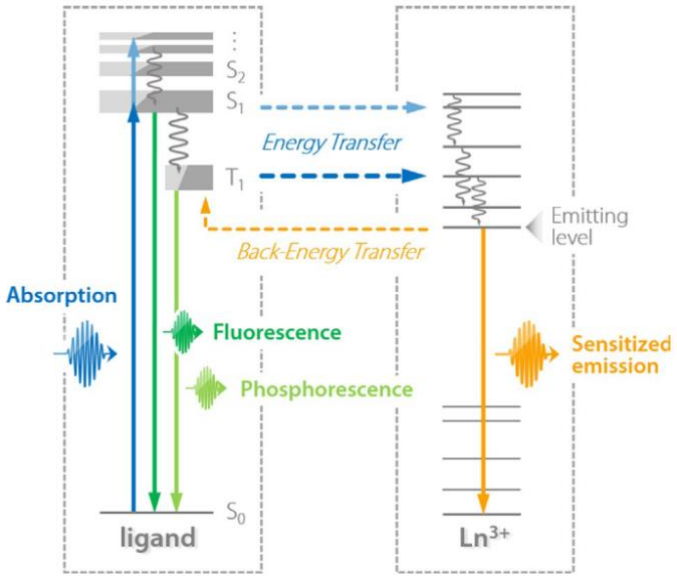

Figure 5. Simplified explanation of sensitization of lanthanoid luminescence for Ln^{3+} complexes. Adapted from *Angew. Chemie - Int. Ed.*, **2021**, *60*, 1728–1746 with permission from John Wiley and Sons.[4]

Energy can also be transferred from charge transfer states with ligand to metal charge transfer (LMCT) in case of Eu, Sm or Yb because they easily adopt the 2+ oxidation state leading to a smaller energy gap between ligand occupied orbital, thus making low energy LMCT transitions.[4,21,39] If no competitive relaxation processes occur, the excited Ln ion relaxes to its ground state through radiative decay by emitting photons.[4,37,38] LMCT states are effective in quenching luminescence if their energy is of the same order or lower than that of the emitting state. At other times, they even improve the quantum yield. Excited state quenching resulting from vibrational energy transfer via a dipole-dipole mechanism is a major cause to the non-radiative deactivation of both ligand and lanthanide excited states. Therefore, this phenomenon needs to be prevented using the appropriate antenna ligands.[26]

3.1 Structure of antenna ligands

Antenna ligands are usually organic molecules that sensitize Ln^{3+} photoluminescence.[4] These light absorption properties are commonly ensured by adding aromatic groups and/or conjugated π-bonds to the structure of a ligand.[4] Even small changes in the scaffold of the ligand can lead to big changes in the properties of a complex. For this reason understanding the influence the ligand scaffold has on the Ln^{3+} luminescence is important in designing multifunctional molecular materials.[37] Through a tailored ligand design it is not only possible to influence the singlet and triplet state positions of the ligand, but also the physico-chemical behavior of the Ln^{3+} complex that are pivotal for achieving sensitized PL.[2,4,37]

Antenna ligands can be designed to absorb light at certain wavelengths by adjusting the length of a conjugated system. Longer conjugated systems with more delocalized π-electrons have lower energy electronic transitions corresponding to a broader absorption spectrum of complex from the UV to NIR region. The delocalization decrease and increase the energies of HOMO and LUMO, respectively.[28] The decrease in the energy gap allows the ligand to absorb light with longer wavelengths, whereas ligands with shorter conjugated systems absorb light over a narrower range and shorter wavelengths resulting in sharper absorptions, particularly in the UV-vis part of the spectrum.[12,28] Furthermore the absorption range can be modified with suitable functional groups and symmetry which also influence the overall quantum yield (Φ_{tot}) by influencing on the intrinsic quantum yield of the metal center (Φ_{Ln}).[21] For example an asymmetric ligand can facilitate forbidden transitions by selection rules.[24]

An antenna ligand should be structurally bulky enough to saturate the Ln^{3+} coordination sphere to prevent coordination of water or other solvents to the Ln ion, because the vibrations of substituents (-OH, -CH) of coordinating solvent molecules (or ligands) are capable of quenching the emissive excited state via a non-radiative energy decay.[21,24] The orientation and position of the ligand relative to the Ln center can be modified by coordinating groups like carboxylates, phosphates, or amines which affect the complex luminescence properties by defining how closely the antenna is coordinated to Ln ion and as mentioned before, also the size and shape of the antenna modulate the ability of sensitization.[25,40,41] For optimal photosensitization it is best that the sensitizer is coordinated directly to the Ln ion because the efficiency of ET from ligand to Ln is highly dependent on the distance between the antenna

ligand and Ln center.[2] The Ln center should be as close as possible to the antenna to ensure a strong overlap of wavefunctions between Ln center and antenna ligand for efficient energy transfer.[9,26]

Additional functional groups can be used to tune the emission color of some Ln ions like Eu^{3+} by modifying the electron structure of antenna ligand. By substituting electron withdrawing groups like fluorides or electron donating groups such as amines into the framework of the ligand it is possible to modulate the ET efficiency between the antenna and Ln ion resulting in a change of the emission color.[37,42] Eu^{3+} and Tb^{3+} can form strong luminescent complexes with most organic ligands but the place of emitting levels of terbium and europium limits the possible photosensitizers to those which absorb in the blue or UV part of the spectrum at the best. With correct ligand Tb^{3+} and Eu^{3+} can emit pure green and red light, respectively, at almost any environment and without the influence of external factors.[2,3] Their light emission is due to the redistribution of electrons in the 4f orbitals.[3] Functional group can also enable the selective binding to analyte or other targets in luminescent sensor applications.[42]

Many different types of light-absorbing molecules can act as antenna ligands, but certain requirements are imposed by the application-related considerations such as the metal ion being used and internal photonic energetics.[2] For example, the most commonly used antenna ligands for Ln ions are β-diketones, such as acetylacetonate (AcAc) and 2-thenoyltrifluoroacetone (tta), because they exhibit strong absorption in the UV-vis range and form stable complexes with the Ln ions. β-diketonates have two carbonyl groups in their structure and since Ln ions prefer coordination with oxygen, they can easily form complexes with Ln ions.[8,38]

3.2 Energy transfer mechanisms

Antenna ligands can transfer energy to the Ln^{3+} ions with different mechanisms. The quantum efficiency, which refers to the probability of photon emission after the system has been excited to its emitting state, is directly influenced by the ET efficiency. ET efficiency depends on many factors including the specific ET mechanism involved, overlap of emission and absorption spectra of antenna ligand and Ln^{3+} ion, orientation of antenna with respect to Ln center, and distance between these two as mentioned above.[9,26] There are two main energy transfer

mechanism that can occur in Ln based systems, namely Förster resonant energy transfer and Dexter electron exchange. The latter mechanism takes place more often if the factors mentioned above are fullfilled.[9,26,43] In addition to these two methods, energy can be conveyed to the Ln^{3+} ion through other mechanisms. One example is LMCT, where electrons are transferred from ligand-character orbitals to metal-character orbitals. The opposite process, metal-to-ligand charge transfer (MLCT), is not usually observed due to the large ionization energies of Ln^{3+}, which makes the transitions very high in energy. After LMCT, the reduced Ln ion can be oxidized back to its stable +3 state by an electron transfer from the reduced Ln to the oxidized ligand. In LMCT, the transition energy is typically lower compared to intraligand absorption due to the electrons needing to migrate over a greater distance. True LMCT transitions are rare in Ln ions, but they can occur among the most easily reduced Ln^{3+} ions such as Eu^{3+}, Yb^{3+}, and Sm^{3+}.[5,9]

In some cases, energy can be transferred directly from the singlet state to the Ln emitting state if the S_1-T_1 intersystem crossing is slow. However, this is not usually the case due to magnetic moments and the heavy atom effect, which makes ISC very efficient and fast.[27,39] A straightforward ET from the singlet state of the ligand can occur in cases involving Eu^{3+} or Tb^{3+} chelates if the ligand triplet state lies below or close to the emitting level of Ln ion, which typically quenches the lanthanide based luminescence due to the back-energy transfer from a Ln ion to a ligand. One example is europium complexes with certain coumarin sensitizing groups, where the Eu $^5D_1$ state is populated and subsequently undergoes vibrational relaxation to the longer-lived $^5D_0$ Eu emissive state.[27,39]

Förster resonant energy transfer mechanism and Dexter electron exchange mechanism are both presented in Scheme 1. These mechanisms have different energetic requirements for sensitizer ligands and they populate different accepting excited 4f states of Ln.[43] For the radiative relaxations the Frank–Condon principle is valid and the spin and symmetry selection rules are also valid for the emission and absorption of photon.[9] The Franck-Condon principle states that the timescale of electronic transitions is significantly faster than that of nuclear vibrations and therefore the internuclear distances do not change during the transition. This implies that the transitions are vertical and potentially end up on different vibrational states of the next electronic excited state. When the electron is excited to a higher vibrational state, the spectral absorption energy is increased, which is seen as a shift in the spectrum.[9]

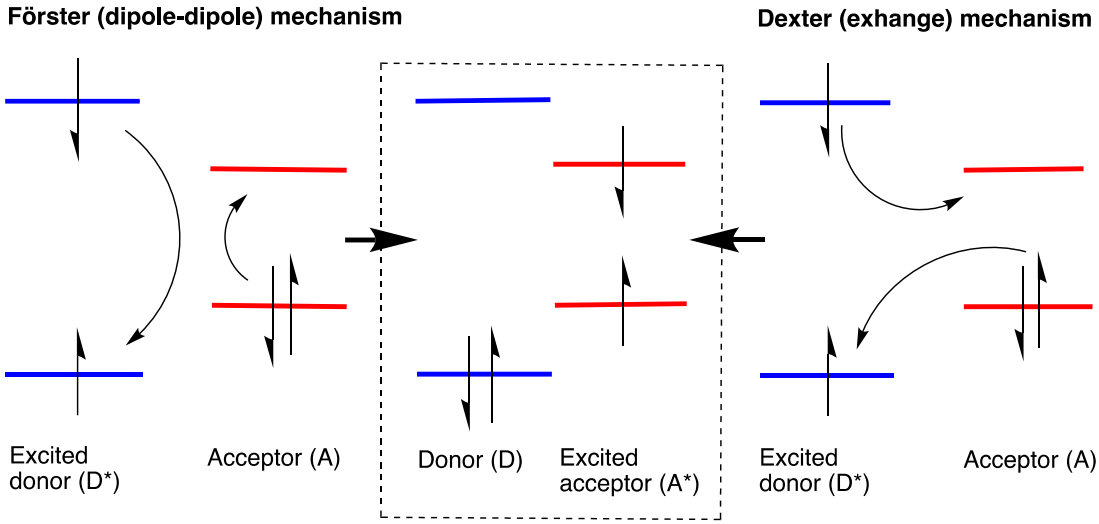

Scheme 1. Mechanism for singlet-singlet Förster and Dexter energy transfer from donor to acceptor.

Dexter electron exchange requires direct orbital overlapping and is thus a short range process where an electron is exchanged between donor singlet states and acceptor singlet states. Dexter mechanism requires change in the spin multiplicity of antenna and Ln and when it occurs from the ligand triplet state.[43] It depends also from the orientation of Ln and antenna, and distance between these two has to be less than 10 Å for the electron transfer to occur.[9,26,44] The electron transfer rate k_{EnT} is proportional to the negative natural exponential function to the power of twice the distance, *i.e.*, $k_{EnT} \propto \exp(-2R_0)$, where R_0 represents the distance between the energy donor and acceptor center.[25]

Förster resonant energy transfer is based on resonant Columbic interaction through space and dipole-dipole couplings, where an acceptors electron is promoted when donors excited electron relaxes back to the ground state by a non-radiative transition.[43] The Förster transfer happens when Ln^{3+} ions and it's antennas transitions are both dipole allowed, coupled and distance between the ligand and the Ln center is less than 100 Å. Förster transition happens from the singlet state and the energy transfer rate is proportional to the inverse sixth power of the distance, *i.e.*, $k_{EnT} \propto \frac{1}{R_0^6}$,. [25,43,44] This mechanism is favored when distance between antenna and Ln ion is longer, for example in case where an antenna is not directly attached to the Ln ion. In a case like this there is no close contact that would enable an electronic exchange and ET selectively happens through Försters mechanism.[9,21,26]

4 Acetylacetonate ligands as antennas

As mentioned before, most of antenna ligands are organic compounds with aromatic substituents and/or conjugated π-electrons in their structure.[4,12] Some of the most used and studied antenna ligands are based on acetylacetonate (AcAc) (**1**) which chemical structure is shown in Figure 6 together with its protonated precursor acetylacetone (AcAcH) (**2**). AcAc belongs to β-diketonate ligand family and it has many derivatives, like 1,1,1-trifluoroacetylacetonate (tfac), 1,1,1,5,5,5-hexafluoroacetylacetonate (hfac) and 2-thenoyltrifluoroacetonate (tta) that are shown in Figure 7. All of these compounds function as antenna ligands.[8,45] AcAc ligands are widely used in coordination chemistry and material science. They are particularly important in the synthesis of metal-organic complexes, coordination polymers, metal-containing materials and molecular magnetic materials showing spin-crossover and/or SMM properties.[23]

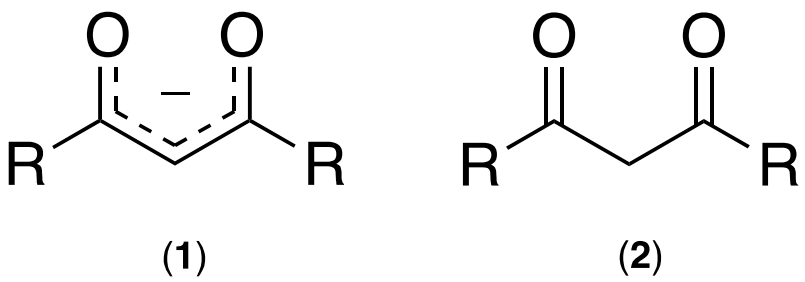

Figure 6. (**1**) acetylacetonate; AcAc and (**2**) acetylacetone; AcAcH

AcAc ligands are stable molecules with long excited-state lifetimes and their absorption range can be modified through simple structural changes. The carbonyl groups of AcAc make the bidentate coordination mode possible and enables the easy modification of the ligand backbone around of carbon chain.[24,44,46] Bidentate coordination also enhances the magnetic properties, such as high spin states or long relaxation times of complex.[4,34,37]

AcAc and its many derivatives are commercially available at reasonably low prices, but they can also be easily synthesized through a Claisen condensation reaction between a deprotonated methyl ketone and a methyl or an ethyl ester.[44] AcAc derivatives are simply made by substituting CH_3 groups with other groups. Substitution by other groups influence numerous properties of ligand but typically there is only small variation in the T_1 state energy among

complexes when considering different AcAc moieties.[8,37,45] The first singlet and triplet states of AcAc are located at about 33 600 cm^{-1} and 24 800 cm^{-1}, respectively, while the first triplet levels of tfac is located at 22 700 cm^{-1} and hfac at 22 200 cm^{-1}.[37,46] Methyl groups in AcAc are electron-donor groups with quenching bonds, whereas trifluoromethyls in hfac are electron withdrawing groups and phenyl groups in dbm are electron donor groups without quenching bonds.[24,37] Substitution of methyl group/groups by trifluoromethyls eliminates high energy C – H vibrations resulting in improved luminescence properties like increased quantum efficiency, longer PL lifetimes and enhanced resistance of thermal quenching.[11] Also, the acidity of AcAc ligand depends on the substituent. Derivatives with electron withdrawing groups are more acidic than derivatives with electron donating groups.[44]

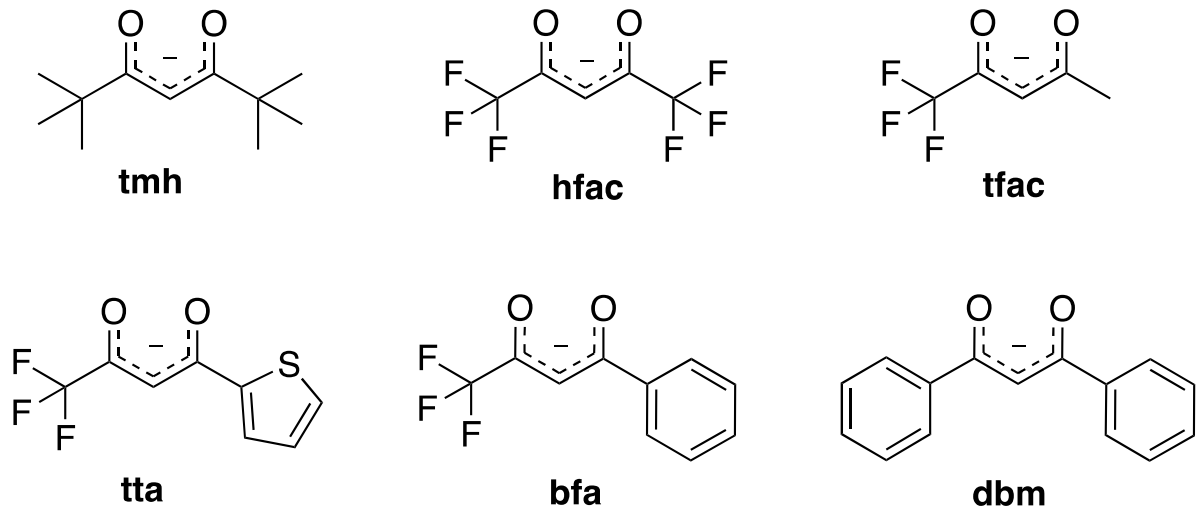

Figure 7. Some selected AcAc derivatives which have been used as antenna ligands for Ln ions. 2,2,6,6-Tetramethylheptadionate (tmh), 1,1,1,5,5,5-hexafluoroacetylacetonate (hfac), 1,1,1-trifluoroacetylacetonate (tfac), 2-thenoyltrifluoroacetonate (tta), 3-benzoyl-1,1,1-trifluoroacetonate (bfa) and dibenzoylmethane (dbm).

AcAc ligands have an efficient capacity for energy transfer process in Ln^{3+} complexes and they usually form tris complexes with Ln ions.[24,44,46] The coordination mode and geometry define the orbital overlapping and distance between oxygen donor atom and Ln center.[28] The high molar absorption coefficients of AcAc ligands in the UV range and their suitable excited energy levels and steric hindrance allows efficient ET to the visible and NIR emitting Ln ions.[8,12,24,34] The chelate ring formed from bidentate coordination of AcAc to Ln provides more stable and rigid coordination complexes which also leads to highly thermodynamically stable and photoluminescent compounds.[4,34,37] By adding different substituent on the ligand backbone,

the ligand field around the Ln ion is influenced. This kind of energy level modification leads to tunable luminescence properties of Ln compounds.[37,46] Selection of the AcAc ligand and the Ln ion is critical when considering the synthesis and design of luminescent complexes. [28,44]

In a solution, the AcAc ligand offers a shielding effect for the Ln ion against the high-energy oscillators (O−H, N−H, C−H) present in the solvent. This shielding reduces the nonradiative decay rate as well as prevents the quenching of luminescence and ligand dissociation leading to the enhanced luminescent properties of a complex.[18,42] One of the most popular luminescent Ln complexes is [Eu(tta)$_3$(phen)] which has been used for example in electroluminescent devices,[34] oxygen sensing materials,[8] and luminescent temperature sensors.[12]

4.1 Luminescent acetylacetonate lanthanoid complexes

Luminescent Ln^{3+} AcAc complexes consist of Ln^{3+} ion(s), coordinated AcAc ligand/ligands, and auxiliary ligand(s) if the coordination sphere is not fulfilled by AcAc ligand(s) and/or solvent molecules.[8] In this chapter, some luminescent Ln AcAc complexes are introduced and their photonic properties are discussed. Both, AcAc and auxiliary ligands, can be used to modulate the photophysical properties of complexes like emission intensity, lifetime, and wavelength.[8,46] By introducing auxiliary ligands, the electron density around the Ln ion can be altered and/or steric bulk around the coordination sphere can be increased.[18,47] Auxiliary ligands can also improve the solubility and stability of the complex,[46] and additionally, the use of chiral ligands can result in circularly polarized luminescence, which has potential applications in chiral sensing and optoelectronics.[26]

4.1.1 Centrosymmetric complex [Tb(AcAc)$_3$(phen)]

In 2018, AcAc terbium complex [Tb(AcAc)$_3$(phen)] (**3**) (phen = 1,10-phenanthroline) was synthesized to study the relationship between structure and triboluminescence properties of rare earth metal complexes. [Tb(AcAc)$_3$(phen)] showed an intensive PL and TL which makes it a promising material for use in various applications such as sensors, optoelectronics, and lighting devices. Complex was synthesized by adding $TbCl_3$ dropwise into a mixture of AcAcH

and phen in ethanol while heating and intensively stirring. NaOH was used as a base. The reaction yielded the complex **3** that is presented in Scheme 2.[29]

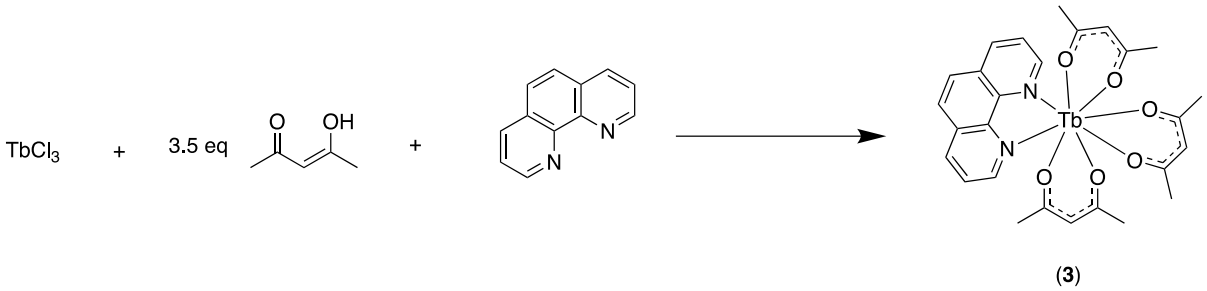

(**3**)

Scheme 2. The synthesis route for **3.**

Complex **3** is isostructural with known [Ln(AcAc)$_3$(phen)] complexes of Sm, Eu, Dy, Er and Lu. The complex crystallizes in the monoclinic crystal system in space group *P*21/*n*. Crystals were colorless and transparent. Molecular structure of the complex in the crystal is presented in Figure 8. The crystal structure of the complex reveals that Tb^{3+} ion is coordinated by three acetylacetonate ligands and one phenanthroline ligand. Ligands create a distorted square antiprism geometry around Tb^{3+} ion. The packing of these complexes within the crystal lattice is determined by Van der Waals interactions. Weak Van der Waals interactions create the potential for cleavage planes in crystals. These cleavage planes are regions where the crystal's linkage is weakened leading to potential cracking.[29]

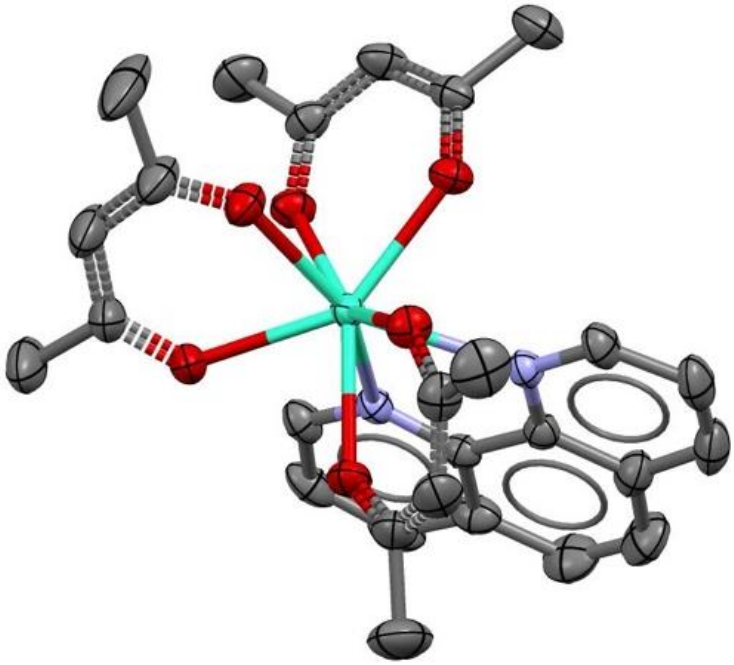

Figure 8. Crystal structure of **3** where green = Tb, red = O, purple = N. Hydrogens are omitted for clarity and thermal ellipsoids are drawn at the probability level of 50%. CSD: SEQGON.[29]

Complex **3** shows intensive PL when irritated with UV light. Internal $\pi \rightarrow \pi^*$ transitions of AcAc and phen cause a broad band in excitation spectrum between 230-330 nm. TL studies were carried out by crushing the crystal material with 110 g steel ball falling from height of 1 m. TL and PL spectra $^5D_4 - {}^7F_5$ transitions are identical which proves that no essential changes occur in the crystal field symmetry of Tb^{3+} during the process of crystal fracture. TL and PL maxima are at wavelength of 547 nm. The TL properties of the crystal were combined with the structural properties of crystal. The cracking of the cleavage planes results in the ionization of AcAc until eventual detachment of AcAc ions. This causes charge formation to in the destruction zone which leads to TL. When AcAc ionizes, it acts as a charge carrier and creates oppositely charged cleavage surfaces, which generate an electric field that excites electrons and leads to the excitation of the ligand to triplet state. Energy is transferred intramolecularly to the emitting state $^5D_4$ of Tb^{3+}. TL intensity correlates with the width of destruction zone which is equal to 6.414 Å in the investigated system.[29]

4.1.2 [{Ln(AcAc)$_3$}$_2$(μ-bpm)]

In 2009 luminescent bimetallic [{Ln(AcAc)$_3$}$_2$(μ-bpm)] (bpm = 2,2'-bipyrimidine) complexes of Eu (**4**), Sm (**5**), and Tb (**6**) were synthesized. Complexes were intended for dopants for OLEDs that could generate white electroluminescence. bpm was chosen as the auxiliary ligand because it has been shown to efficiently sensitize emission in the visible range of the electromagnetic spectrum. Complexes were synthesized by reacting commercial Ln(AcAc)$_3$·xH$_2$O with solution of bpm in CH$_3$CN (Scheme 3).[34]

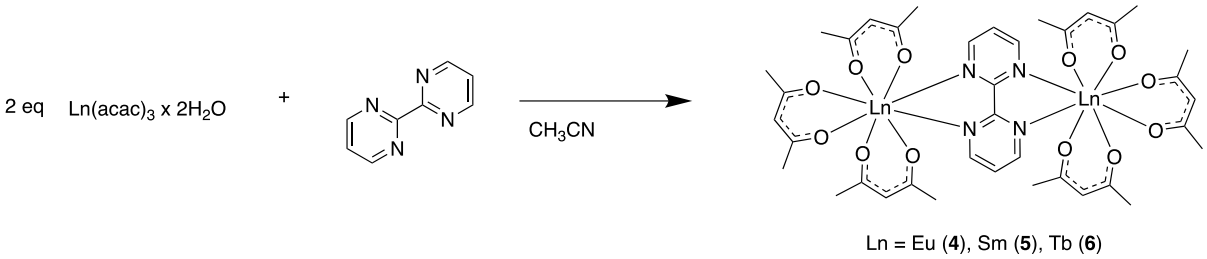

Scheme 3. The synthesis route for **4**, **5** and **6**.

Complexes were characterized by the single-crystal X-ray diffraction (SCXRD) and found to be isomorphous. The aromatic N-heterocyclic ligand bridges two Ln ions as seen in Figure 9. Complexes crystallize in the triclinic crystal system in space group $P\bar{1}$.[34]

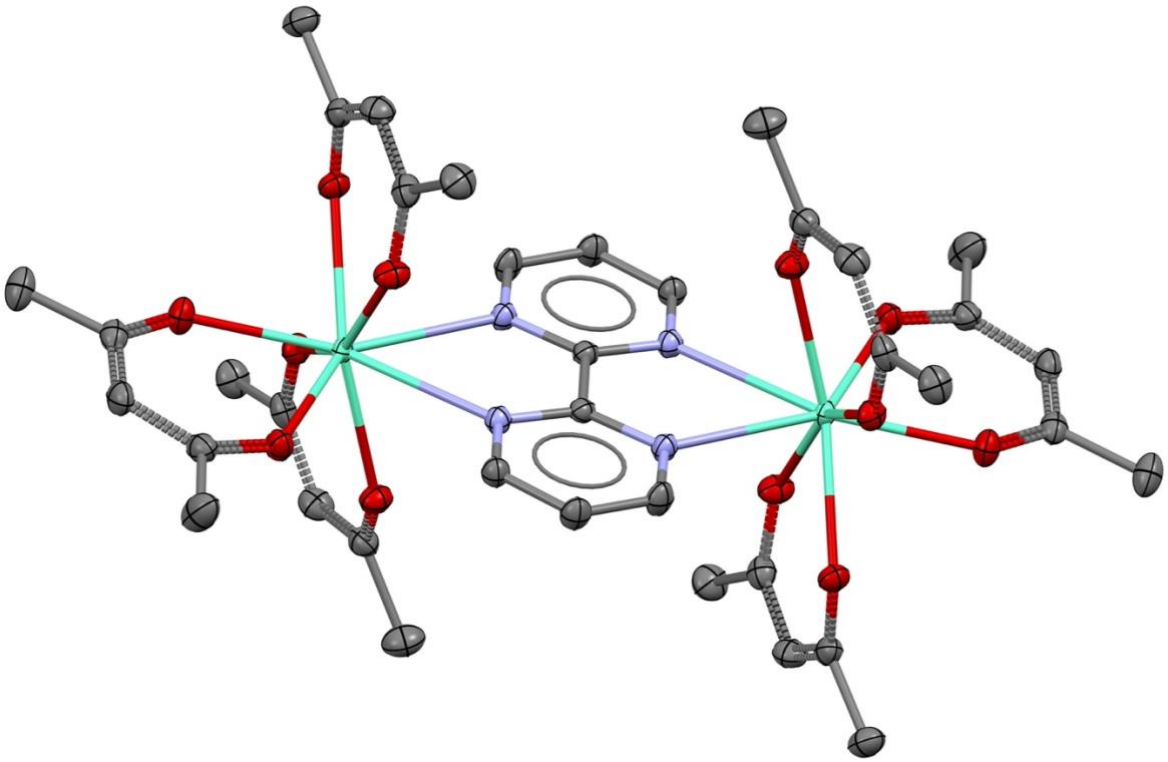

Figure 9. The crystal structure for complex [{Eu(AcAc)$_3$}$_2$(μ-bpm)] where green = Eu, red = O, purple = N. Hydrogens are omitted for clarity and thermal ellipsoids are drawn at the probability level of 50%. CSD: XUNYIP.[34]

When the complexes are excited with UV light (230-360 nm), the photoluminescence of each complex is detected with characteristic sharp emission lines. Photoluminescence spectra are presented in Figure 10. The $^5D_0 \rightarrow {}^7F_J$ (J= 0–4) transitions of Eu3+ ion show peaks at 579 nm, 589 nm, 612 nm, 652 nm, 702 nm, respectively; the $^5D_4 \rightarrow {}^7F_J$ (J = 6–2) transitions of Tb3+ appear at 489 nm, 545 nm, 584 nm, 620 nm, 655 nm, and Sm3+ ion emission bands were observed at 565 nm ($^4G_{5/2} \rightarrow {}^6H_{5/2}$), 606 nm ($^4G_{5/2} \rightarrow {}^6H_{7/2}$), 649 nm ($^4G_{5/2} \rightarrow {}^6H_{9/2}$), and 710 nm ($^4G_{5/2} \rightarrow {}^6H_{11/2}$).[34]

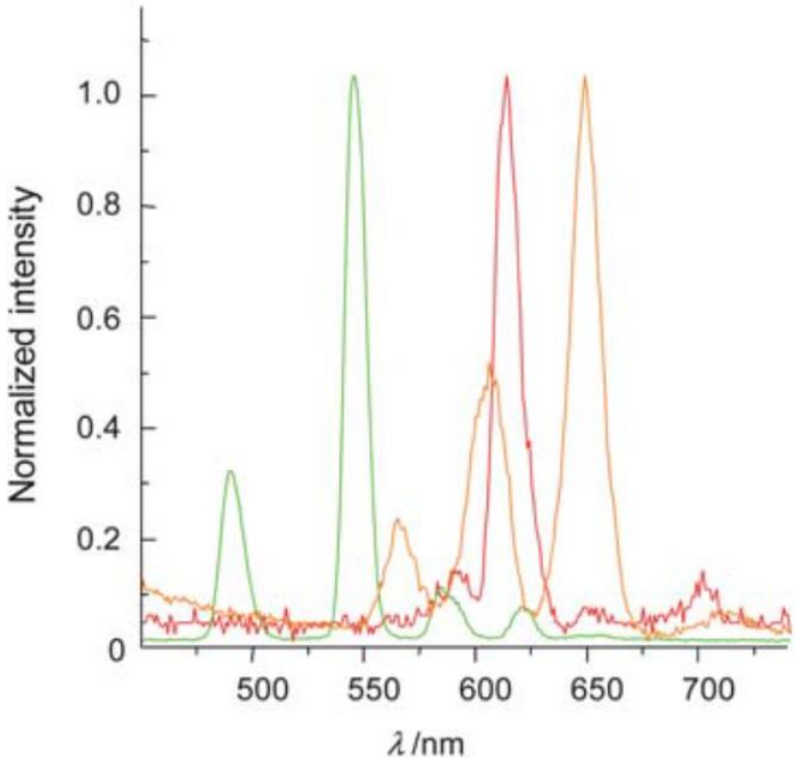

Figure 10. Normalized photoluminescence spectra of the [{Ln(acac)$_3$}$_2$(μ-bpm)] complexes where (Ln = Eu is red with λ_{exc} = 320 nm, Tb is green with λ_{exc} = 326 nm, and Sm is orange with λ_{exc} = 330 nm).[34] – Adapted from *J. Mater. Chem.*, **2010**, *20*, 2114-2120 with permission from The Royal Society of Chemistry.

Luminescent devices build using [{Ln(AcAc)$_3$}$_2$(μ-bpm)] show broad emission caused by an exciplex formation between the 4,4′-Bis(N-carbazolyl)-1,1′-biphenyl (CBP) host (Figure 11) and dopant emission layer.[34] Exciplex formation involves the formation of an excited state complex between two different molecules, typically a donor and an acceptor molecule. The excited state complex then emits light as it returns to its ground state.[27] The combination of europium's red emission and emission formed by exciplex produce an overall white electroluminescence from devices built with [{Eu(AcAc)$_3$}$_2$(μ-bpm)]. Same phenomena was also observed with the [{Eu(tta)$_3$}$_2$(μ-bpm)] complex which was reported at the same study. The host material serves as both a charge transporter and energy donor for the dopant, but it can also interact with it in other ways. In this particular case, the exciplex formation resulted in a change in the overall emission color of the device.[34]

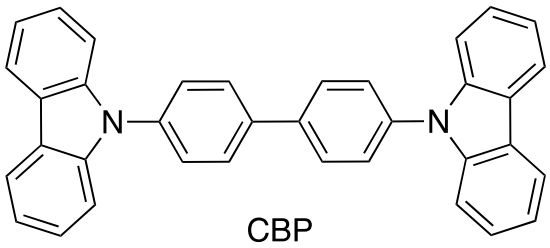

Figure 11. Structure of CBP host material.

One of the advantages of OLED based white light sources over white LEDs is the diminished light pollution and reduce energy consumption. The significant dependence of Rayleigh scattering on the wavelength of light implies that cool white LEDs have the potential to contribute more to light pollution compared to other sources.[34,48]

4.1.3 [Ln(AcAc)$_3$(PyAm)]

Series of Ln AcAc complexes including 2-amidinopyridine (PyAm) as auxiliary ligand were synthesized in 2020. Three of these complexes show characteristic PL properties depending on the temperature. Complexes were synthesized by reacting [Ln(AcAc)$_3$] · H_2O and N-2-pyridylimidoyl-2-pyridylamidine (Py_2ImAm) where Py_2ImAm goes through metal assisted hydrolysis yielding the ligand PyAm, which then coordinates to the Ln ion resulting complexes [Ln(AcAc)$_3$(PyAm)] where Ln = Eu (**7**), Gd (**8**), Tb (**9**), and Dy (**10**).). The lanthanide series was complemented with their analogue **11** (Ln = Y) which was used for nuclear magnetic resonance (NMR) studies. Synthesis of complexes is shown in Scheme 4.[46]

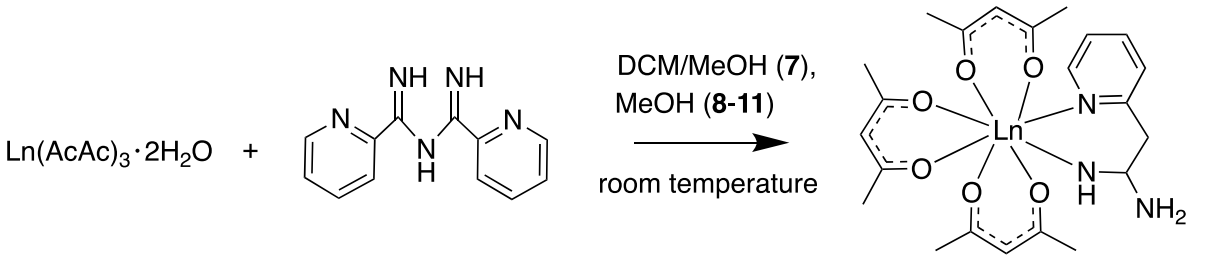

Scheme 4. Simplified synthesis route for **7**, **8, 9**, **10** and **11**.

The complexes containing Eu, Gd, Tb and Dy ions formed pale yellow crystals on evaporation which were suitable for SCXRD studies. Complexes were isomorphous and crystallize in the monoclinic space group $P2_1/n$. Figure 12. shows the crystal structure of **7**.[46]

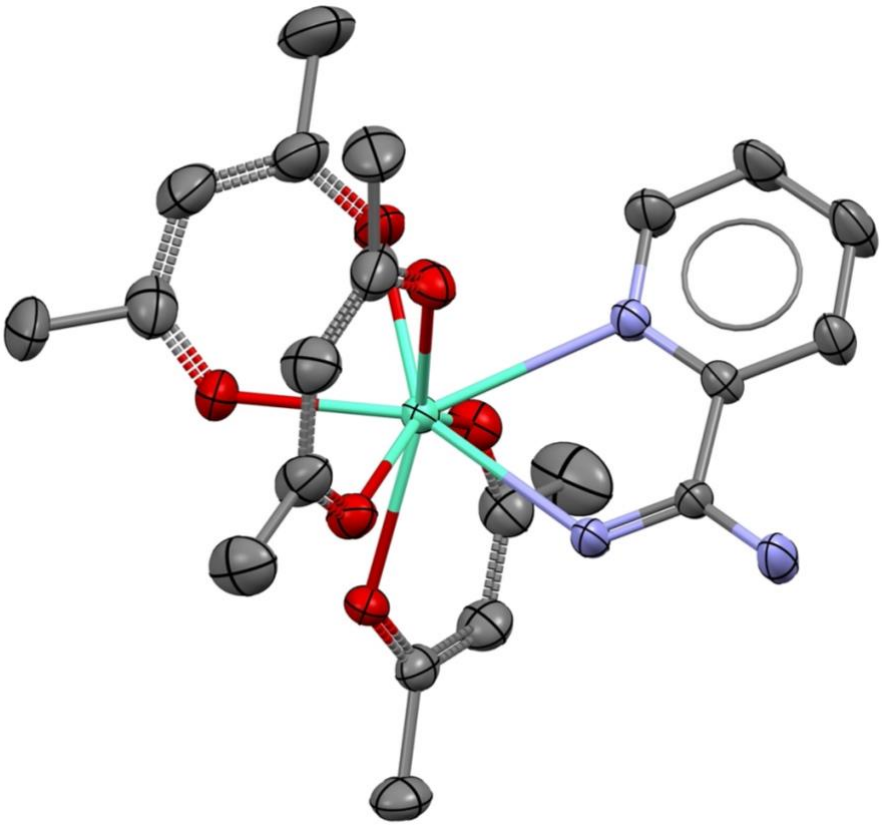

Figure 12. The crystal structure for complex [Eu(AcAc)$_3$(PyAm)] where green = Eu, red = O, purple = N. Hydrogens are omitted for clarity and thermal ellipsoids are drawn at the probability level of 50%. CSD: NUVSUV.[46]

In Eu^{3+} complex, the triplet state energy of AcAc ligand and LMCT state were in par for the ligand-centered sensitization but at the temperature of 300K the direct excitation of 4f states of Eu^{3+} ion were more efficient than the ligand-centered sensitization. At the temperature of 25 K the sensitization occurs through the ligand, and it was observed from the excitation spectrum that there needs to be a thermal quenching for the LMCT at 300 K. The characteristic emission of red light of Eu^{3+} complex was measured with quantum yield of 3%, whereas for Tb^{3+}, and Dy^{3+} complexes the characteristic emissions of green, and yellow light were measured with quantum yields of 65%, and 8%, respectively. It was observed that the auxiliary ligand, PyAm has suitable energy levels matching those of Tb^{3+} and Dy^{3+} and it was acting as an effective cosensitizing antenna for these ions. Changes in thermal populations of Stark sublevels in Tb^{3+}

and Dy^{3+} complexes offer the opportunity to use them as efficient optical thermometers. These complexes exhibit maximum relative sensitivities of up to 2% K^{-1}, enabling precise temperature measurements based on the changes in their luminescent spectra. The discoveries highlight the potential of [Ln(acac)$_3$(PyAm)] complexes for various applications in the fields of lighting technologies, optical thermometry, and other areas that require photoluminescent materials.[46]

4.1.4 [Ln(tppz)(AcAc)(NO$_3$)$_2$]·AcAc

New highly luminescent Ln^{3+} AcAc complexes [Ln(tppz)(AcAc)(NO$_3$)$_2$]·AcAcH (tppz=2,3,5,6- tetra-2-pyridinylpyrazine) (Ln = Tb^{3+} (**12**), Er^{3+} (**13**), Y^{3+} (**14**)) were synthesized in 2018 with the purpose to investigate their potential as Et$_2$O sensors. Complexes were synthesized with bis-tridentate ligand tppz which enabled the construction of tridentate chelated lanthanide complexes with one coordinated AcAc ligand and one non-coordinating AcAcH molecule in the crystal structure. Complexes were made by dissolving tppz in CHCl$_3$ and Ln(NO$_3$)$_3$·6H$_2$O in AcAc and then mixing the solutions and letting them stand overnight. The resulting mixture was filtered, and the filtrate was evaporated slowly to obtain crystals suitable for single crystal X-ray determination. The synthesis route for the complexes is presented in Scheme 5.[14]

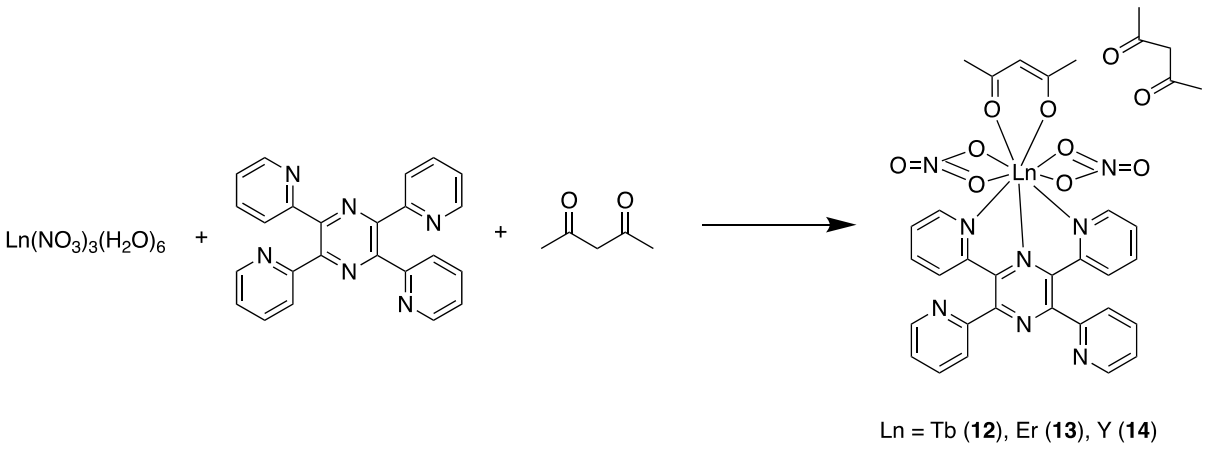

Scheme 5. The synthesis route for [Ln(tppz)(AcAc)(NO$_3$)$_2$]·AcAcH.

In these complexes the AcAc was acting as co-sensitizer and the tppz ligand offers the energy transfer to Ln ion. All three complexes were fully characterized, and they found to be

isostructural. Complexes crystallizes in the triclinic crystal system in space group *P-1* and the coordination atoms arranged in a distorted one-capped quadrangular mode. tppz forms tridentate chelate ring with Tb center and the AcAc is nearly in plane with tppz, with only small, twisted angle of 27.656° between these moieties. The crystal structure for Tb complex is shown in Figure 13.[14]

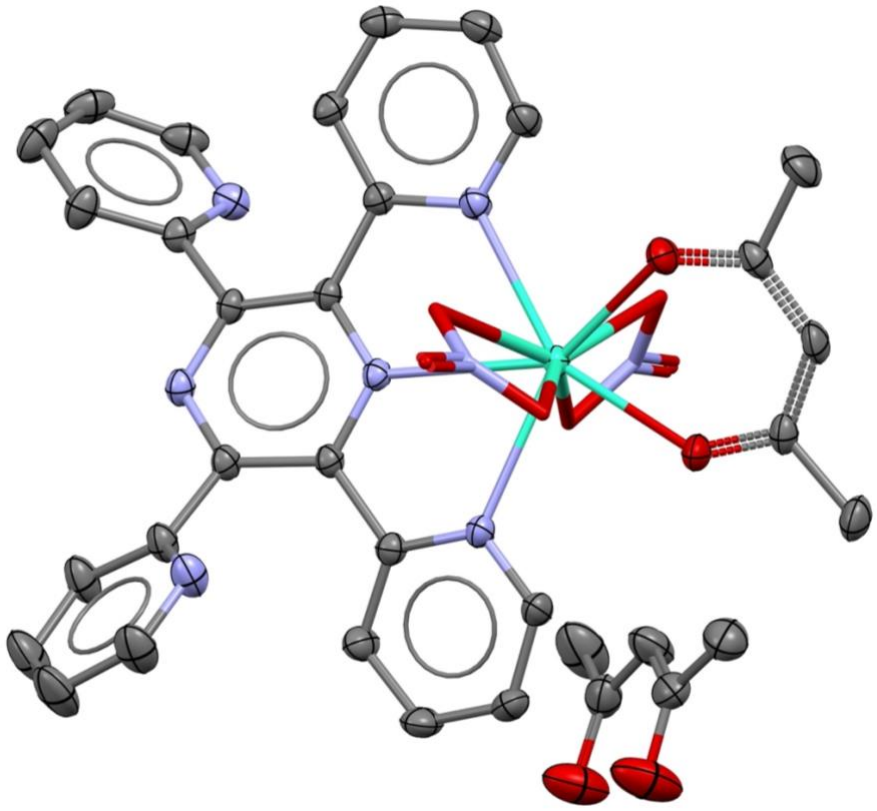

Figure 13. The crystal structure for complex **12** where green = Tb, red = O, purple = N. Hydrogens are omitted for clarity and thermal ellipsoids are drawn at the probability level of 50%. CSD: BIKQEU

The complex **12** containing the Tb^{3+} ion as a metal center exhibits luminescence with quantum yield of 69% and functions as sensitizer for Et_2O. The high quantum yield is a result of energy transfer from the triplet state of tppz which matches well with the emitting state of Tb^{3+} ($^5D_4$). The luminescent spectra of **12** were measured at room temperature, showing its strongest green emission peaks at 489 nm, 547 nm, 582 nm, and 620 nm with a lifetime of 1.35 ms at 298 K when excited with 391 nm. These correspond to transitions of $^5D_4 \rightarrow {}^7F_6$, $^5D_4 \rightarrow {}^7F_5$, $^5D_4 \rightarrow {}^7F_4$, and $^5D_4 \rightarrow {}^7F_3$, respectively. The largest emission intensity peak was observed for the transition $^5D_4 \rightarrow {}^7F_5$. Complex **12** luminescence was measured in several solvents to study if it has

sensitivity for some of them. Oscillations of O-H, N-H, and C-H were found to quench the metal centered luminescence of complex **12** in Et_2O, thus it can be used as turn-off sensor for Et_2O.[14]

4.2 Luminescent molecular sensors

As technology continues to advance, sensors are being increasingly utilized in everyday consumer products like smartphones and gaming devices. In such applications, there is often a requirement to create a tunable response, which can be accomplished by applying independent external stimuli, such as pressure, temperature, magnetic fields, or humidity.[23] Sensors play a vital role in numerous fields, including environmental monitoring, medical diagnostics, and industrial process control, where precise monitoring of parameter changes is necessary.[49]

The luminescent molecular sensor is a system that transforms sensor-analyte interactions into detectable light signals, enabling analyte sensing through optical or structural changes. Luminescent molecular sensors offer several advantages, such as small size, fast response, non-destructive detection, selectivity, low costs, high sensitivity, and often the possibility of reuse. The sensitivity and response of these sensors are influenced by the detection method used and the extent of change in the complex's luminescence properties caused by the detected target. For these reasons the availability of different types of luminescent sensors in various applications is important.[12,26]

4.2.1 Sensor applications of luminescent acetylacetonate lanthanoid complexes

The compounds presented in Chapter 4.1 demonstrated sensing abilities through energy transfer, antenna effect, and interaction with various sensing targets. The use of AcAc as an antenna ligand for Ln-based luminescence is well established in the literature and many trivalent Ln ions have been successfully complexed with different kinds of AcAc compounds to yield complexes that show enhanced luminescence utilized in a wide range of sensing applications.[28,30,42,50] Luminescence of AcAc Ln complexes is highly sensitive to changes in

the local environment like temperature, pH, or coordination of certain molecules which can, for example quench the luminescence by oscillations. Additionally, their relatively easy synthesis and tunable luminescence properties through the choice of Ln ion, number of AcAc ligands, and auxiliary ligands further contribute to their capability to sensing applications.[2,7,12,28,44] Auxiliary ligands are usually incorporated into complexes to broaden the excitation band and to avoid quenching the emission by additional coordination of water molecules.[47] Sensitivity and selectivity of a complex can be tailored by designing ligands that have specific affinity towards the target analyte like metal ions calcium, zinc, or copper. Luminescent AcAc Ln complexes can also be incorporated into various sensing platforms, such as optical fibers or thin films.[8]

Enhanced luminescence by AcAc ligands with different emission colors of Ln ions are key ingredients to many luminescent sensing applications. For example, Eu^{3+} complexes typically exhibit red luminescence, while Tb^{3+} complexes show green luminescence.[28,44] Narrow and sharp emission bands of AcAc Ln^{3+} complexes from UV to NIR region with their long emission lifetimes enables time gated detection and multiplexing. In multiplexing several Ln based probes with different emitting wavelengths are integrated in the same application. This allows the detection of multiple analytes at once or the capture of multicolor images of a studied target.[4,20] High quantum yields and large stokes shifts of AcAc Ln sensors enables also low limits of detection, minimized self-absorption, maximized signal to noise ratio and avoidance of light scattering and background autofluorescence. Resistance to photobleaching (self-absorption) makes them better than many organic dyes of fluorophores particularly in applications with longer monitoring times and continuous sensing where sensor stability is crucial.[4,20,26,51]

4.2.2 Luminescent temperature sensor

Temperature is one of the most important fundamental physical quantities in science. Many phenomena like rates of chemical reactions and colors of stars depend on the temperature. Temperature sensors play a vital role in industrial applications, where they are essential for monitoring and controlling processes. The accurate measurement and control of temperature is crucial as it directly impacts the kinetics of various processes and influences the overall

functionality of industrial systems. Current technology requires increasingly advanced contactless temperature monitoring in real time to meet the challenges of different fields in handling, storage, and use of materials, for example, in nanoelectronics, photonics, nanomedicine and nanofluidics. In the field of temperature sensors, the goal is that the old-fashioned infrared thermometers could be replaced by cheaper, more reliable remote-readable temperature sensors. Integrating Ln ions to hybrid materials is a promising way to get non-invasive thermometers. Contactless temperature sensors do not disturb the investigated substance and are necessary, for example, for fast-moving or small samples.[13,23,51,52] They also have good spatial resolution and signal stability and are considered as nontoxic.[51]

Luminescent temperature sensors are likely the most studied type of sensors that are based on luminescent Ln AcAc complexes.[7,12,26] The most common measurement methods for luminescent molecular thermometers are luminescence lifetime, intensity, and bandwidth, with the last being based on electron-phonon interactions sensitive to temperature. In the case of luminescent molecular thermometers where the AcAc ligand is chelated to the Ln ion, lifetime thermometry is perhaps the most used technique.[51] Figure 14 shows an example of luminescence thermometry, which has been explored using intensity ratio and lifetime measurements. Lifetime measurements are immune to possible fluctuations of the excitation source or detection system, which can make PL intensity measurements from single Ln emission uncertain.[51] Temperature induced intensity change of emission is typically coming from temperature-activated quenching mechanisms or population redistribution over electronic levels according to the Boltzmann statistics.[1,51] Lifetime thermometry involves observing how the population of excited state decreases by time. Decay can happen by radiative process or nonradiative process including Förster resonant transfer and cross relaxation between lanthanide ions.[51]

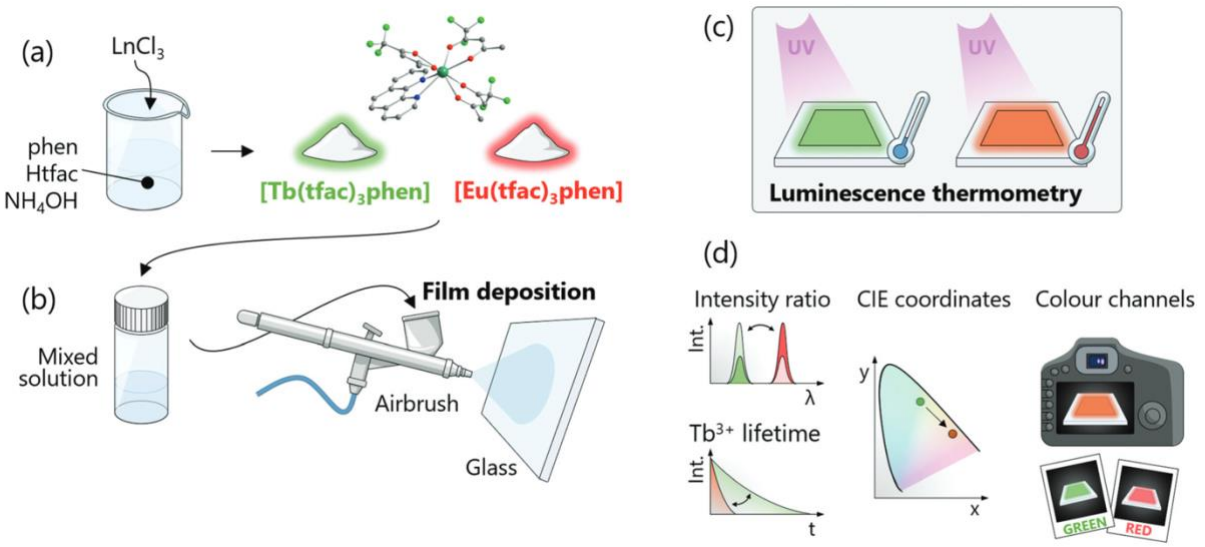

Figure 14. Explanation of how luminescent Ln AcAc complexes can be utilized in luminescent temperature sensing sprayed film. a) Synthesis of [Ln(tfac)$_3$(phen)] complexes. b) Deposition of the film with this mixed chloroform solution. c) Preparation of temperature-dependent luminescent films. d) Strategies used to explore the ways to obtain a quantitative thermal readout, including intensity ratios between Tb^{3+} and Eu^{3+} emission bands, changes in Tb^{3+} luminescence lifetime, variations in the CIE coordinates describing the color of the films, and analysis of the green and red parts of pictures taken under UV light.[52] – Adapted from *J. Mater. Chem. C*, **2022**, *10*, 1767–1775. with permission from The Royal Society of Chemistry.

Many different kind of luminescent Ln temperature sensors have been designed and Ln molecular thermal sensors can be adapted in various sensing platforms like nanoparticles (NP).[51] They can be embedded also in sol-gel glasses,[7] Langmuir-Blodgett films and polymer films,[7] or even biological fluids.[1] Many Eu^{3+} and Tb^{3+} AcAc compounds work as luminescent sensor for temperature like [Eu(tta)$_3$].[1,7,37] The emission intensity ratios of Eu and Tb vary with temperature, with Eu showing changes in the range of 150 to 250 K, while Tb exhibits variations in the range of 200 to 300 K.[26]

[Eu(tta)$_3$] complex is an illustrative example of the temperature sensor where the sensing is obtained by following the changes in the quantum yield or emission lifetime. Its luminescence lifetime is approximately 200 µs at the room temperature and it has thermal sensitivity of 2.1% K^{-1}. Its big advance is that it is not very sensitive to oxygen consentration.[7] It has been used for various applications such as imaging temperature of integrated circuits by placing it in a matrix of poly(methyl methacrylate). This sensor achieved a spatial resolution of 0.7 µm. The

[Eu(tta)$_3$] was also injected in living cells to image receptor-activated heat production.[12] Chemically similar kind of complex [Eu(tta)$_3$(phen)] has been used in nm thin Langmuir–Blodgett films of poly-(N-dodecylacrylamide) which has the same sensitivity of 2.1% K^{-1} as [Eu(tta)$_3$] in the temperature range of 320–370 K.[12]

Other good examples of temperature sensors are [Eu(hfac)$_3$(tppo)$_2$] (tppo = triphenylphosphine oxide) and [Tb(hfac)$_3$(tppo)$_2$] complexes that have been used in vinyltriethoxysilane Sol-gel glasses as energy transfer thermometers. The system is promising candidate to developing optical fiber sensor for temperature measurements. ET from Tb^{3+} to Eu^{3+} by Förster resonant process causes temperature-dependent changes in the luminescence intensity ratios of Tb^{3+} and Eu^{3+} emission bands. As a result, the samples emit different colors at different temperatures, shifting from orange at 10 K to red at 293 K.[7]

When developing an effective luminescent AcAc Ln sensor to measure the temperature, it is important to consider the same factors as in the development of luminescent AcAc Ln complexes. To achieve the best sensitivity, it is essential to find the optimal combination of Ln, AcAc ligand(s), and auxiliary ligand(s) in the complex where other physical parameters have minimal impact on the luminescence compared to temperature. The lifetime thermometry decay time primarily depends on three factors: (i) the type and number of ligands, (ii) polymer matrix, and (iii) complex concentration. Higher concentrations result in shorter lifetimes and increased temperature sensitivities.[7] Despite recent progress, fundamental challenges persist in the development of thermometers, including achieving optimal temperature readout and creating stable and sufficiently sensitive sensors. These issues have long been associated with thermometer development, and the design strategies for optimal luminescent thermometers are still in the process of being improved.[1]

4.2.3 Luminescent chemical and pressure sensors

Ln AcAc complexes can also be used as luminescent chemical and pressure sensors. Chemical and pressure sensors are one of the most used sensors, together with temperature sensors, in industry.[23] Luminescent chemical sensors can be used to monitor pH changes in biological systems, detect metal ions in water samples, or measure dissolved oxygen consentrations.[7,26,53]

Oxygen can also be detected using luminescent pressure sensors, which are occasionally referred to as oxygen sensors due to the significant interest in developing pressure-sensitive paints to detect oxygen.[12,53] Industrial processes and health industry rely on the everyday use of numerous chemicals, some of which have the potential to be harmful to the environment or disrupt the processes themselves. Therefore, portable tools for real-time analytics measurement of chemical species are essential to optimize production and reduce waste generation.[49]

Luminescent chemical sensors can be categorized into two groups: one where the analyte directly coordinates to the Ln center, and the other where this coordination does not occur. The latter can involve non-coordinative interactions with the antenna or electrostatic interactions with the complex. These new interactions cause changes in the luminescence properties of the material, usually luminescent quenching which enables the measurement of the target molecule's concentration.[49,53] Binding to target molecule or ion can be pH depended and this way with specific kind of molecules a chemical sensor can also act as a pH sensor.[26,49,53] Illustrative example of the detection of acid-base vapors with the Ln acac complexes are given in Figure 15.

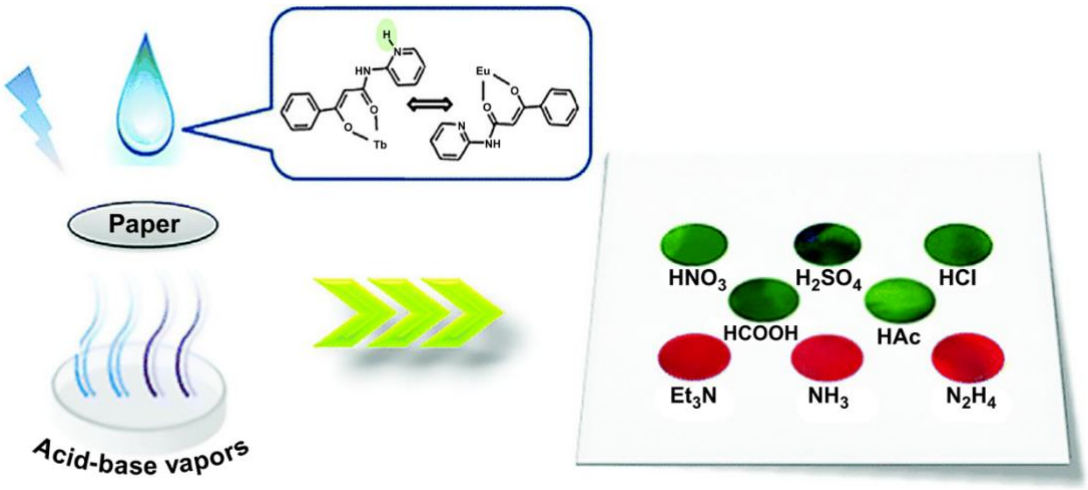

Figure 15. Ln AcAc complexes used as sensors for acid-base vapor detection. [54] – Adapted from *Inorg. Chem. Front.*, **2016**, *3*, 1014–1020 with permission from The Royal Society of Chemistry.

A good example of a Ln^{3+} complex used to measure the concentration of a chemical analyte is $[Tb(acac)_3]$, which has been used to measure the concentration of acetazolamide in

pharmaceutical tablets and serum samples. Acetazolamide quenches the [Tb(acac)$_3$] luminescence in DMSO at 545 nm when pH is 6.8 and λ_{ex}= 350 nm. Limit of detection (LOD) for this is 4.0 × 10^{-9} mol/L and limit of quantification (LOQ) is 1.21 × 10^{-8} mol/L respectively.[10]

[Eu(tta)$_3$(phen)] has been found to be very effective luminescent compound for monitoring oxygen concentration in gas phase when it is doped into a poly(styrene-*co*-trifluoroethylmethacrylate) film.[7,53] Exactly the same compound was used in pressure sensitive paints to measure oxygen pressure in wind tunnel experiments. The pressure sensing ability of luminescent pressure sensitive paints is based on oxygen adsorption and quenching. Quenching happens from the triplet state of antenna ligand to oxygen molecule because the ground state spin of oxygen is normally a triplet state. Quenching depends on the energy level of triplet state of antenna ligand, its emission lifetime, and energy transfer rate to Ln ion.[12,53,55]

Pressure can induce changes in molecular packing and shortening of interionic distance that can increase or decrease the crystal field strength around Ln ion. These changes have direct effect on the luminescent properties of Ln ion and can be used to detect pressure changes. Pressure sensors can offer high sensitivity, fast response times, and non-electrical readout, making them suitable for applications where electrical sensors are not ideal.[8,12,55] Also all triboluminescent crystals can be used as pressure sensors because they glow under pressure.[29,31,53] Luminescent AcAc Ln pressure sensors are suitable for harsh environments like strong electric fields or high temperatures. They can be integrated into the solid matrix of various applications using techniques such as luminescent coating, which finds applications in diverse fields like materials science and biomechanics. [12,53,55]

4.3 Ketoiminate ligands

NacAc ligands are nitrogen derivatives of AcAc ligand, which can be synthesized through a condensation reaction between AcAc and amines. During the reaction one O atom will be replaced with N atom.[16,17] NacAc ligands are important ligands in coordination chemistry, and their transition metal complexes are known for their catalytic properties in organometallic chemistry and application in catalysis.[15,16,40,56] NacAc ligands are more modifiable than AcAc

ligands because of the nitrogen which makes it possible to add more substituents to this molecule. An addition of new substituent to a ligand framework makes it possible to adjust physical and chemical properties like steric factors and triplet state position of the ligand.[37,40,57] This way it is possible to tune the ligand absorption properties for certain Ln ions that potentially leads to more efficient luminescence. However, the luminescence properties of NacAc Ln complexes have not been extensively studied.[15–17,19,41,57,58] No other fundamental reason is given in the literature for this other than that nitrogen is usually one of the factors that can quench Ln luminescence. Nitrogen atoms can introduce additional non-radiative relaxation pathways (because of SOC) that can compete with the desired radiative decay, potentially decreasing the luminescence efficiency. The effects of NacAc ligands on the PL properties of Ln complexes have not yet been studied in detail, so it presents an intriguing research problem. The NacAc ligand and its protonated precursor are illustrated in Figure 16.

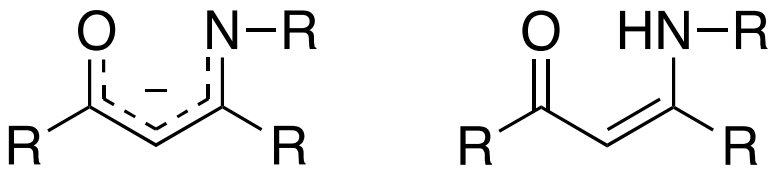

(**15**) (**16**)

Figure 16. (**15**) NacAc and (**16**) NacAcH

Although the luminescence of NacAc complexes has not been studied extensively, many nitrogen ligands, such as diimines, have been used as effective antenna ligands with Ln ions. This is because chelating nitrogen ligands can function as π acceptors and σ donors.[59] Moreover, nitrogen ligands can stabilize and activate the Ln center, leading to a stable and appropriate coordination sphere.[13,25] Many Ln tris-(β-diketonate) complexes have been made where unsaturated coordination sphere of Ln^{3+} ion has been completed by several nitrogen ligands like biby, phen and 2,2′:6′,6″-terpyridine. The saturation of coordination sphere prevents coordination of solvent molecules which would result nonradiative deactivations by vibronic couplings if solvent contains O-H oscillators.[18] The phen ligand is an efficient energy donor, forming a bidentate coordination to the Ln ion through its two free nitrogen electron pairs, creating a stable coordination compound. N-(2-pyridinyl)benzoylacetamide (HPBA) has been used in Tb and Eu based polymer hybrids to create tunable photoluminescent films where emission could be tuned from green to red depending on the OH concentration in hybrid

compounds from.[25] The success of using chelating nitrogen ligands in luminescent complexes together with AcAc ligands supports the expectation that changing one oxygen to nitrogen could result in good antennas.

4.3.1 Ketoiminate lanthanoid complexes

Coordination complexes of Ln NacAc have been synthesized, but their chemistry is still relatively new, with the first homoleptic Ln NacAc complex being synthesized in the 2000s.[41] In Figure 17 there are some NacAc ligands which have been coordinated successfully with Ln ions.

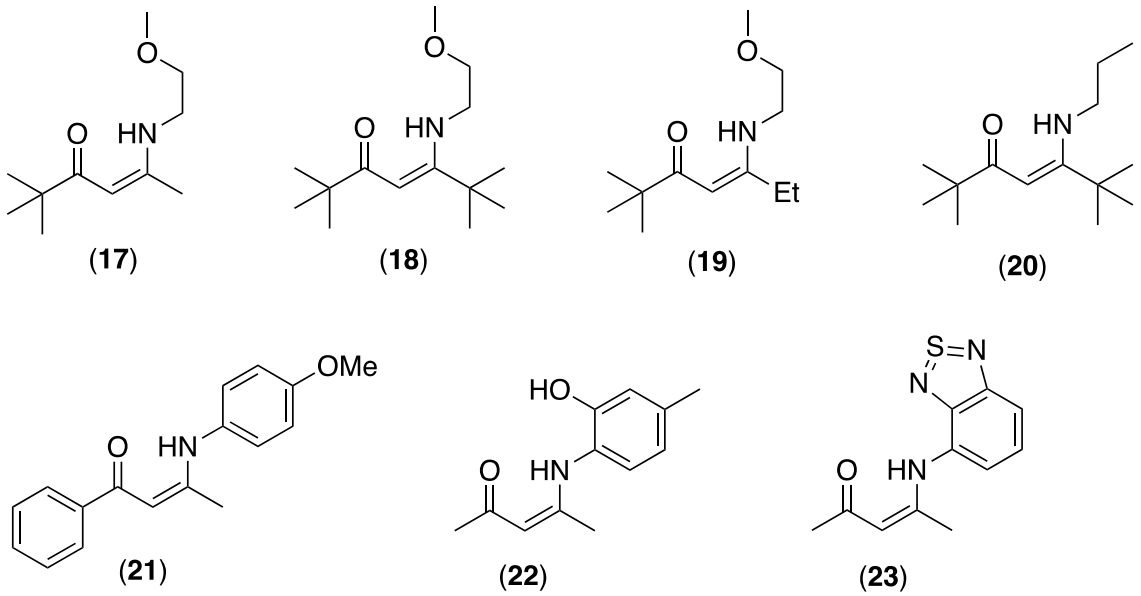

Figure 17. NacAc ligands which have been complexed with Ln ions. (**17**) 2,2-dimethyl-5-N-(2-methoxyethyl-imino)-3-hexanone,[19] (**18**) 2,2,6,6-Tetramethyl-5-N-(2-methoxyethyl-imino)-3-heptanone,[57] (**19**) 2,2-Dimethyl-5-N-(2-methoxyethyl-imino)-3-heptanone,[57] (**20**) 2,2,6,6-tetramethyl-5-(propylamino)hept-4-en-3-one,[41] (**21**) 1-phenyl-3-N-(p-methoxyphenylimino)-1-butanone,[15] (**22**) 4-((2-hydroxy-5-methylphenyl)amino)pentenone,[16] (**23**) 4-(2,1,3-benzothiadiazol-4-ylamino)pent-3-en-2-one.[58]

All ligands **17-23** were synthesized by a condensation reaction between corresponding AcAcH and amines, and their Ln complexes were made by a general metathesis reaction.[15–17,19,41,57,58] Ln complexes prepared with ligands **17-20** were synthesized to be used as dopants in chemical

vapor deposition because fluorine-free dopants are needed for more stable devices, and ketone/imino sites offer possibilities to tune melting point and volatility. Especially Ce^{3+} precursors were made with this in mind.[19,41,57] Ligand **21** was complexed with Y, Sm, Nd, and Yb to serve as catalysts for the ring-opening polymerization of rac-lactide. This polymerization process produces polylactic acid (PLA), a biodegradable and biocompatible polymer with properties similar to conventional plastics.[15] Ln complexes of Y, Yb, Tb, Nd, and Sm with ligand **22** were synthesized for the purpose of studying the synthesis, reactivity, and characterization of neutral complexes made by metathesis reactions with the sodium salt of N-aryloxo-functionalized -ketoiminate.[16] Lastly, Eu, Sm, and Gd complexes with ligand **23** were synthesized to study the structures and luminescent properties of these complexes. These are the only Ln^{3+} NacAc complexes with luminescence that have been studied, and more details of their properties are explained below.[58]

4.3.1.1 Tris4-(2,1,3-Benzothiadiazol-4-ylimino)pent-2-en-2-olato)- Ln

In 2019 new Ln complexes of 4-(2,1,3-benzothiadiazol-4-ylamino)pent-3-en-2-onate (L^-) were synthesized with samarium (**24**), gadolinium (**25**) and europium (**26**) to get $[Ln(L)_3]$. The complexes were made to get information of their coordination modes and luminescence properties. Ligand was selected because some Ln ions with 2,1,3-Benzothiadiazole (Btd) derivatives have shown interesting photophysical properties and 4-(2,1,3-benzothiadiazol-4-ylamino)pent-3-en-2-one (LH) has intense emission and high quantum yield and it can be easily deprotonated to form chelating ligand toward Ln ions. Ln amides $Ln(N(SiMe_3)_2)_3$ (Ln = Sm, Gd) and ketoimine LH were synthesized with known procedures. Reactions of silylamides of Sm and Gd with LH were performed in tetrahydrofuran (THF) or toluene resulting $Ln(L)_3$. $EuCl_3$ was reacted with LH in the presence of $KN(SiMe_3)_2$ as a strong base in THF. All reactions are presented in Scheme 6.[58]

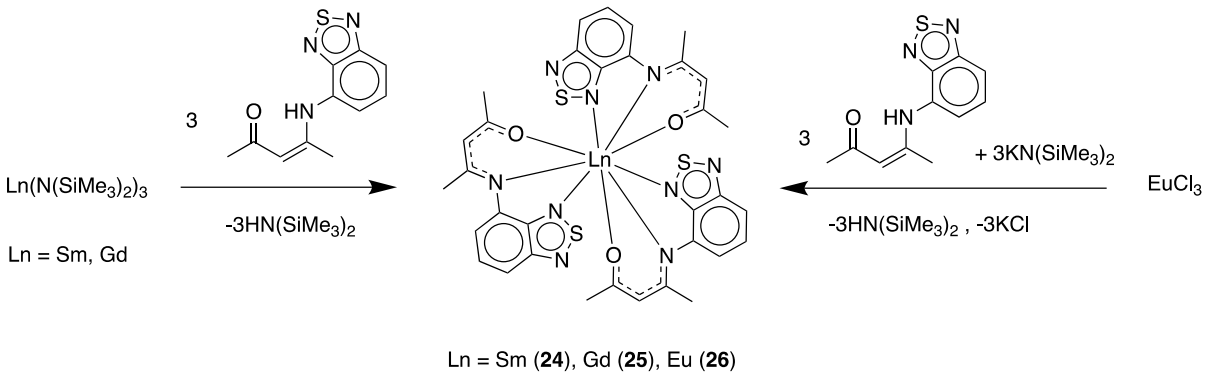

Scheme 6. Two methods used to synthesize lanthanoid complexes with 4-(2,1,3-benzothiadiazol-4-ylamino)pent-3-en-2-one.

Complexes were isomorphous and crystallizes in the monoclinic crystal system in space group $P2_1/c$. Structure is unique because the metal atom and one of the ligands display disorder in two positions. Additionally, the ligand fragments adopt a head to tail arrangement, occupying the same volume. This configuration potentially leads to the crystal lattice breakdown. In addition to the atoms of the ketoiminate moiety, the N atom of the heterocycle coordinates to the Ln center, which is why the L^- is a tridentate ligand in these compounds. Tridentate coordination explains why the Ln atoms are disordered 0.8 Å from the ketoiminate fragment plane. The nitrogen-Ln bonds varied between 2.58–2.77 Å in both thiadiazole and imino group. Thus, the arrangement of the ligands was more affected by steric effects, rather than the type of nitrogen atom. Crystal structure for **24** is shown in Figure 18.[58]

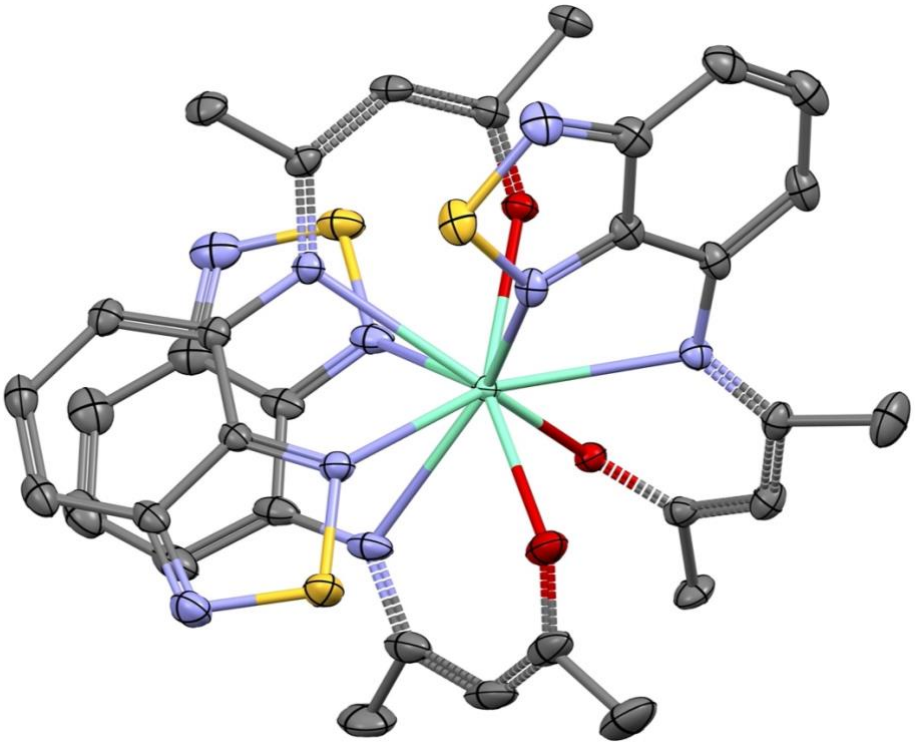

Figure 18. The crystal structure for complex **24** where green = Sm, red = O, purple = N, yellow = S. Hydrogens are omitted for clarity and thermal ellipsoids are drawn at the probability level of 50%. CSD: PODTEK

Luminescence measurements were done for $Sm(L)_3$ complex. In the crystal structure thiadiazole moieties were close to the central atoms which is important for the excitation ET from ligand to Ln center. However, the colors of the $Ln(L)_3$ complexes were red which indicates that the emission bands of Sm^{3+} and Eu^{3+} ion are emergently too close to the absorption band of the complex. This means that ET from ligand to these Ln ions leading to luminescence is not very probable. In $Sm(L)_3$ emission spectra only the board band of interligand transitions are observed and no characteristic Ln-centered luminescence is seen. Compared to the free ligand's maximum band of 595 nm, the maximum band of assigned intraligand transitions at 625 nm has shifted to a longer wavelength range. In earlier studies it has been noted that bonding from heterocyclic N atom to center metal causes a bathochromic shift in the absorption and emission spectra.[58]

5 Experimental part

5.1 Aim of the work

Aim of the experimental part was to prepare new luminescent lanthanoid complexes based on NacAc ligands. They are nitrogen analogues of the well-known β-diketonate ligands which readily form complexes with Ln ions with excellent luminescence properties.[8,20,28,47] Although AcAc ligands are widely known antenna ligands for Ln ions, the luminescence properties of NacAc Ln complexes have not been investigated much before. As mentioned in the literature part, NacAc ligands are more modifiable than AcAc ligands because they contain nitrogen atom where new substituents can be introduced to. 2,4,6-trimethylmesityl and 2,6-diisopropylphenyl were chosen as nitrogen substituents because they crystallize easily and are bulky enough to protect the coordination center from molecules such as water, which can quench the luminescence.[7,38,42] They also contain the aromatic group which is common for antenna ligands.[21,25] In addition to this the coordinating atoms might also have little effect to the triplet state.[24,28,37] The complexes were mainly characterized with NMR, and because the most interesting Ln ions from a luminescence aspect are paramagnetic, diamagnetic yttrium was used in the syntheses instead as a model system to obtain easily interpretable spectra. Studies of new antenna ligands are important to get new luminescent Ln complexes suitable for different kinds of applications. Especially excitation with longer wavelengths are required in some applications.[2,24] If NacAc ligands turn out to be good antennas, then NacAc Ln compounds could be used in applications such as in 3D-printable molecular sensors. Modified literature procedures were utilized in the synthesis of the ligands. All synthesized complexes were characterized by IR and NMR spectroscopy as well as X-ray crystallography and elemental analysis.

5.2 General considerations

Both commercial and non-commercial reagents were used in reactions (Table 1). Non-commercial reagents were synthesized by other researchers in the lab. All syntheses were performed under argon atmosphere using Schlenk line techniques and argon atmosphere

gloveboxes. Solvents were dried by distillation using CaH_2 and sodium as drying agents. The ^{1}H, ^{19}F and ^{13}C NMR spectra were measured at 30°C with Bruker Avance III HD 300 MHz NMR-spectrometer. Deuterated solvents were used in the NMR samples. IR spectra were measured with Bruker Alpha FTIR-spectrometer. The crystals were measured with the Rikagu Oxford Supernova X-ray diffractometer using Cu-Kα (λ = 1.54184) radiation. EA samples were measured with Elementar vario EL III elemental analyzer. The limit value for the measurements was set at the RSC's value of ± 0.5 %.

Table 1. Reagents used

Reagent	Purity (%)	Supplier	M (g/mol)
Acetylacetone	≥99	Sigma-Aldrich	100.12
2,4,6-trimethylmesityl	>99.0	TCI	135.21
2,6-diisopropylphenyl	>90.0	TCI	177.29
Hexafluoroacetylacetone	>95.0	TCI	208.06
$YI_2(THF)_5YI_4(THF)_2$	*	*	*
KHMDS 0.7M in toluene		Acros	
Formic acid	>99	VWR	46.03
KHMDS	*	*	*
Methanol	>99.8	Honeywell	32.04
Tetrahydrofuran-d8	99.5	Eurisotop	80.16
Toluene	100	VWR	92.14
Toluene-d8	99.5	Eurisotop	100.19
n-Hexane	>97	Honeywell	86.18
n-Heptane	99	Abcr	100.23
Petroleum ether (60–80 °C)	≤ 100	Honeywell	
Diethyl ether	100	VWR	74.12
C_6D_6	99.5	Eurisotop	84.15
$CDCl_3$	99.5	Eurisotop	120.38

*Reagent prepared in the laboratory of the University of Jyväskylä

6 Results and discussion

The work was started by preparing trimethylmesityl and diisopropylphenyl substituted NacAc ligands. However, it was soon observed that diisopropylphenyl derivatives were more difficult to crystallize in contrast to trimethylmesityl derivatives, thus, it was decided to focus on the trimethylmesityl substituted NacAc ligands and their yttrium complexes. The ligands were deprotonated with KHMDS to give potassium salts, from which yttrium complexes were synthesized in 3:1 (ligand:metal) ratios. Scheme 7 shows the general reaction pathway to ligands, alkali salts and yttrium complexes.

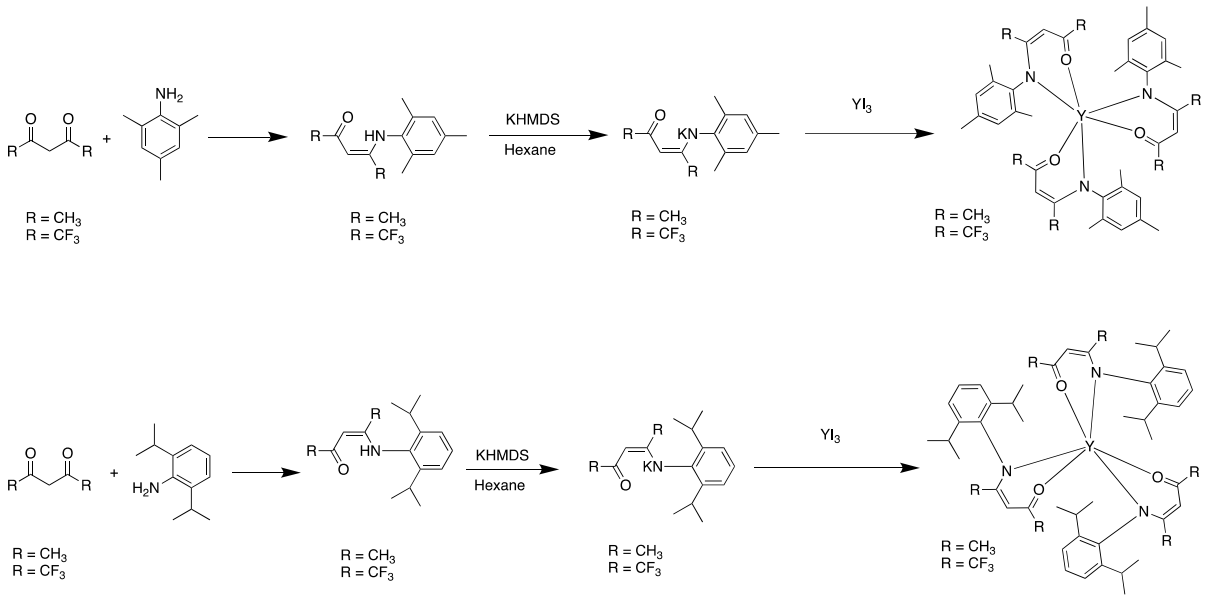

Scheme 7. Synthesis routes to NacAc yttrium complexes.

Detailed synthetic protocols and characterization of the products are presented in Chapter 9 Syntheses. All collected NMR spectra and crystal data are given in Appendices. Syntheses were only done with yttrium but due to the similarity to Ln ions, the reactions presented in this master thesis would generally also work with other LnI_3.

6.1 Ligands

6.1.1 (*Z*)-4-(mesitylamino)pent-3-en-2-one (27)

(*Z*)-4-(mesitylamino)pent-3-en-2-one (**27**) was prepared through the condensation reaction between acetylacetone and 2,4,6-trimethylmesityl as reported in the literature (Scheme 8).[40] The condensation reaction was carried out at the room temperature in methanol and two drops of formic acid were used as a catalyst. Product **27** was crystallized from petroleum ether as large white crystals in 61 % yield after vacuum filtration and petroleum ether wash.

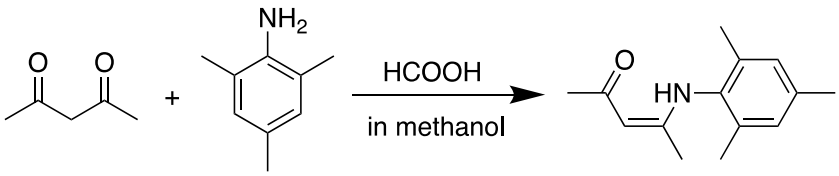

(**27**)

Scheme 8. Synthetic route for (z)-4-(mesitylamino)pent-3-en-2-one.

It has been reported that the product should be yellowish solid and the reaction should give the yield of 86 %, but without the crystallization steps. It is possible that a small amount of impurity has remained in the previously reported product, which causes the difference in color. The ^{1}H NMR of the product was in agreement with the reported values (Appendix 1). The EA results were also close to the calculated values although they differ by 1.2 % for carbon, 0.8 % for hydrogen and 0.1 % for nitrogen. The carbon and hydrogen values are slightly above the ±0.5 % limit, but since no impurities were observed by NMR, these differences are approximated to be insignificant, and it is safe to assume that the correct ligand was obtained. Because the reaction worked well, it was repeated with the same amounts of substances.

6.1.2 (Z)-4-((2,6-diisopropylphenyl)amino)pent-3-en-2-one (28)

(Z)-4-((2,6-diisopropylphenyl)amino)pent-3-en-2-one (**28**) was prepared through the condensation reaction between acetylacetone and 2,6-diisopropylphenyl as reported in the

literature (Scheme 9).[40] The condensation reaction was carried out overnight in methanol at 85°C and 5 drops of formic acid were used as catalyst.

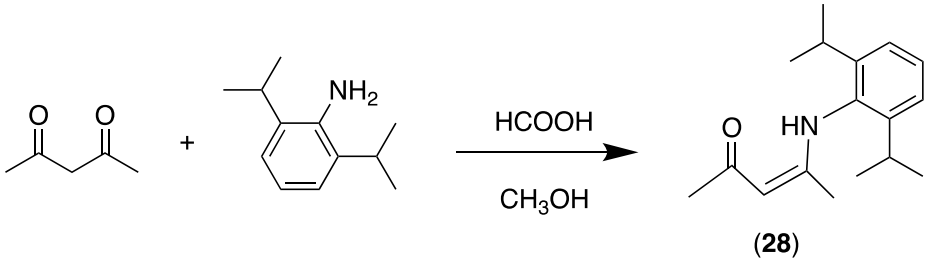

Scheme 9. Synthetic route for (Z)-4-((2,6-diisopropylphenyl)amino)pent-3-en-2-one.

^{1}H NMR measured from the reaction product indicated that there were still signals from the acetylacetone and 2,6-diisopropylphenyl so the reaction was not complete (Appendix 2). Between 1.11-1.31 ppm there are three doublets of integral 6, while in the correct ligand or in 2,6-diisopropylphenyl there should be only one doublet with the integral of 12. Some product was obtained but it was not pure. Attempts were made to crystallize the product from petroleum ether to obtain pure product, but crystals were never obtained. The reaction should have been heated longer and later it was concluded that the product could have been purified also by flash distillation, in which case the reaction might have given pure product.

6.1.3 (Z)-1,1,1,5,5,5-hexafluoro-4-(mesitylamino)pent-3-en-2-one (29)

(*Z*)-1,1,1,5,5,5-hexafluoro-4-(mesitylamino)pent-3-en-2-one (**29**) was prepared using a synthesis route modified from a literature synthesis of NacNac ligands.[45] The condensation reaction between hexafluoroacetylacetone and 2,4,6-trimethylmesityl was carried out in toluene at 140°C in the presence of molecular sieves (Scheme 10). Molecular sieves were used to remove water.

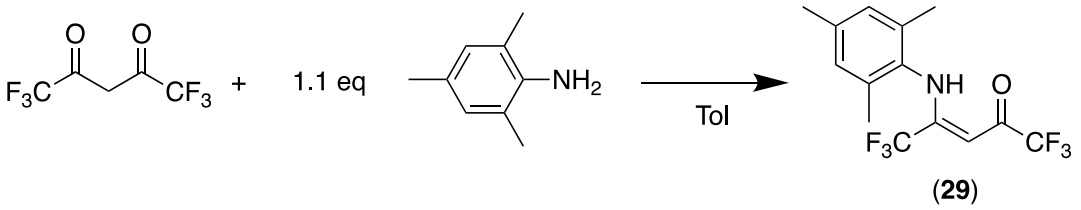

Scheme 10. Synthetic route for (Z)-1,1,1,5,5,5-hexafluoro-4-(mesitylamino)pent-3-en-2-one.

During reflux the solution turned purple. The dark purple mixture was filtered giving oily crude product. Purification of the crude product was attempted by crystallization from methanol or petroleum ether, but crystals were not obtained. However, flash distillation of the purple solution yielded an orange oily distillate. By dissolving the orange distillate into methanol and letting it stand at room temperature, **29** was obtained as needle-like yellow crystals. After the reaction conditions were optimized, the reaction was repeated with yield of 40 %. According to ^{19}F and ^{1}H NMR (Appendix 3 and 4) the product was pure, but the crystals always contained methanol as shown by the characteristic peak of methanol in ^{1}H NMR at 3.49 ppm. To remove the methanol before deprotonation reactions, crystals were dissolved in hexane and then vacuum dried to give **29** as a methanol free white powder. The EA values differed from the calculated values for carbon by 0.19%, for hydrogen by 0.03% and for nitrogen by 0.05% so all values were within the error limits. Single crystal X-ray crystallography was used to determine the crystal structure of **29** which was previously unknown (Figure 19).

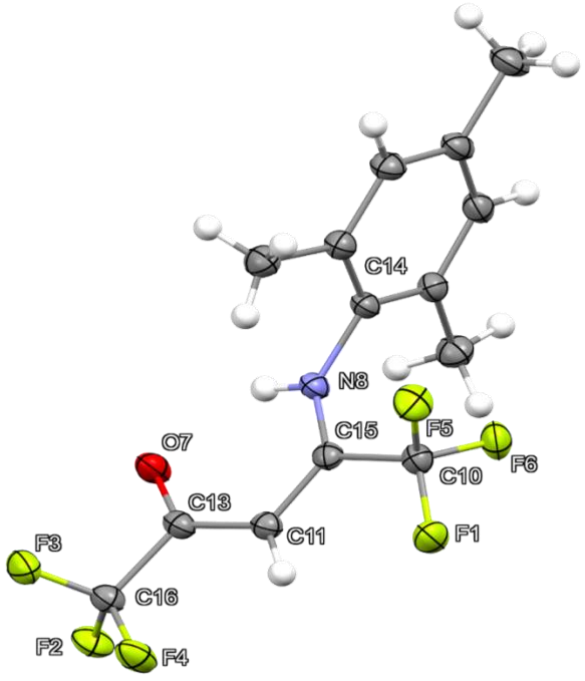

Figure 19. The molecular structure of **29**. Thermal ellipsoids are drawn at the probability level of 50%.

Compound **29** crystallizes in the monoclinic crystal system in space group $P2_1/n$. The crystal structure along with EA and NMR proved that the product was the targeted compound. The

unit cell dimensions and refinement parameters of the crystal structure are given at Appendix 28.

6.1.4 (Z)-4-((2,6-diisopropylphenyl)amino)-1,1,1,5,5,5-hexafluoropent-3-en-2-one (30)

(Z)-4-((2,6-diisopropylphenyl)amino)-1,1,1,5,5,5-hexafluoropent-3-en-2-one (**30**) was prepared using a modified literature synthesis.[45] The condensation reaction between hexafluoroacetylacetone and 2,6-diisopropylphenyl was carried out in toluene in the presence of molecular sieves like for **29** (Scheme 11).

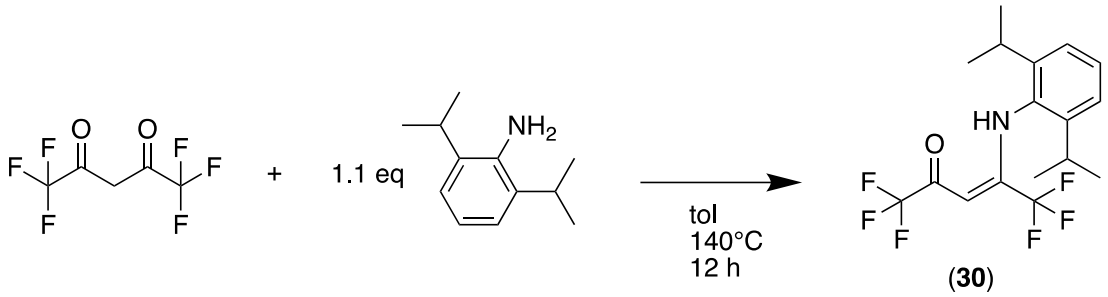

Scheme 11. Synthetic route for (Z)-4-((2,6-diisopropylphenyl)amino)-1,1,1,5,5,5-hexafluoropent-3-en-2-one.

The reaction solution was stirred and refluxed overnight yielding the brownish mixture. The product was filtered, and the toluene was evaporated from the solution. The crude product crystallized as large yellow crystals from methanol in several crops. To speed up the crystallization process, it may be worthwhile to purify the product by flash distillation before crystallization. According to ^{1}H and ^{19}F NMR spectra, respectively, the product was pure (Appendices 5 and 6).

6.2 Potassium salts

The potassium salts of ligands **27**, **29**, and **30** were prepared by deprotonating them with a strong base, namely KHMDS. Potassium salts were initially prepared using a 0.7 M KHMDS

solution in toluene, but after a few failures it was concluded that the KHMDS solution was not completely pure. For this reason, KHMDS was crystallized out from the concentrated toluene solution. The crystals of KHMDS were isolated with filtration and dried under a vacuum overnight. With crystallized KHMDS, the deprotonation was more successful.

6.2.1 Potassium (*Z*)-1,1,1,5,5,5-hexafluoro-4-(mesitylimino)pent-2-en-2-olate (31)

Ligand **29** was deprotonated on two occasion with 0.7 M KHMDS toluene solution in hexane (Scheme 12). Attempts to purify white solid reaction products (**31**) from both reactions were made by crystallization in different solvents. A successful crystallization was achieved using diethyl ether which gave **31** as small blocks with a yield of 57%.

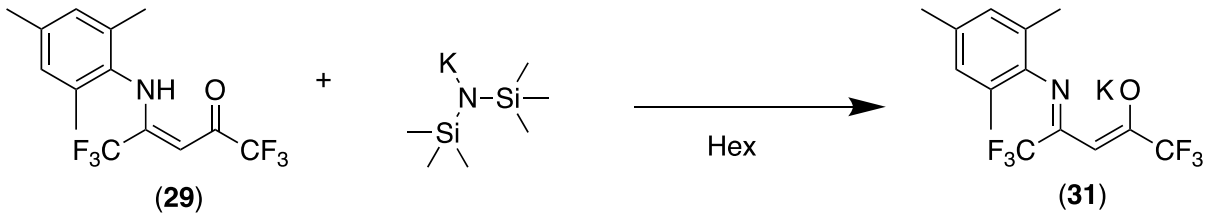

Scheme 12. Deprotonation of **29**.

Due to impurities observed in ^{1}H NMR before crystallization (Figure 20) the reaction was also repeated with the crystalline KHMDS. The ligand was dissolved in hexane and slowly added over crystalline KHMDS in ice bath producing bright yellow solid product. The product was crystallized from diethyl ether with a yield of 88%. Figure 20 shows the spectra of the crude and crystallized products obtained from the reaction using 0.7 M KHMDS toluene solution and crystalline KHMDS.

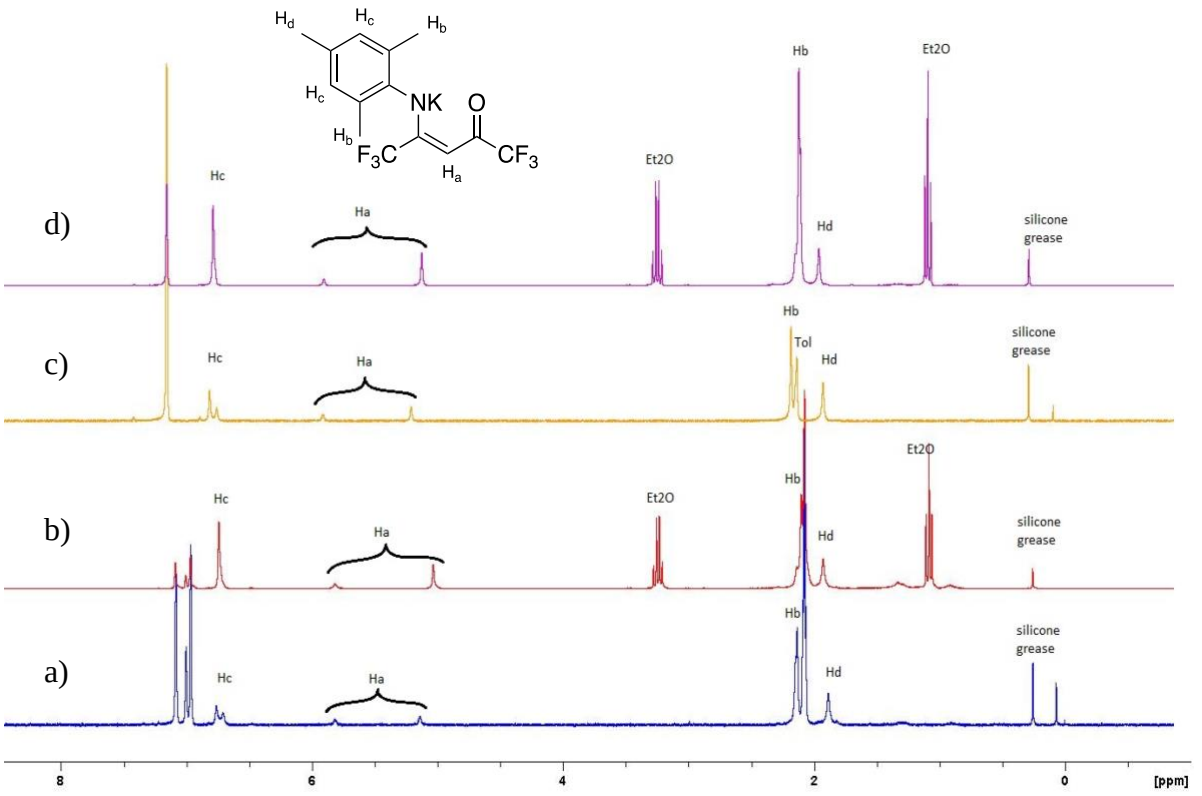

Figure 20. ^{1}H NMR spectra for raw and crystallized product of **31**. a) blue is raw product from reaction with 0.7M KHMDS solution and b) red is crystallized product from same reaction. Blue and red are measured in toluene-d8. c) yellow spectrum is raw product from reaction with crystallized KHMDS and d) purple is crystallized product from same reaction. Yellow and purple are measured in C_6D_6.

From blue ^{1}H NMR it can be seen that the reaction was complete; ligand peaks are not observed. The product contained hexane at 1.22 ppm and 0.88 ppm. The α-hydrogen signal was split, but it was not possible to explain why until closer examination of the crystal structure, which revealed two ligands coordinated to potassium (see below). Impurity peaks coming from impure KHMDS solution can be observed below 0.20 ppm. Same observation is made for yellow spectrum even though the reaction was performed with crystalline KHMDS. After crystallization, the only impurity observed in Figure 31b) and 31a) spectra is silicon crease. Diethyl ether can be observed at 1.11 ppm and 3.25 ppm. In the ^{19}F NMR spectra, there were three peaks instead of the expected two (Appendices 8 and 10). This is likely due to interactions between the α-hydrogen and one of the fluorine atoms. ^{13}C NMR shows silicon grease peak at 1.02 ppm and diethyl ether at 15.13 ppm and 65.49 ppm in addition to the product signals (Appendix 11). Many product signals are also slightly split in two, but they are so close to each other that it is safe to assume that they belong to same carbon atom(s).

The downside of crystallization is that product dissolves in a very small amount of ether, after which it precipitated out as a hard solid mass. After this, more than ten times the amount of ether must be added before the product dissolves again. It was also impossible to crystallize the product from such a large amount of diethyl ether and it crystallized only when the solution was concentrated to about 1/4 of the volume. Diethyl ether is therefore perhaps not the most efficient crystallization solvent for **31**, even though it yields a clean crystalline product as a diethyl ether adduct (see below). Interestingly, the potassium salt is readily soluble in toluene, but after diethyl ether coordinates to the potassium salt, its solubility into toluene is significantly decreased and heating is required to fully dissolve the diethyl ether adduct. The same observation was made when the product was dissolved in benzene. ^{19}F NMR of the pure product shows 3 peaks, so it is possible that one of the fluorine atoms of a CF_3 group interacts with hydrogen which would explain the splitting of α hydrogen signal (Appendix 10). Measured EA values differ from calculated for carbon by 0.67 %, for hydrogen by 0.53 %, and for nitrogen by 0.16 %. Carbon and hydrogen values are slightly above the ± 0.5 % for this compound as well. Crystal structure of compound was previously unknown, and it is shown in Figure 21. The compound forms small, sphere-like, yellow crystals. The particular crystal that was analyzed by SCXRD was a twin which affected the quality of the data. Compound **31** crystallizes in the triclinic crystal system in space group *P*-1. The unit cell dimensions, and refinement parameters are given in Appendix 30.

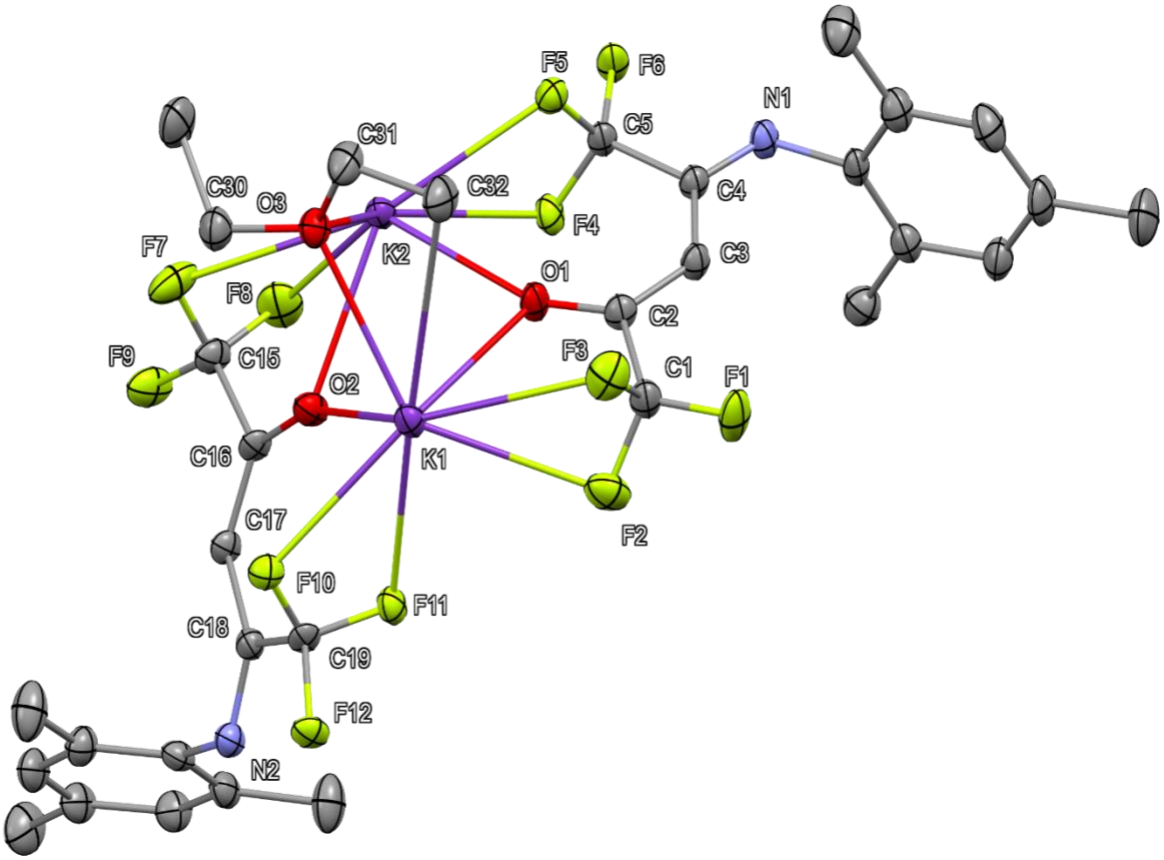

Figure 21. Molecular structure of **31**. Hydrogens are omitted for clarity and the thermal ellipsoids are drawn at the probability level 50%

In addition to diethyl ether, which coordinates to both potassium atoms from oxygen, it was also observed that potassium atoms act as bridging atoms between two ligands. Both ligands coordinate to potassium from the oxygen atom as well as two fluorines of both trifluoromethyl groups, and not from nitrogen as it was first hypothesized.

6.2.2 Potassium (*Z*)-4-(mesitylimino)pent-2-en-2-olate (32)

potassium (*Z*)-4-(mesitylimino)pent-2-en-2-olate (**32**) was prepared twice using 0.7 M KHMDS toluene solution the same way as **31**, but by replacing **29** with **27** (Scheme 13). Pure white solid product was obtained from the reaction with a yield of 64 %.

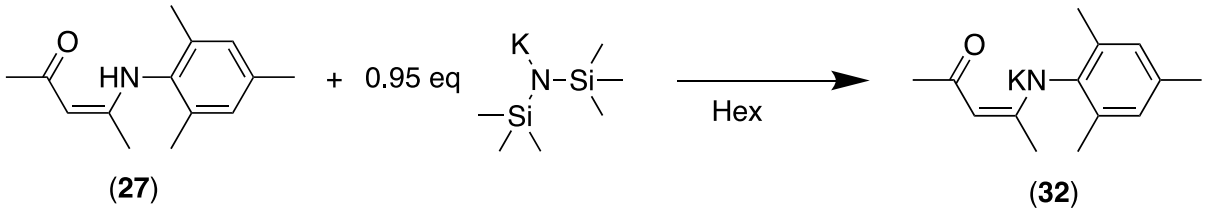

(**27**) (**32**)

Scheme 13. Deprotonation of **27**.

In ^{1}H NMR, NH proton was not observed anymore and the remaining peaks, based on the integrals and positions of the peaks, can be assigned to **32** indicating a successful reaction (Appendix 12). The product also contains hexane and its peaks can be seen at 0.88 ppm and 1.22 ppm as well as a small amount of silicon grease observed at 0.30 ppm.

The reaction was repeated with crystalline KHMDS giving a yield of 62 %. The reaction was done by dissolving KHMDS in toluene and adding this solution into the hexane solution of the ligand in ice bath to ensure that all KHMDS would react. Toluene was preferred over hexanes because KHMDS does not dissolve in hexane. Unfortunately, this caused a problem because the potassium salt of the ligand dissolves in toluene very easily and hexane had to be added in large quantities before all of the product precipitated out from the solution. ^{1}H NMR results were same as in the first reaction and are presented in Appendix 13. The product was otherwise pure but it also contained a small amount of silicon grease and hexane. Hexane can also be seen in ^{13}C NMR at 13.95, 22.66 and 31.58 (Appendix 14). EA values differ from calculated for carbon by 0.78 %, for hydrogen by 0.33 %, and for nitrogen by 0.06 %.

6.2.3 Potassium (Z)-4-((2,6-diisopropylphenyl)imino)-1,1,1,5,5,5-hexafluoropent-2-en-2-olate (33)

30 was deprotonated only with commercial 0.7 M KHMDS solution in toluene producing potassium (Z)-1,1,1,5,5,5-hexafluoro-4-(2,6-diisopropylphenylimino)pent-2-en-2-olate (**33**) as fine and dusty white powder (Scheme 14). Purification of the crude product was attempted by crystallization from toluene and diethyl ether without success. Thus, it was washed with hexane to get rid of diethyl ether.

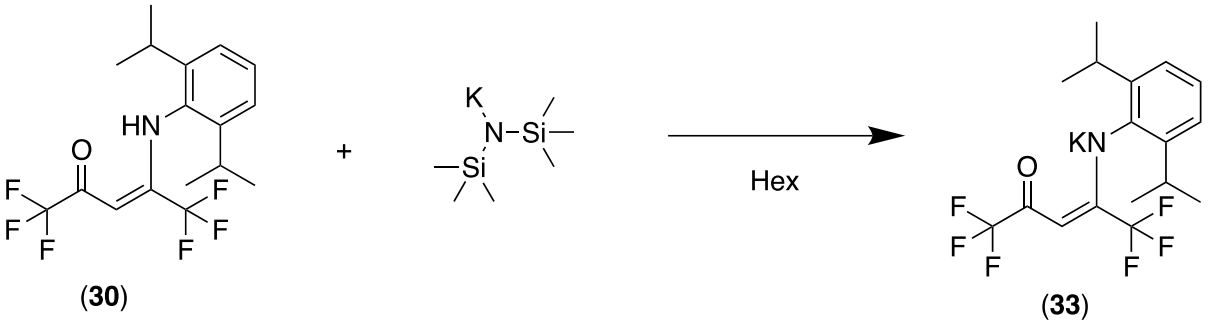

Scheme 14. Deprotonation of **30**.

Based on the ^{1}H NMR the targeted potassium salt was obtained but ^{1}H NMR also indicated the presence of hexane at 0.89 ppm and 1.29 ppm and other impurities originating likely from the commercial KHMDS solution at 0.09ppm, 0.05ppm and -0.11ppm (Appendix 15). In ^{19}F NMR there are two peaks that can be intergrated to three as expected for the targeted product (Appendix 16). The reaction was repeated on a larger scale to facilitate the crystallization process. Unfortunately, no crystals were obtained as the product readily dissolved in diethyl ether in the same way as **31**. The product containing the impurities from the KHMDS solution was obtained with yield of 66 %. Based on ^{1}H and ^{19}F NMR (Appendix 17 and 18), the reaction was complete, but the same impurities that were seen after the first synthesis attempt were observed in the newly recorded ^{1}H NMR spectrum as well, in addition to toluene, which gave resonances at 2.31 ppm, 7.10 ppm, and 7.19 ppm. The ^{19}F NMR spectra were identical. There was no time to repeat the reaction with crystalline KHMDS.

6.3 Yttrium complexes

6.3.1 Tris(4-((2,6-diisopropylphenyl)imino)-1,1,1,5,5,5-hexafluoropent-2-en-2-olato)-yttrium (34)

Tris(4-((2,6-diisopropylphenyl)imino)-1,1,1,5,5,5-hexafluoropent-2-en-2-olato)-yttrium complex (**34**) was synthesized in NMR scale by reacting **33** with $[YI_2THF_4][YI_4THF_2]$ in THF as shown in Scheme 15.

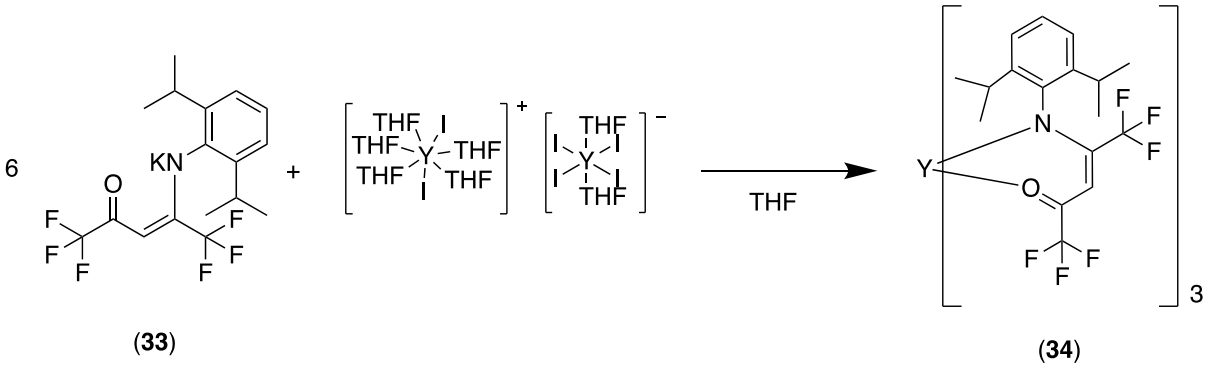

Scheme 15. Synthetic route for **34**.

Both, ^{1}H and ^{19}F NMR, revealed complicated spectra. ^{19}F NMR spectrum (Appendix 20) contained more than twenty peaks indicating a mixture of compounds when there should be only two peaks. A closer inspection of ^{1}H NMR (Appendix 19 and Figure 22) showed full consumption of the potassium salt, but also a degree of protonation of the ligand **30**, suggesting the presence of a proton source. However, the proton source could not be determined.

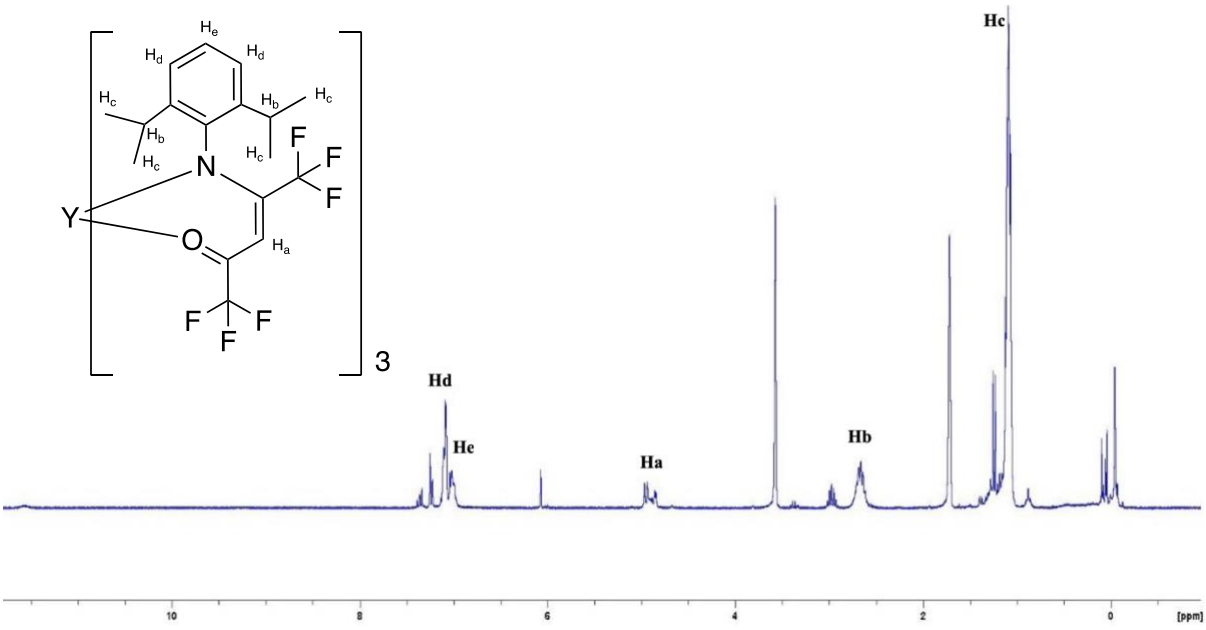

Figure 22. ^{1}H NMR spectrum of **34** in THF-d_8. Only the product peaks are labelled.

Despite the complicated NMR spectra one product with split signals was observed in ^{1}H NMR spectrum along with hexane and impurities originating from the commercial KHMDS solution. The CH_3 peaks of the isopropyl groups of the complex overlap with the CH_3 peaks of the ligand, which is why the peak at 1.10 ppm integrates to 14.4 instead of 12. There are two main reasons that could have led to the complicated reaction mixture in this reaction. First, THF is

probably not the best solvent for the reaction because subsequent reactions with other potassium salts in toluene or diethyl ether worked well (see below). Second, by using the potassium salt synthesized from the crystallized KHMDS could have removed all the impurities originating from the commercial 0.7 M KHMDS solution in toluene. It is possible that THF coordinates to some of the complexes and causes a splitting of the signals. THF also made a very unclear spectrum with (**35**). Thus, the reaction should have been repeated in the different reaction conditions and with the pure starting reagents.

6.3.2 Tris(4-(mesitylimino)pent-2-en-2-olato)-yttrium (35)

Yttrium complex Tris(4-(mesitylimino)pent-2-en-2-olato)-yttrium (**35**) was first made in NMR scale with 3:1 ratio between **32** and $[YI_2THF_4][YI_4THF_2]$] in toluene (Scheme 16).

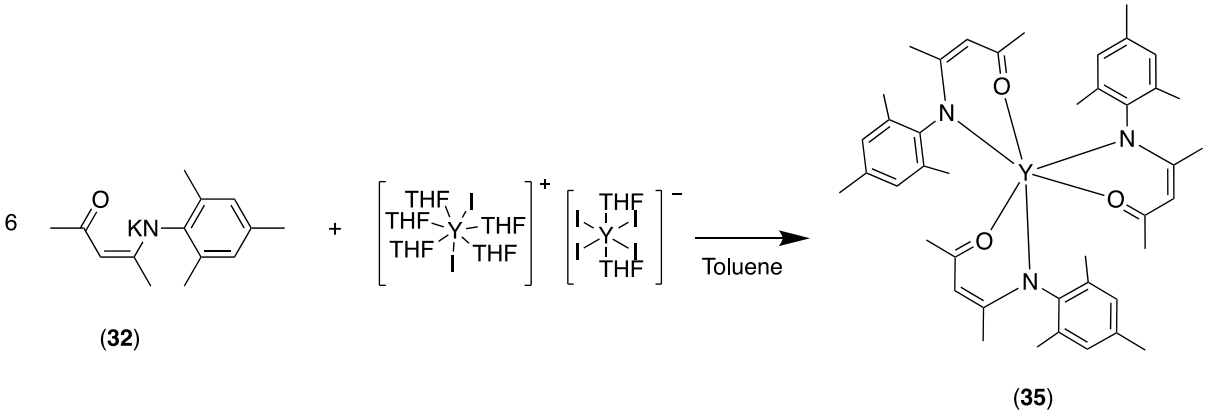

Scheme 16. Synthetic route for **35**.

According to the ^1H NMR (Figure 23 and Appendix 21) it is very likely that 3:1 complex was obtained but crystal structure could not be obtained to further confirm the hypothesis. Also signals from the protonated ligand also appeared at 6.60 , 5.06 , 1.321 , and 1.967 ppm. The NH signal of the ligand was so far downfield that it was not visible, but it was estimated to be located at 12.25 ppm based on the ligand spectrum. Additionally, other signals, most likely from 1:1 and 2:1 complexes, as well as diethyl ether, were observed in the spectrum. For this reason, 1:1 and 2:1 reactions were tested on an NMR scale. Both reactions resulted in the formation of a mixture of complexes and protonated ligands (Appendix 22). All three products also contained hexanes. Of all the complicated spectra, the 3:1 spectrum was the easiest to interpret, so the 3:1 reaction was repeated on a larger scale.

The large-scale 3:1 reaction was carried out in toluene by adding the potassium salt to $[YI_2THF_4][YI_4THF_2]$ at room temperature. The reaction result was a brown solution of **35** with a white residue of KI, leading to the conclusion that the reaction had been exposed to air based on its color. Based on the ^1H NMR measured from sample of the brown solution after evaporation, the same complex as in the NMR scale reaction was obtained (Appendix 23). Therefore, crystallization of the solid residue was attempted from toluene and diethyl ether, but without success. After 72 hours, mostly protonated ligand was left in the crystallization, which indicates that the product had been exposed to moisture. The reaction was repeated twice, once in toluene and once in diethyl ether, both times in dry ice bath was used to slow down the reaction rate and to ensure the formation of only one complex. The ^1H NMR spectra of both complexes are shown in Figure 23, together with the 3:1 NMR scale reaction spectrum.

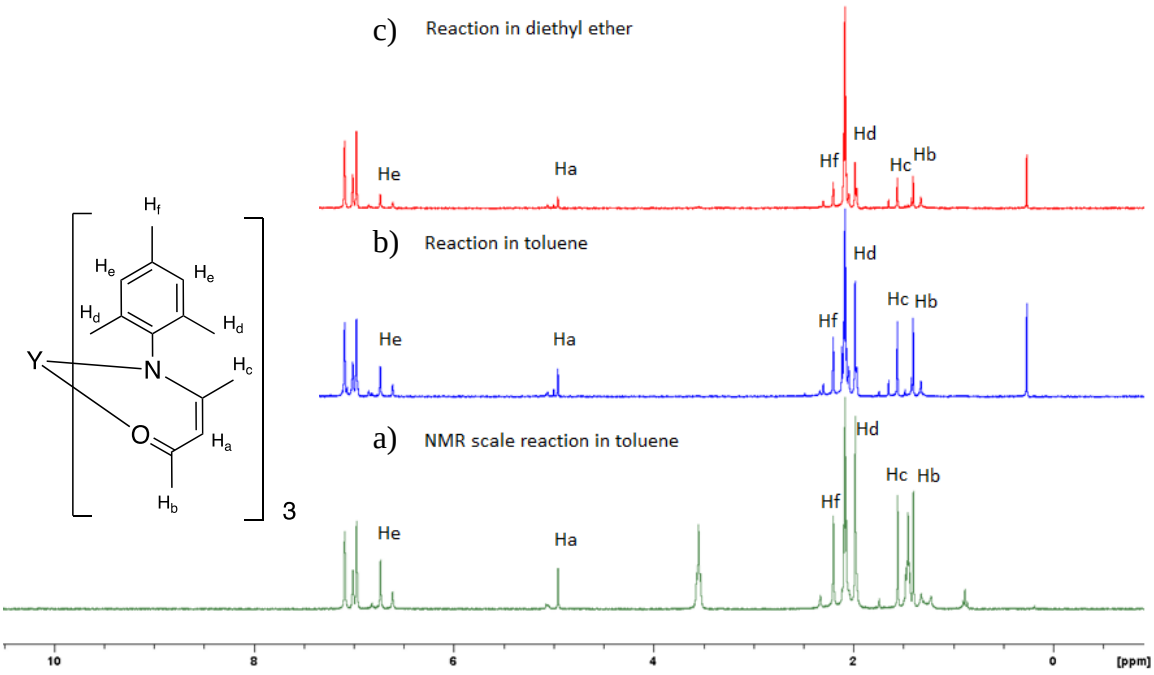

Figure 23. 3:1 reaction ^1H NMR spectra of **35** from the 3:1 reactions under various conditions. a) green: in NMR scale in toluene. b) blue: reaction in toluene. c) red: reaction in diethyl ether. Only the products peaks are labelled.

When the reactions were carried out in a dry ice bath, the product obtained was a yellow solution with white residue. Crystallization from diethyl ether and heptane resulted in very low yields, and crystals suitable for x-ray analysis were not obtained. Since diethyl ether

coordinates to the product, heptane might be a better solvent for crystallization. However, when the reaction was performed in toluene, it took three days to reflux, whereas in diethyl ether, it only took one day to reflux. Reaction time in toluene was monitored by ^{1}H NMR measurements. According to the ^{1}H NMR spectrum, all reactions produced the same main product but reaction mixtures also contained protonated ligand (Figure 23). However, the NH proton was so far downfield that it could not be observed in the chosen measurement window. A completely pure product was never obtained.

6.3.3 Tris(1,1,1,5,5,5-hexafluoro-4-(mesitylimino)pent-2-en-2-olato)-yttrium (36)

Reactions of **31** with $[YI_2THF_4][YI_4THF_2]$ in 3:1 ratio (Scheme 17) produced tris(1,1,1,5,5,5-hexafluoro-4-(mesitylimino)pent-2-en-2-olato)-yttrium complexes tentatively assigned as (**36**) and (**37**). NMR scale reaction was carried out in benzene giving **36** and large-scale reaction in diethyl ether in cold giving **37**.

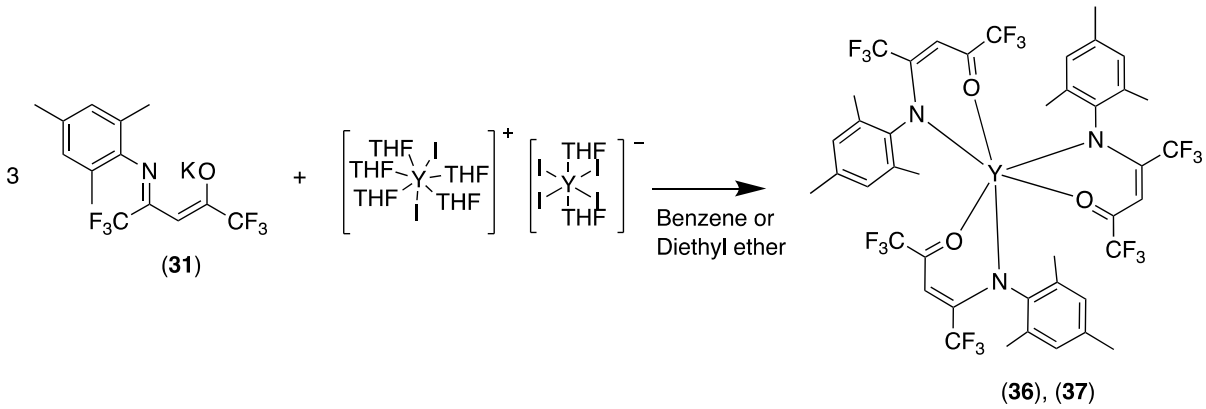

Scheme 17. Synthetic route to **36** and **37**.

^{1}H NMR of the NMR scale reaction product **36** showed the full consumption of the potassium salt (Appendix 24). However, both ^{1}H and ^{19}F NMR spectra are quite complex, with many signals being split. Due to this complexity, the ^{1}H NMR spectrum of **36** was interpreted using the ^{1}H NMR spectrum of the potassium salt as guidance. Assigments of the product peaks in ^{1}H NMR are presented in Figure 24.

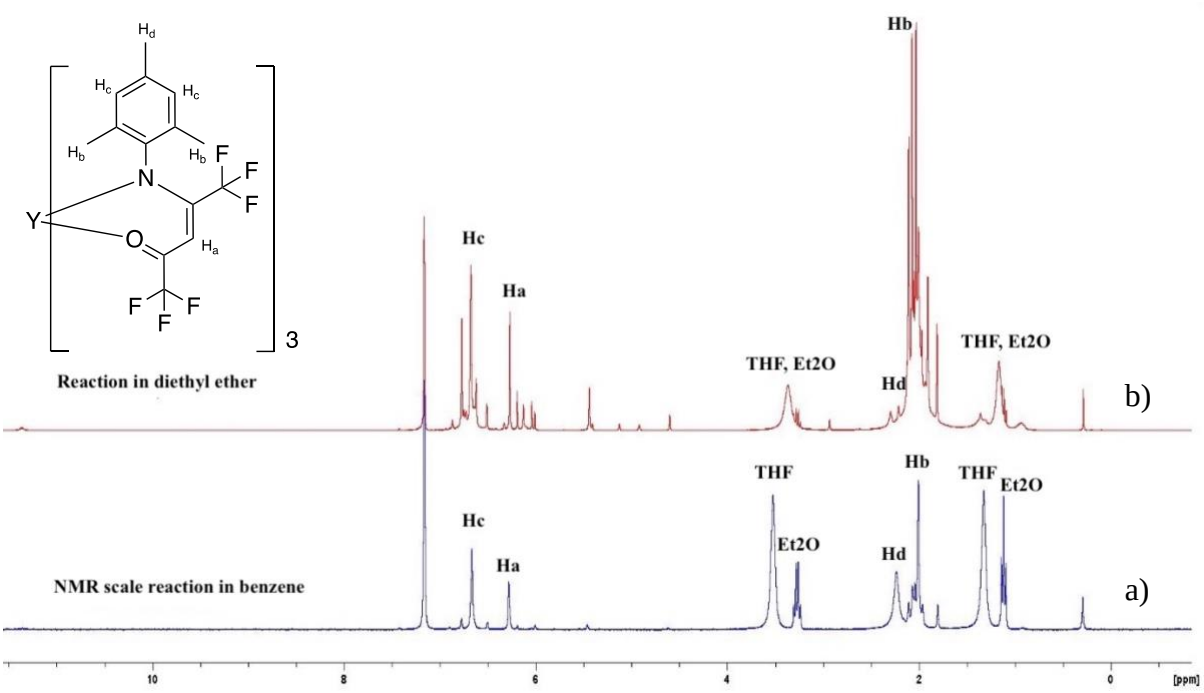

Figure 24. ^{1}H NMR spectra of **36** and **37**. a) blue **36**: large-scale reaction in diehtyl ether in cold. b) red **37**: NMR scale reaction in benzene at room temperature.

In the ^{1}H NMR spectrum of **36**, diethyl ether can be observed at 1.12 ppm and 3.27 ppm, while THF can be seen at 1.34 ppm and 3.54 ppm. Additionally, there are some impurity peaks and silicon grease at 0.29 ppm. In the ^{19}F NMR spectrum, two main signals can be observed at -7.78 ppm and 0.72 ppm, both with the same intensity (Appendix 25). In addition, smaller peaks can be seen in the spectrum.

In the large-scale reaction, the product was obtained as a clear yellow solution, and attempts were made to crystallize it without success. The product was then vacuum dried to give a fluffy yellow solid, **37**. The ^{1}H and ^{19}F NMR spectra of **37** are quite complex. The sample also contains a protonated ligand, and the NH proton can be detected at 11.35 ppm in the ^{1}H NMR spectrum (Appendix 26). The THF and ether peaks are almost overlapping in the spectrum at 1.16 ppm and 3.36 ppm. By comparing the ^{1}H NMR spectra of **37** and **36**, it is possible to integrate the main product, which is shown in Figure 24. However, there are other compounds present as well. The ^{19}F NMR spectrum has been integrated and it is presented in Appendix 27.

7 Summary

Developing antenna ligands for Ln ions is important for new applications where current emissive materials are not suitable. Knowledge of the electronic properties and luminescence of lanthanides, coupled with the research on antenna ligands, has established a strong foundation for the development of novel antenna ligands and a better understanding of energy transfer processes. Acetylacetonate ligands currently represent the most widely used antennas in combination with Ln ions, and various derivatives of acetylacetonate ligands work effectively as antennas. Nitrogen-containing ligands are frequently employed as auxiliary ligands in luminescent Ln AcAc complexes, and the incorporation of both oxygen and nitrogen donors into a single ketoiminate ligand offers a new approach to antenna ligand design.

The possibility of adding one more substituent to the ketoiminate ligand enables more flexible ligand design and offers promising opportunities for optimizing the antenna effect in Ln complexes. The study of luminescent Ln AcAc complexes and their applications in luminescent sensors highlights the importance of these compounds. The potential of ketoiminate ligands as efficient lanthanide antennas opens exciting possibilities for their utilization as emissive materials in luminescent sensors. With nanotechnology and 3D printing, the complexes could be adapted for use in almost any sensing platform.

The synthesis and preliminary study of two new NacAc yttrium complexes are important steps to progressing in this field. Although their luminescence properties remain to be fully explored, their successful syntheses imply that similar experiments could be conducted with other Ln ions, allowing for future luminescence measurements. Several syntheses had to be repeated multiple times to achieve success, and it is possible that even four ligands could fit into the coordination environment. Notably, all ligand crystals appeared almost clear when washed with cold methanol or petroleum ether, but they exhibited a yellowish or orange hue upon storage in the lab, underscoring the importance of storing the ligands in a glovebox. In addition, the change in color could also occur due to reaction with light, and thus storing the ligand in dark could provide useful. These compounds represent a steppingstone for future research and hold great promise for advancing NacAc lanthanoid compounds as emissive materials.

8 Syntheses

8.1 (*Z*)-4-(mesitylamino)pent-3-en-2-one (27)

Compound **27** was prepared according to the published procedure.[40] A magnetic stirring bar and 10 mL of methanol were added to a 50 mL round-bottom flask. 2.60 mL (25,2 mmol) of acetylacetone was added and after that 3.50 mL (24,9 mmol) of 2,4,6-trimethylmesityl was slowly added. Two drops of formic acid were added as a catalyst. The reaction solution was stirred overnight at the room temperature. The solvent was evaporated by a rotary evaporator and the remaining orange oil was dried under a vacuum. With intense stirring the oil started to solidify which was dissolved in 20 mL petroleum ether. The solution was kept in the freezer over night during which the first crop of yellow crystals formed. The crystals were vacuum filtered and washed with cold petroleum ether to give white crystals. Two more crops of crystals were isolated from the solution using the same procedure. Yield 3.333 g (61 %). ^{1}H NMR ($CDCl_3$; 300 MHz; ppm): 1.62 (3H, s, CH_3), 2.10 (3H, s, CH_3), 2.15 (6H, s, CH_3), 2.28 (3H, s, CH_3), 5.20 (1H, s, CH), 6.89 (2H, s, aromatic), 11.84 (1H, s, NH), (Appendix 1). IR (cm^{-1}): 2918, 1605, 1566, 1298, 1269, 1210, 1186, 1015, 855, 740. EA calcd for $C_{14}H_{19}NO$: C, 77.38; H, 8.81; N, 6.45; O, 7.36. Found: C, 76.18; H, 7.975; N, 6.571.

8.2 (*Z*)-4-((2,6-diisopropylphenyl)amino)pent-3-en-2-one (28)

(*Z*)-4-((2,6-diisopropylphenyl)amino)pent-3-en-2-one **28** was prepared according to the published procedure.[40] 2.60 mL (25,3 mmol) of acetylacetone was added to a 100 mL round-bottom flask charged with a magnetic stirring bar and 40 mL of methanol. To this solution, 5.20 mL (24,8 mmol) of 2,6-diisopropylphenyl was added slowly followed by five drops of formic acid as a catalyst. The reaction solution was refluxed overnight at 85 °C with stirring. After that, the solvent was evaporated by a rotary evaporator and the remaining orange oil was dissolved to 10 mL of petroleum ether. The solution was kept in the freezer overnight but no crystals were obtained. Flask was put into the ethanol-liquid nitrogen bath (-30°C) and stirred hard, but no crystallization occurred. The mixture was thrown away because the ^{1}H NMR did not match to the correct product.. ^{1}H NMR ($CDCl_3$; 300 MHz; ppm): 1.15 (6H, d, CH_3), 1.22

(6H, d, CH_3), 1.28 (6H, d, CH_3), 1.63 (3, s, CH_3), 2.12 (3H, s, CH_3), 3.03 (2H, m, CH), 5.21 (1H, s, CH), 7.18 (2H, d, aromatic), 7.30 (1H, t, aromatic), (Appendix 2).

8.3 (*Z*)-1,1,1,5,5,5-hexafluoro-4-(mesitylamino)pent-3-en-2-one (29)

Z)-1,1,1,5,5,5-hexafluoro-4-(mesitylamino)pent-3-en-2-one **29** was prepared using a synthesis route modified from a literature synthesis of NacNac ligands.[45] A magnetic stirring bar and molecular sieves were added to a 50 mL ampoule. To this ampoule 20 mL of toluene, 4.4 mL (29,9 mmol) of hexafluoroacetylacetone and 4.7 mL (32,7 mmol) of 2,4,6-trimethylmesityl were added with a syringe. The reaction mixture sepatared in two phases. The top one was orange and bottom phase was pink. The reaction mixture was stirred and refluxed in oil bath at 140°C overnight. During the reflux, the solution turned to purple. The solution was allowed to cool to the room temperature after which it was filtered gravimetrically through a filter paper to a 50 mL round-bottom flask. The product was purified with flash distillation. The distillate contained the product and toluene. Toluene was then evaporated to the outer cold trap and remaining orange oily product was dissolved in methanol. The product crystallized out the solution at room temperature overnight. The obtained yellow crystals were vacuum filtered and dissolved in methanol and placed in a freezer to recrystallize. After overnight storage in a freezer the first crop of yellow crystals formed. The crystals were vacuum filtered and washed with cold methanol when they turned almost white. One more crop of crystals was isolated from the solution using the same procedure. Yield 3.8528 g (40 %). ^{1}H NMR ($CDCl_3$; 300 MHz; ppm): 2.18 (6H, s, CH_3), 2.30 (3H, s, CH_3), 6.03 (1H, s, CH), 6.92 (2H, s, aromatic), 11.40 (1H, s, NH), (Appendix 3) ^{19}F NMR ($CDCl_3$; 282 MHz; ppm): -10.60 (3F, s, CF_3), -0.93 (3F, s, CF_3), (Appendix 4). IR (cm^{-1}): 3154, 2925, 1636, 1591, 1360, 1260, 1185, 1149, 1128, 1097, 856.1, 795.3, 730.8, 690.5, 598.1, 564.5. EA calcd for $C_{14}H_{13}F_6NO$: C, 51.70; H, 4.03; F, 35.05; N, 4.31; O, 4.92. Found: C, 51.89; H, 4.00; N, 4.36.

8.4 (*Z*)-4-((2,6-diisopropylphenyl)amino)-1,1,1,5,5,5-hexafluoropent-3-en-2-one (30)

Complex **30** was prepared using the modified literature synthesis.[45] A magnetic stirring bar and about 5 mL of molecular sieves were added to a 50 mL ampoule. To this ampoule 15 mL of toluene, 5.4 mL (27.8 mmol) of 2,6-diisopropylphenyl, and 3.7 mL (25,2 mmol) of hexafluoroacetylacetone were added with a syringe resulting an orange/brown solution which was refluxed in oil bath at 140°C overnight. During the reflux, the solution turned to brown. The solution was allowed to cool to the room temperature after which it was filtered gravimetrically through filter paper to a 50 mL round-bottom flask. The residue was washed with 30 mL of toluene. The combined toluene phases were then evaporated by a rotary evaporator to dryness. The residue was dissolved in 30 mL of methanol. The methanol solution was stored in the freezer overnight during which the first crop of yellow crystals formed. The crystals were vacuum filtered and washed with cold methanol. Three more crops of yellow crystals were isolated from the solution using the same procedure. Unfortunately, the rest of the product fell on the floor which is why the yield was only 0.7186 g (8 %). ^{1}H NMR ($CDCl_3$; 300 MHz; ppm): 1.13 (6H, d, CH_3), 1.26 (6H, d, CH_3), 2.94 (2H, m, CH) 6.04 (1H, s, CH), 7.19 (1H, s, aromatic), 7.21 (1H, s, aromatic), 7.37 (1H, t, aromatic), 11.64 (1H, s, NH), (Appendix 5). ^{19}F NMR ($CDCl_3$; 282 MHz; ppm): -10.50 (3F, s, CF_3), 0.16 (3F, s, CF_3), (Appendix 6).

8.5 Potassium(*Z*)-1,1,1,5,5,5-hexafluoro-4-(mesitylimino)pent-2-en-2-olate (31)

Free ligand **29** (1.3887 g, 4.27 mmol) was weighed to a 100 mL Schlenk tube equipped with a magnetic stirring bar. Crystalline KHMDS (809 mg, 4.05 mmol) was weighed to a separate 100 mL ampoule with a magnetic stirring bar. KHMDS was mixed with 5 mL of hexane and the ligand was dissolved into 20 mL of hexane. Then the ligand was added over the KHMDS in an ice bath while stirring and the reaction was stirred overnight. The pale yellow residue of **31** was filtered and dried under a vacuum. The dried residue was then analyzed by NMR spectroscopy. Attempts were made to crystallize the product from diethyl ether. At first, the product dissolved well in ether, but it soon precipitated out of solution, and more than ten times the original amount of ether had to be added to re-dissolve everything again. However, crystals were not obtained from the dilute solution but after concentrating the solvent to ¼ of the original volume crystallization of **31** did initiate at –20°C. Yield 1,3 g (88 %). ^{1}H NMR (C_6D_6;

300 MHz; ppm): 1.96 (1H, s, CH_3), 2.14 (8H, s, CH_3), 5.13 (1H, s, CH), 6.78 (2H, s, aromatic), (Appendix 9). ^{19}F NMR (C_6D_6; 282 MHz; ppm) -7.45 (3F, s, CF_3) -2.39 (2F, s, CF_3) -0.84 (1F, s, CF_3), (Appendix 10). ^{13}C NMR (C_6D_6; 75.5 MHz; ppm): 17.22, 20.35, 81.80, 119.37, 120.02, 123.19, 123.68, 125.91, 129.17, 132.71, 144.14, 153.96, 154.39, 162.18, 162.55 (Appendix 11) ATR-RTIR (cm^{-1}) 800, 1100, 1150, 1550, 2900. EA calcd for $C_{32}H_{38}F_{12}K_2N_2O_3$: C, 47.75; H, 4.76; F, 28.33; K, 9.72; N, 3.43; O, 5.96. Found: C, 48.42; H, 4.23; N, 3.59.

Product was also made with 0.7 M KHMDS toluene solution, but the KHMDS solution turn out to be impure. 1.1446 g (3.52 mmol) of ligand (29) was weighed to a 100 mL ampoule charged with a magnetic stirring bar. 15 mL of hexane and 4.7 mL (3.3 mmol 0.7 M) of KHMDS solution was added to the ampoule with a syringe. The yellow mixture was stirred overnight. The white residue of **31** was filtered and washed with 10 mL of hexane. Product was vacuum dried with external cold trap and ^1H and ^{19}F NMR were measured in toluene (Appendices 7 and 8).

8.6 Potassium (*Z*)-4-(mesitylimino)pent-2-en-2-olate (32)

Reaction with the KHMDS solution: 1.19 g (5.48 mmol) of ligand **27** was weighed to a 50 mL Schlenk flask charged with magnetic stirring bar. 15 mL of hexane and 7.43 mL (5.20 mmol) of 0,7 M KHMDS solution was added to the Schlenk flask with a syringe resulting in a yellow solution. After 10 minutes of stirring white solids started to precipitate out of the solution, but the reaction mixture was stirred overnight to complete the reaction. The solution was filtered, and the remaining white solids of **32** were washed with 5 mL hexane and dried under a vacuum yielding 900 mg (64 %) of product. ^1H NMR is presented in Appendix 12.

Reaction with crystalline KHMDS: 1.8804g (8.65 mmol) of ligand **27** was weighed to a 100 mL Schlenk flask and a magnetic stirring bar was put in the flask. 1.644g (8.22 mmol) of crystalline KHMDS was weighed to a 50 mL ampoule and magnetic stirring bar was added to the ampoule. First, **27** was dissolved into 8 mL of hexane, stirred for 10 minutes, and vacuum dried to get methanol out of the crystal structure. Then 25 mL of hexane was added as a solvent. KHMDS was dissolved in 10 mL of toluene and added over **27** in an ice bath. The reaction was stirred overnight. The yellow solution was filtered, and the remaining white solids were dried

under a vacuum. The filtrate was concentrated to 2 mL under a vacuum, and then 20 mL of hexane was added to precipitate out more white solids. The second crop was also isolated by the filtration and dried under a vacuum. Yield 1.3g (62 %). ^{1}H NMR (Toluene-d_8; 300 MHz; ppm): 1.32 (3H, s, CH_3), 1.55 (3H, s, CH_3), 2.01 (6H, s, CH_3), 2.24 (3H, s, CH_3), 4.70 (1H, s, CH), 6.79 (2H, s, aromatic) (Appendix 13). ^{13}C NMR (C_6D_6; 75.5 MHz; ppm): 18.32, 20.48, 22.20, 28.41, 94.18, 128.91, 129.77, 149.14, 165.44, 178.53 (Appendix 14). IR (cm^{-1}): 2909, 1588, 1462, 1416, 1222, 1192, 1146, 998.6, 921.3, 852.0, 789.7, 737.5, 641.0, 530.6. EA calcd for $C_{14}H_{18}KNO$: C, 65.84; H, 7.10; K, 15.31; N, 5.48; O, 6.26. Found: C, 66.62; H, 7.433; N, 5.422.

8.7 Potassium (Z)-4-((2,6-diisopropylphenyl)imino)-1,1,1,5,5,5-hexafluoropent-2-en-2-olate (33)

Free ligand **30** (1.232 g, 3.35 mmol) was weighed to a 50 mL two-neck round-bottom flask and vacuum dried on Schlenk line. 20 mL of hexane was added with a syringe followed by 4.8 mL (3.36 mmol 0.7 M) of KHMDS. A pale yellow reaction mixture was stirred for 48 h. The solution mixture was filtered leaving a light-colored solid residue of **33**. The solids were washed with 10 mL of hexane and then dried under a vacuum. Yield 900 mg (66 %). ^{1}H NMR (THF-d8; 300MHz; ppm): 1.08 (12H, q, CH_3), 2.83 (2H, m, CH), 4.39 (1H, s, CH), 6.85 (1H, t, aromatic), 6.99 (2H, d, aromatic). ^{19}F NMR (THF-d_8; 282 MHz; ppm): -8.53 (3F, s, CF_3), -2.99 (3F, s, CF_3). NMR spectra are presented in Appendices 15-18.

8.8 Tris(4-((2,6-diisopropylphenyl)imino)-1,1,1,5,5,5-hexafluoropent-2-en-2-olato)-yttrium (34)

34 was synthesized by 3:1 reaction between **33** and $[YI_2THF_4][YI_4THF_2]$ in THF-d_8. 20 mg (0.049 mmol) of **33** and 13 mg (0.009 mmol) of $[YI_2THF_4][YI_4THF_2]$ were weighed into an NMR tube and dissolved in 0.6 mL of THF-d_8. The reaction produced bright yellow solution and white residue of potassium iodide on the bottom of the NMR tube. ^{1}H NMR (THF-d_8; 300MHz; ppm): 1.09 (14H, m, CH_3), 2.67 (2H, m, CH), 4.94 (1H, m, CH), 7.02 (1H, m, aromatic), 7.09 (2H, m, aromatic) (Appendix 19). ^{19}F NMR (THF-d8; 282 MHz; ppm): -11.51

(1F, s, CF_3), -6.46 (3F, m, CF_3), -0.20 (1F, s, CF_3) (Appendix 20).

8.9 Tris(4-(mesitylimino)pent-2-en-2-olato)-yttrium (35)

Potassium salt **32** (587 mg, 2.30 mmol) was weighed to a 100 mL Schlenk tube charged with a magnetic stirring bar. Next 544 mg (0.377 mmol) of $[YI_2THF_4][YI_4THF_2]$ was weighed to a 100 mL ampoule charged with a magnetic stirring bar. The potassium salt was dissolved into 25 mL of diethyl ether and 2 mL of diethyl ether was added to the yttrium iodide ampoule. Potassium salt was added to $[YI_2THF_4][YI_4THF_2]$ in dry ice bath and reaction was stirred overnight. The reaction was refluxed at 36°C for 3h and after that the solid potassium iodide was separated from the liquid by filtration. The solution of **35** was vacuum dried resulting in yellow micro crystals with yield of 347 mg. The NMR and IR spectra of product were measured. Crystallization of the product from heptane was tried with 50 mg of material but the yielded only 1 mg of crystals. The rest of the product was used for crystallization from Et_2O but only 9 mg of crystals were obtained. NMR of crystals were measured in benzene. The reaction was also done in toluene using the same procedure, but in toluene the reaction was refluxed 2 days and then stirred 1 day without heat, instead of just refluxing it 3 h in diethyl ether. ^{1}H NMR (Toluene-d_8; 300 MHz; ppm): 1.39 (3H, s, CH_3), 1.56 (3H, s, CH_3), 1.98 (6H, s, CH_3), 2.20 (3H, s, CH_3), 4.95 (1H, s, CH), 6.73 (2H, s, aromatic). IR (cm^{-1}): 2915, 2856, 1567, 1503, 1396, 1256, 1229, 1195, 1146, 1010, 936.2, 850.9, 761.3, 587.7, 480.4. NMR spectra are presented in Appendices 21-23.

8.10 NMR scale reaction of tris(1,1,1,5,5,5-hexafluoro-4-(mesitylimino)pent-2-en-2-olato)-yttrium (36)

In the 3:1 NMR scale reaction, 16 mg (0.044 mmol) of **31** was weighed into an NMR tube and 10.5 mg (0.0072 mmol) of $[YI_2THF_4][YI_4THF_2]$ was added. The reagents were dissolved in 0,6 mL of C_6D_6 resulting in yellow solution of **36** and white residue of potassium iodide. Reaction was refluxed overnight at 89°C during which the solution turned brown. ^{1}H NMR was measured in benzene after the addition of $[YI_2THF_4][YI_4THF_2]$, after one hour of the

reaction and after one night of refluxing the reaction. ^{1}H NMR (C_6D_6; 300 MHz; ppm): 2.00 (6H, m, CH_3), 2.24 (3H, s, CH_3), 6.27 (1H, m, CH), 6.66 (2H, m, aromatic) (Appendix 24). ^{19}F NMR (C_6D_6 ; 282 MHz; ppm): -10.36 (0.2F, s, CF_3), -7.78 (3F, m, CF_3), -6.04 (0.2F, s, CF_3), -2.94 (1F, s, CF_3), -0.91 (1F, s, CF_3), 0.72 (15F, m, CF_3) (Appendix 25).

8.11 Larger scale reaction of tris(1,1,1,5,5,5-hexafluoro-4-(mesitylimino)pent-2-en-2-olato)-yttrium (37)

Potassium salt **31** (407 mg, 1.026 mmol) was weighted to a 100 mL Schlenk tube with magnetic stirring bar. $[YI_2THF_4][YI_4THF_2]$ (234 mg, 0,162 mmol) was weighted to a 100 mL ampoule charged with magnetic stirring bar. The potassium salt was dissolved into 30 mL of diethyl ether and 5 mL of diethyl ether was added to $[YI_2THF_4][YI_4THF_2]$. The potassium salt was added slowly into the diethyl ether solution of $[YI_2THF_4][YI_4THF_2]$ in cold (-78°C). Reaction was stirred overnight and then refluxed 3 h at 36°C. The yellow solution was filtered to get rid of solid potassium iodide and then the solution was concentrated and taken to freezer for crystallization. White powder of potassium iodide was characterized by IR and thrown away. Crystals were not obtained from the freezer, so the solution was dried under a vacuum. A fluffy yellow product was obtained and according to NMR the product was impure. It was then stored in a glovebox and weighed to be 220 mg. ^{1}H NMR (C_6D_6; 300 MHz; ppm): 1.97 (6H, m, CH_3), 2.11 (3H, s, CH_3), 6.27 (1H, s, CH), 6.67 (2H, s, aromatic) (Appendix 26). ^{19}F NMR (C_6D_6 ; 282 MHz; ppm): -10.37 (0.2F, s, CF_3), -7.85 (2F, m, CF_3), -6.09 (1F, s, CF_3), -2.98 (1F, s, CF_3), -0.99 (0.2F, s, CF_3), 0.52 (3F, m, CF_3) (Appendix 27).

References

1. Brites, C. D. S.; Balabhadra, S. ja Carlos, L. D., Lanthanide-Based Thermometers: At the Cutting-Edge of Luminescence Thermometry, *Adv. Opt. Mater.*, **2019**, *7*, 1–30.
2. Werts, M. H. V., Making sense of lanthanide luminescence., *Sci. Prog.*, **2005**, *88*, 101–131.
3. Zeng, Y.; Qiu, B.; Wang, F. F.; Zhou, L. ja Li, Y., Transparent films based on functionalized Poly(ionic liquids) coordinating to photoactive Lanthanide(Eu^{3+},Tb^{3+})

and Poly(methyl methacrylate): Luminescence and chemical sensing, *Opt. Mater. (Amst).*, **2020**, *107*, 110149.

4. Marin, R.; Brunet, G. ja Murugesu, M., Shining New Light on Multifunctional Lanthanide Single-Molecule Magnets, *Angew. Chemie - Int. Ed.*, **2021**, *60*, 1728–1746.
5. Duward Shriver, Mark Weller, Tina Overton, Jonathan Rourke, F. A., *Inorganic Chemistry. 6th edition. Oxford university press, 2014. pp. 626-643*.
6. Errulat, D.; Marin, R.; Gálico, D. A.; Harriman, K. L. M.; Pialat, A.; Gabidullin, B.; Iikawa, F.; Couto, O. D. D.; Moilanen, J. O.; Hemmer, E.; Sigoli, F. A. ja Murugesu, M., A Luminescent Thermometer Exhibiting Slow Relaxation of the Magnetization: Toward Self-Monitored Building Blocks for Next-Generation Optomagnetic Devices, *ACS Cent. Sci.*, **2019**, *5*, 1187–1198.
7. Binnemans, K., Lanthanide-based luminescent hybrid materials, *Chem. Rev.*, **2009**, *109*, 4283–4374.
8. Nehra, K.; Dalal, A.; Hooda, A.; Bhagwan, S.; Saini, R. K.; Mari, B.; Kumar, S. ja Singh, D., Lanthanides β-diketonate complexes as energy-efficient emissive materials: A review, *J. Mol. Struct.*, **2022**, *1249*, 131531.
9. Andres, J. ja Chauvin, A., Luminescence, David A. Atwood. (ed.), *The Rare Earth Elements*, John Wiley & Sons Ltd, The Atrium, Southern Gate, Chichester, West Sussex, United Kingdom, 2012.
10. Youssef, A. O., A highly selective and sensitive Tb^{3+}-acetylacetone photo probe for the assessment of acetazolamide in pharmaceutical and serum samples, *Spectrochim. Acta - Part A Mol. Biomol. Spectrosc.*, **2018**, *195*, 47–52.
11. Anderson, B. R.; Gunawidjaja, R. ja Eilers, H., Soluble Sm-based ternary complexes for non-contact molecular thermometry, *J. Lumin.*, **2018**, *204*, 341–348.
12. Wang, X. D.; Wolfbeis, O. S. ja Meier, R. J., Luminescent probes and sensors for temperature, *Chem. Soc. Rev.*, **2013**, *42*, 7834–7869.
13. Vanden Bussche, F.; Kaczmarek, A. M.; Veerapandian, S. K. P.; Everaert, J.; Debruyne, M.; Abednatanzi, S.; Morent, R.; De Geyter, N.; Van Speybroeck, V.; Van Der Voort, P. ja Stevens, C. V., N-Rich Porous Polymer with Isolated Tb3+-Ions Displays Unique Temperature Dependent Behavior through the Absence of Thermal Quenching, *Chem. Eur. J.*, **2020**, *26*, 15596–15604.
14. Zheng, K.; Ding, L. W. ja Zeng, C. H., Highly luminescent lanthanide complexes constructed by Bis-tridentate ligand and as sensor for Et_2O, *Inorg. Chem. Commun.*, **2018**, *95*, 95–99.

15. Xia, Q.; Cui, Y.; Yuan, D.; Wang, Y. ja Yao, Y., Synthesis and characterization of lanthanide complexes stabilized by N-aryl substituted β-ketoiminato ligands and their application in the polymerization of rac-lactide, *J. Organomet. Chem.*, **2017**, *846*, 161–168.
16. Peng, H.; Zhang, Z.; Qi, R.; Yao, Y.; Zhang, Y.; Shen, Q. ja Cheng, Y., Synthesis, reactivity, and characterization of sodium and rare-earth metal complexes bearing a dianionic N-aryloxo-functionalized β-ketoiminate ligand, *Inorg. Chem.*, **2008**, *47*, 9828–9835.
17. Sukhikh, T. S.; Ogienko, D. S.; Bashirov, D. A. ja Konchenkoa, S. N., Luminescent complexes of 2,1,3-benzothiadiazole derivatives, *Russ. Chem. Bull.*, **2019**, *68*, 651–661.
18. Bellusci, A.; Barberio, G.; Crispini, A.; Ghedini, M.; La Deda, M. ja Pucci, D., Synthesis and luminescent properties of novel lanthanide(III) β-diketone complexes with nitrogen p,p′-disubstituted aromatic ligands, *Inorg. Chem.*, **2005**, *44*, 1818–1825.
19. Belot, J. A.; Wang, A.; McNeely, R. J.; Liable-Sands, L.; Rheingold, A. L. ja Marks, T. J., Highly volatile, low-melting, fluorine-free precursors for MOCVD of lanthanide oxide-containing thin films, *Chem. Vap. Depos.*, **1999**, *5*, 65–69.
20. Eliseeva, S. V. ja Bünzli, J. C. G., Lanthanide luminescence for functional materials and bio-sciences, *Chem. Soc. Rev.*, **2010**, *39*, 189–227.
21. Moore, E. G.; Samuel, A. P. S. ja Raymond, K. N., From antenna to assay: lessons learned in lanthanide luminescence, *Acc. Chem. Res.*, **2009**, *42*, 542–552.
22. Hughes, I. D.; Däne, M.; Ernst, A.; Hergert, W.; Lüders, M.; Poulter, J.; Staunton, J. B.; Svane, A.; Szotek, Z. ja Temmerman, W. M., Lanthanide contraction and magnetism in the heavy rare earth elements, *Nature*, **2007**, *446*, 650–653.
23. Ferreira, R. A. S.; Mamontova, E.; Botas, A. M. P.; Shestakov, M.; Vanacken, J.; Moshchalkov, V.; Guari, Y.; Chibotaru, L. F.; Luneau, D.; André, P. S.; Larionova, J.; Long, J. ja Carlos, L. D., Synchronous Temperature and Magnetic Field Dual-Sensing by Luminescence in a Dysprosium Single-Molecule Magnet, *Adv. Opt. Mater.*, **2021**, *9*, 1–8.
24. Arrué, L.; Santoyo-Flores, J.; Pizarro, N.; Zarate, X.; Páez-Hernández, D. ja Schott, E., The role played by structural and energy parameters of β-Diketones derivatives as antenna ligands in Eu(III) complexes, *Chem. Phys. Lett.*, **2021**, *773*.
25. Hasegawa, M.; Ohmagari, H.; Tanaka, H. ja Machida, K., Luminescence of lanthanide complexes: From fundamental to prospective approaches related to water- and

molecular-stimuli, *J. Photochem. Photobiol. C Photochem. Rev.*, **2022**, *50*, 100484.

26. Parker, D.; Fradgley, J. D. ja Wong, K. L., The design of responsive luminescent lanthanide probes and sensors, *Chem. Soc. Rev.*, **2021**, *50*, 8193–8213.
27. Wang, L.; Zhao, Z.; Wei, C.; Wei, H.; Liu, Z.; Bian, Z. ja Huang, C., Review on the Electroluminescence Study of Lanthanide Complexes, *Adv. Opt. Mater.*, **2019**, *7*, 1–49.
28. Ferreira Da Rosa, P. P.; Miyazaki, S.; Sakamoto, H.; Kitagawa, Y.; Miyata, K.; Akama, T.; Kobayashi, M.; Fushimi, K.; Onda, K.; Taketsugu, T. ja Hasegawa, Y., Coordination Geometrical Effect on Ligand-to-Metal Charge Transfer-Dependent Energy Transfer Processes of Luminescent Eu(III) Complexes, *J. Phys. Chem. A*, **2021**, *125*, 209–217.
29. Bukvetskii, B. V.; Mirochnik, A. G. ja Shishov, A. S., Triboluminescence and crystal structure of centrosymmetric complex Tb(AcAc)3Phen, *J. Lumin.*, **2018**, *195*, 44–48.
30. Ilmi, R.; Khan, M. S.; Sun, W.; Zhou, L.; Wong, W. Y. ja Raithby, P. R., A single component white electroluminescent device fabricated from a metallo-organic terbium complex, *J. Mater. Chem. C*, **2019**, *7*, 13966–13975.
31. Wong, H. Y.; Ting, W.; Chan, K. ja Law, G. L., Triboluminescence of centrosymmetric lanthanide β-diketonate complexes with aggregation-induced emission, *Molecules*, **2019**, *24*.
32. Wong, H. Y.; Lo, W. S.; Chan, W. T. K. ja Law, G. L., Mechanistic Investigation of Inducing Triboluminescence in Lanthanide(III) β-Diketonate Complexes, *Inorg. Chem.*, **2017**, *56*, 5135–5140.
33. Monteiro, J. H. S. K. ja De Bettencourt-Dias, A., Lanthanide ion emission in multicolor OLEDs (Ce^{3+}, Pr^{3+}, Tb^{3+}, Dy^{3+}, Tm^{3+}, and white light Eu^{3+}/Tb^{3+} hybrid systems) and device characterization, Martin-Ramos, P. and Ramos-Silva, M. (eds.), *Lanthanide-Based Multifunctional Materials: From OLEDs to SIMs*, Elsevier Inc., 2018.
34. Zucchi, G.; Jeon, T.; Tondelier, D.; Aldakov, D.; Thuéry, P.; Ephritikhine, M. ja Geffroy, B., White electroluminescence of lanthanide complexes resulting from exciplex formation, *J. Mater. Chem.*, **2010**, *20*, 2114–2120.
35. Dorenbos, P. ja Bos, A. J. J., Lanthanide level location and related thermoluminescence phenomena, *Radiat. Meas.*, **2008**, *43*, 139–145.
36. Weissman, S. I., Intramolecular energy transfer the fluorescence of complexes of Europium, *J. Chem. Phys.*, **1942**, *10*, 214–217.

37. Gálico, D. A.; Marin, R.; Brunet, G.; Errulat, D.; Hemmer, E.; Sigoli, F. A.; Moilanen, J. O. ja Murugesu, M., Triplet-State Position and Crystal-Field Tuning in Opto-Magnetic Lanthanide Complexes: Two Sides of the Same Coin, *Chem. - A Eur. J.*, **2019**, *25*, 14625–14637.

38. Borges, A. S.; Caliman, E. V.; Dutra, J. D. L.; Da Silva, J. G. ja Araujo, M. H., Structure and luminescent investigation of new Ln(III)-TTA complexes containing N-methyl-ε-caprolactam as ligand, *J. Lumin.*, **2016**, *170*, 654–662.

39. Kasprzycka, E.; Trush, V. A.; Amirkhanov, V. M.; Jerzykiewicz, L.; Malta, O. L.; Legendziewicz, J. ja Gawryszewska, P., Contribution of Energy Transfer from the Singlet State to the Sensitization of Eu3+and Tb3+Luminescence by Sulfonylamidophosphates, *Chem. - A Eur. J.*, **2017**, *23*, 1318–1330.

40. Lin, T. H.; Das, K.; Datta, A.; Leu, W. J.; Hsiao, H. C.; Lin, C. H.; Guh, J. H. ja Huang, J. H., Synthesis and characterization of ruthenium compounds incorporating keto-amine ligands. The applications of catalytic transfer hydrogenation and cancer cell inhibition, *J. Organomet. Chem.*, **2016**, *807*, 22–28.

41. Rees, W. S.; Just, O.; Castro, S. L. ja Matthews, J. S., Synthesis and magnetic and structural characterization of the first homoleptic lanthanide β-ketoiminate, *Inorg. Chem.*, **2000**, *39*, 3736–3737.

42. Ilmi, R.; Khan, M. S.; Li, Z.; Zhou, L.; Wong, W. Y.; Marken, F. ja Raithby, P. R., Utilization of Ternary Europium Complex for Organic Electroluminescent Devices and as a Sensitizer to Improve Electroluminescence of Red-Emitting Iridium Complex, *Inorg. Chem.*, **2019**, *58*, 8316–8331.

43. Mara, M. W.; Tatum, D. S.; March, A. M.; Doumy, G.; Moore, E. G. ja Raymond, K. N., Energy Transfer from Antenna Ligand to Europium(III) Followed Using Ultrafast Optical and X-ray Spectroscopy, *J. Am. Chem. Soc.*, **2019**, *141*, 11071–11081.

44. Räsänen, M., *ENERGY TRANSFER IN LUMINESCENT LANTHANOID CHELATES*, Painosalama Oy, Turku, Finland 2020, Ph.D. thesis, University of Turku, Faculty of Science and Engineering, Department of Chemistry, Turku 2020.

45. Carey, D. T.; Cope-Eatough, E. K.; Vilaplana-Mafé, E.; Mair, F. S.; Pritchard, R. G.; Warren, J. E. ja Woods, R. J., Structures and reactions of monomeric and dimeric lithium diazapentadienyl complexes with electrophiles: Synthesis of α-C,C′-dialkyl-β-diimines, and dissolution-reversible synthesis of an α-alkoxylithium- β-diimine, *Dalt. Trans.*, **2003**, 1083–1093.

46. Kitos, A. A.; Gálico, D. A.; Castañeda, R.; Ovens, J. S.; Murugesu, M. ja Brusso, J. L.,

Stark Sublevel-Based Thermometry with Tb(III) and Dy(III) Complexes Cosensitized via the 2-Amidinopyridine Ligand, *Inorg. Chem.*, **2020**, *59*, 11061–11070.

47. Lin, L.; Li, Z.; Wang, Z.; Feng, Z.; Huang, F.; Dai, Q. ja Zheng, Z., Hypersensitive and color-tunable temperature sensing properties of (Eu,Tb)$(AcAc)_3$phen via phonon-assisted energy transfer, *Opt. Mater. (Amst).*, **2020**, *110*, 110532.
48. Kocifaj, M.; Kundracik, F. ja Bilý, O., Emission spectra of light-pollution sources determined from the light-scattering spectrometry of the night sky, *Mon. Not. R. Astron. Soc.*, **2020**, *491*, 5586–5594.
49. Faridbod, F.; Ganjali, M. R. ja Hosseini, M., Lanthanide materials as chemosensors, Martin-Ramos, P. and Ramos-Silva, M. (eds.), *Lanthanide-Based Multifunctional Materials: From OLEDs to SIMs*, Elsevier Inc., 2018.
50. Ilmi, R.; Zhang, D.; Tensi, L.; Al-Sharji, H.; Al Rasbi, N. K.; Macchioni, A.; Zhou, L.; Wong, W. Y.; Raithby, P. R. ja Khan, M. S., Salts of Lanthanide(III) Hexafluoroacetylacetonates [Ln = Sm(III), Eu(III) and Tb(III)] with Dipyridylammonium cations: Synthesis, characterization, photophysical properties and OLED fabrication, *Dye. Pigment.*, **2022**, *203*, 110300.
51. Zaldo, C., Lanthanide-based luminescent thermosensors: From bulk to nanoscale, Martin-Ramos, P. and Ramos-Silva, M. (eds.), *Lanthanide-Based Multifunctional Materials: From OLEDs to SIMs*, Elsevier Inc., 2018.
52. Marin, R.; Millan, N. C.; Kelly, L.; Liu, N.; Rodrigues, E. M.; Murugesu, M. ja Hemmer, E., Luminescence thermometry using sprayed films of metal complexes, *J. Mater. Chem. C*, **2022**, *10*, 1767–1775.
53. Hasegawa, Y. ja Kitagawa, Y., Luminescent lanthanide coordination polymers with transformative energy transfer processes for physical and chemical sensing applications, *J. Photochem. Photobiol. C Photochem. Rev.*, **2022**, *51*, 100485.
54. Li, X.; Chen, H.; Kirillov, A. M.; Xie, Y.; Shan, C.; Wang, B.; Shi, C. ja Tang, Y., A paper-based lanthanide smart device for acid-base vapour detection, anti-counterfeiting and logic operations, *Inorg. Chem. Front.*, **2016**, *3*, 1014–1020.
55. Ferreira da Rosa, P. P.; Kitagawa, Y. ja Hasegawa, Y., Luminescent lanthanide complex with seven-coordination geometry, *Coord. Chem. Rev.*, **2020**, *406*, 213153.
56. Vitanova, D. V.; Hampel, F. ja Hultzsch, K. C., Rare earth metal complexes based on β-diketiminato and novel linked bis(β-diketiminato) ligands: Synthesis, structural characterization and catalytic application in epoxide/CO2-copolymerization, *J. Organomet. Chem.*, **2005**, *690*, 5182–5197.

57. Singh, A. ja Mehrotra, R. C., Synthesis and Characterization of Volatile, Fluorine Free β-Ketoiminate Lanthanide MOCVD Precursors and Their Implementation in Low-Temperature Growth of Epitaxial CeO_2 Buffer Layers for Superconducting Electronics, *Chemtracts*, **2003**, *16*, 743–748.
58. Sukhikh, T. S.; Ogienko, D. S.; Bashirov, D. A.; Kurat'eva, N. V.; Smolentsev, A. I. ja Konchenko, S. N., Samarium, Europium, and Gadolinium Complexes with 4-(2,1,3-Benzothiadiazol-4-ylamino)pent-3-en-2-onate, *Russ. J. Coord. Chem.*, **2019**, *45*, 30–35.
59. Duward Shriver, Mark Weller, Tina Overton, Jonathan Rourke, F. A., *Inorganic Chemistry. 6th edition. Oxford university press, 2014. pp. 210-231*, **2014**, 1–3.

Appendices

APPENDIX 1. The ^{1}H NMR spectrum of **27**

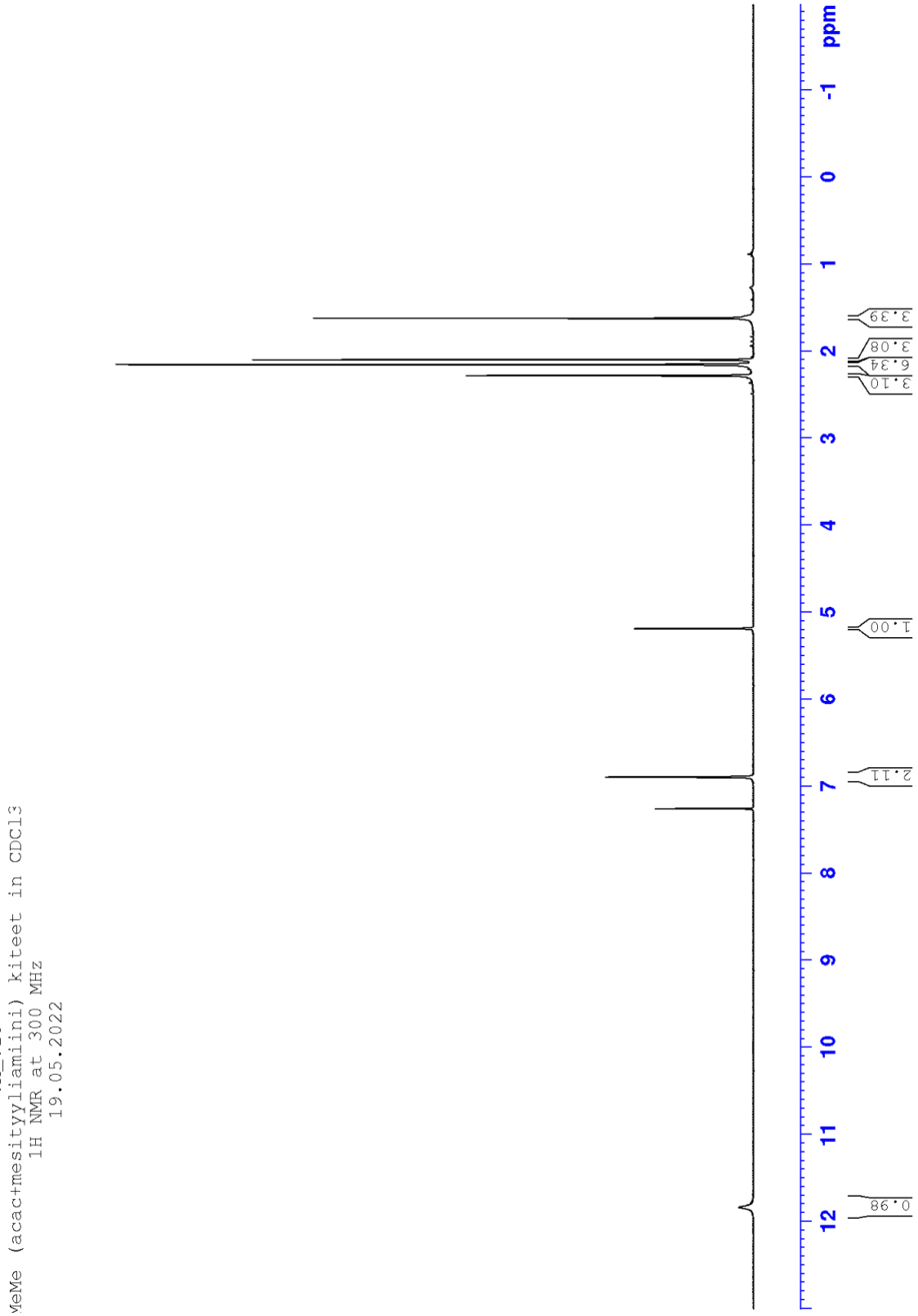

APPENDIX 2. The ^{1}H NMR spectrum of **28**

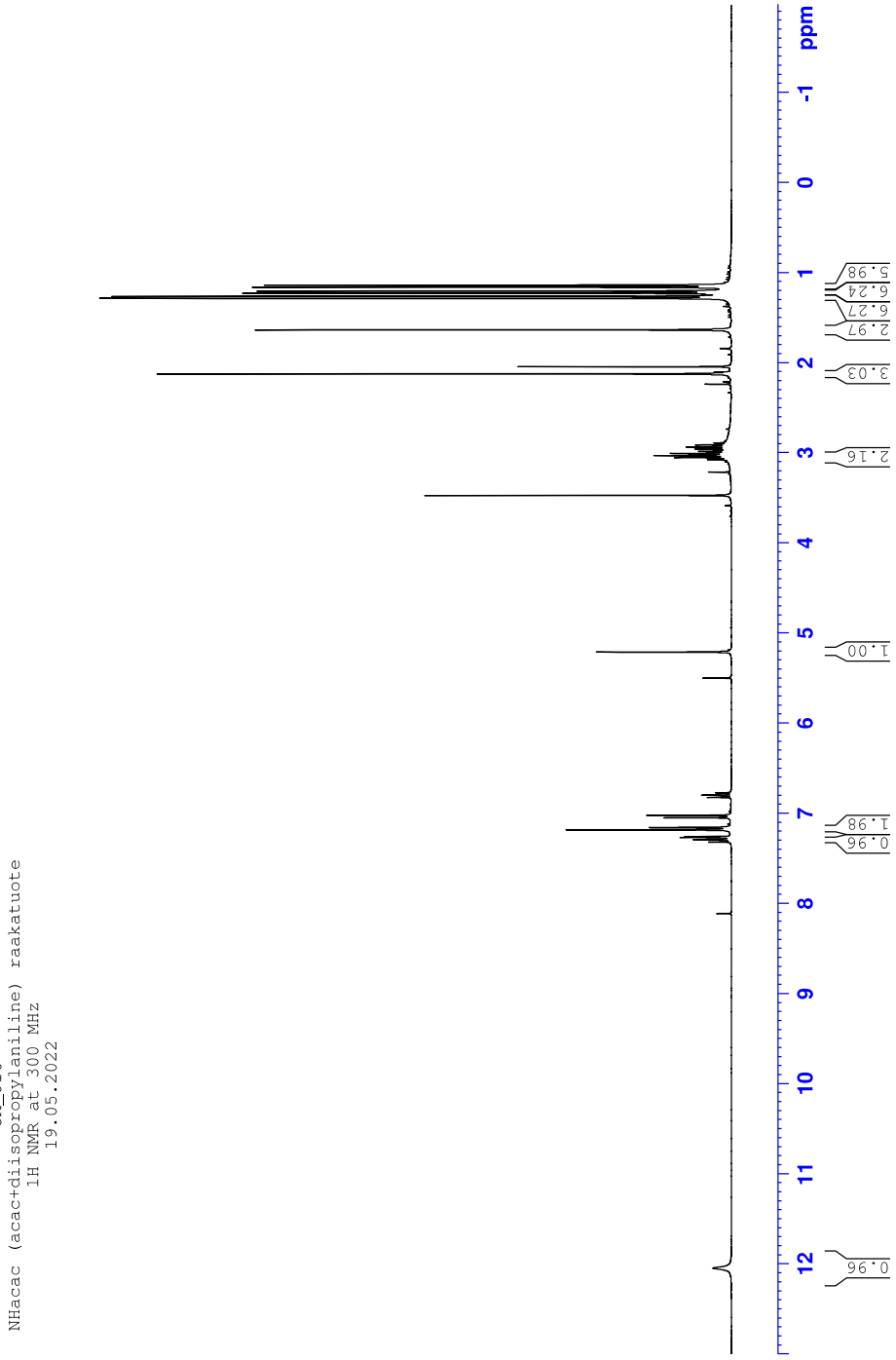

APPENDIX 3. The ^{1}H NMR spectrum of **29**

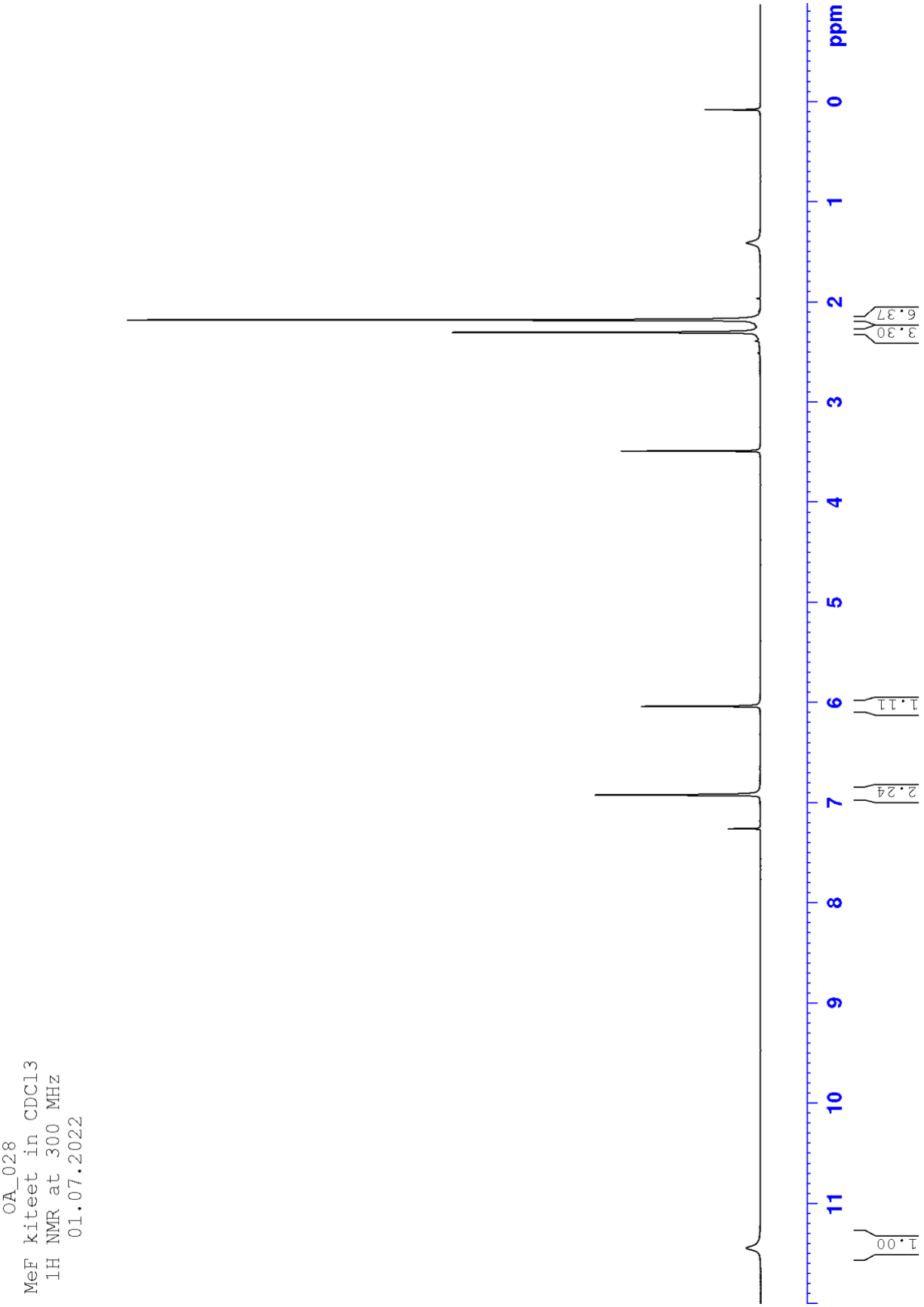

APPENDIX 4. The ^{19}F NMR spectrum of **29**

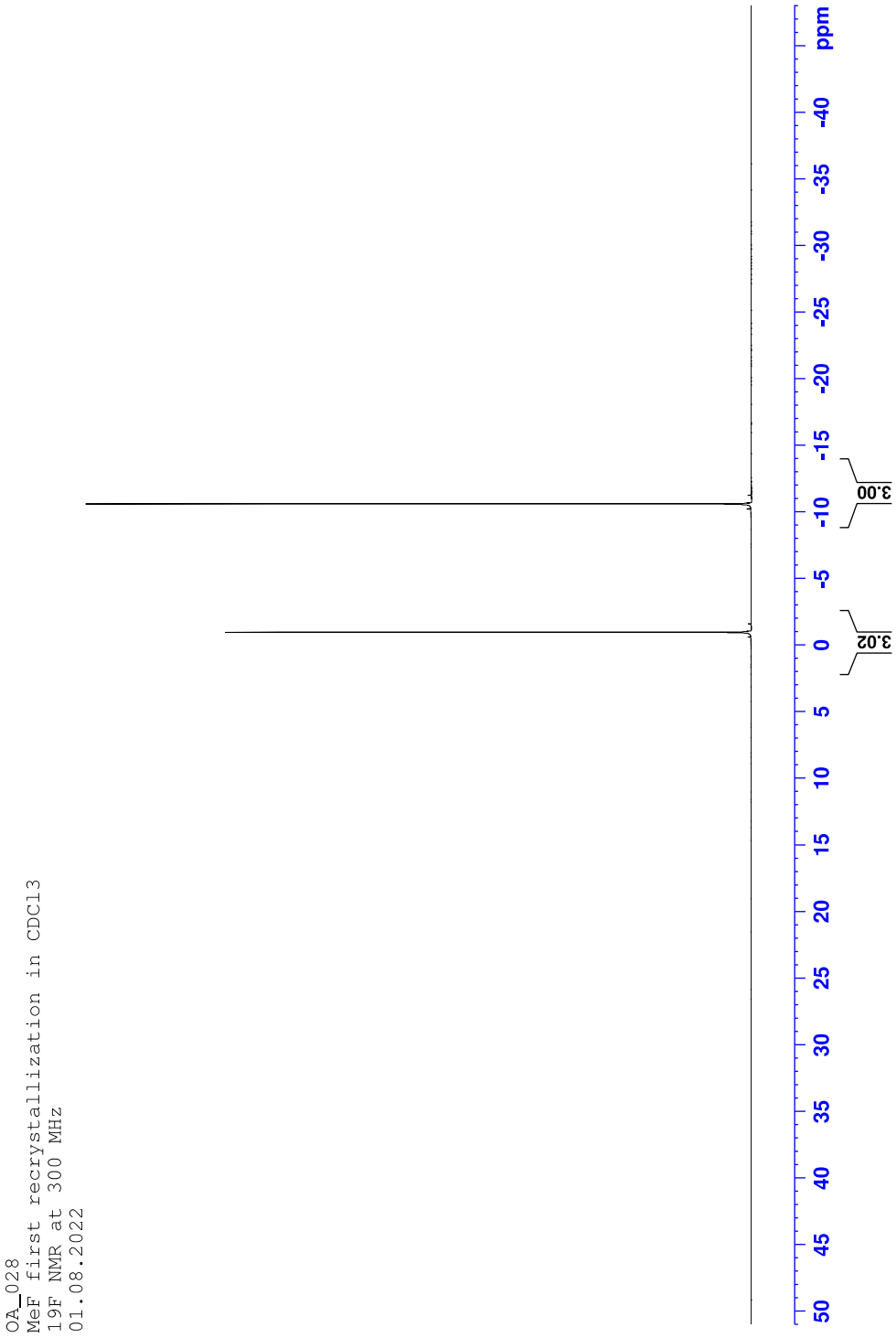

APPENDIX 5. The ^{1}H NMR spectrum of **30**

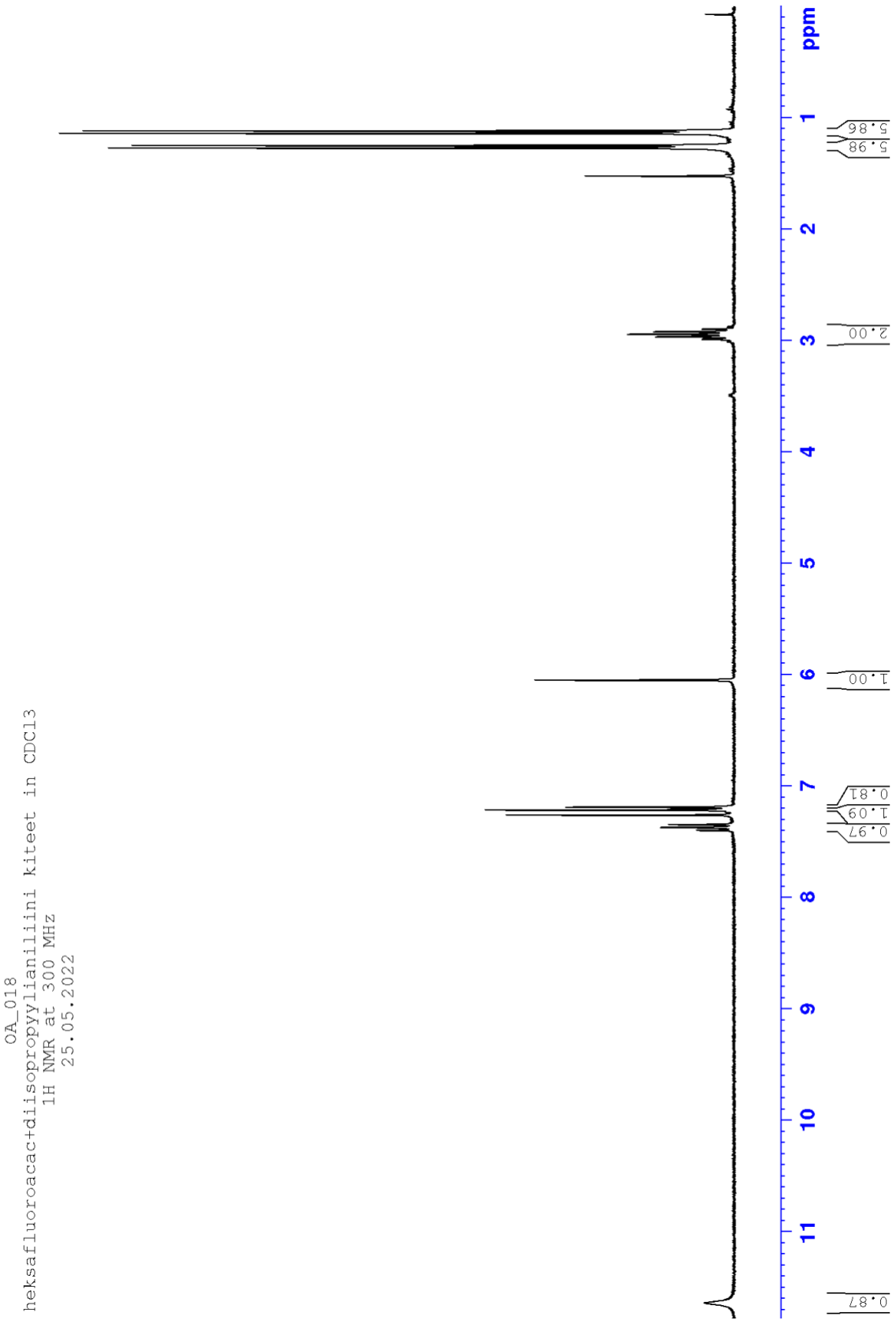

APPENDIX 6. The ^{19}F NMR spectrum of **30**

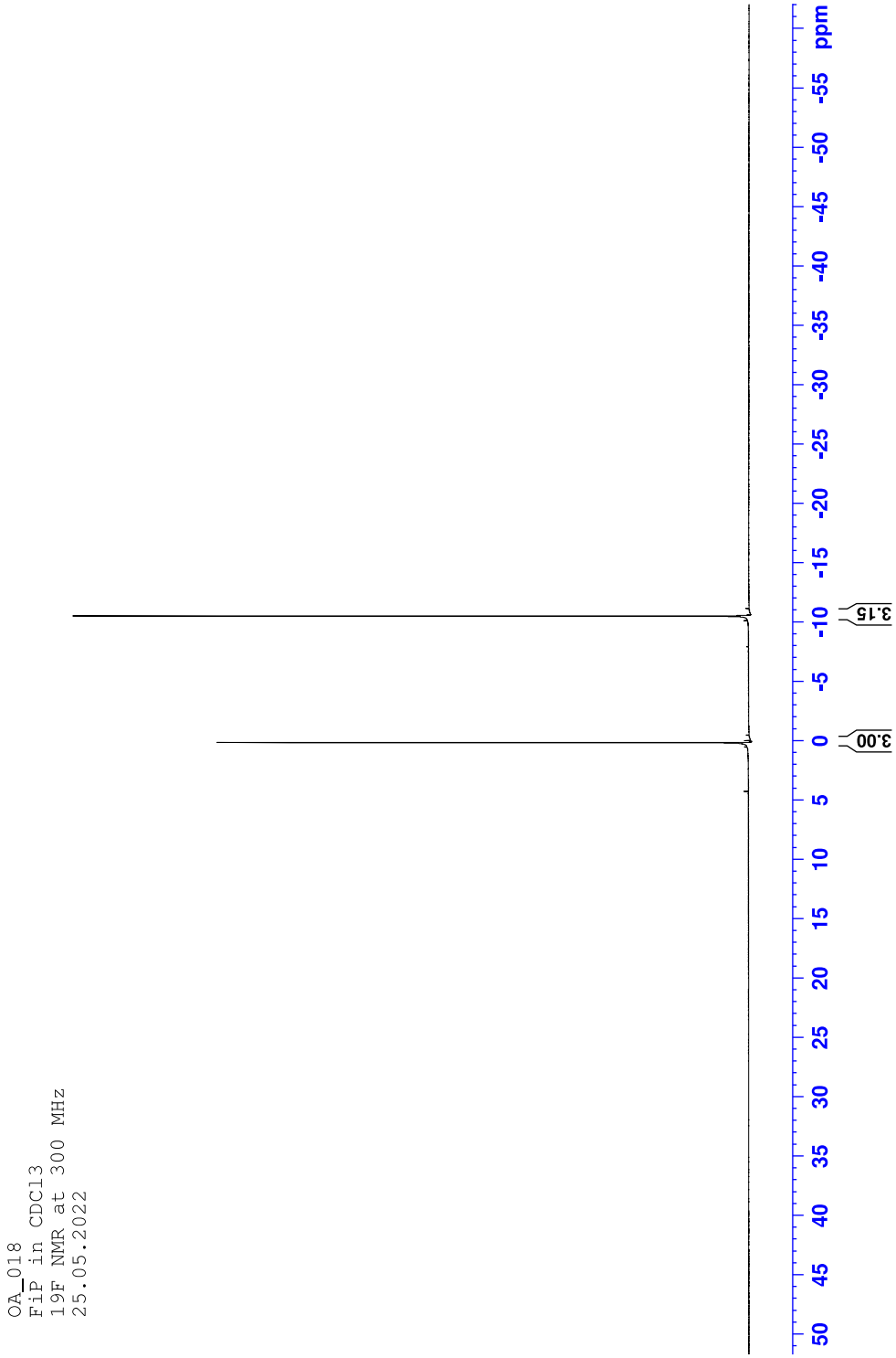

APPENDIX 7. The ^{1}H NMR spectrum of **31** in toluene

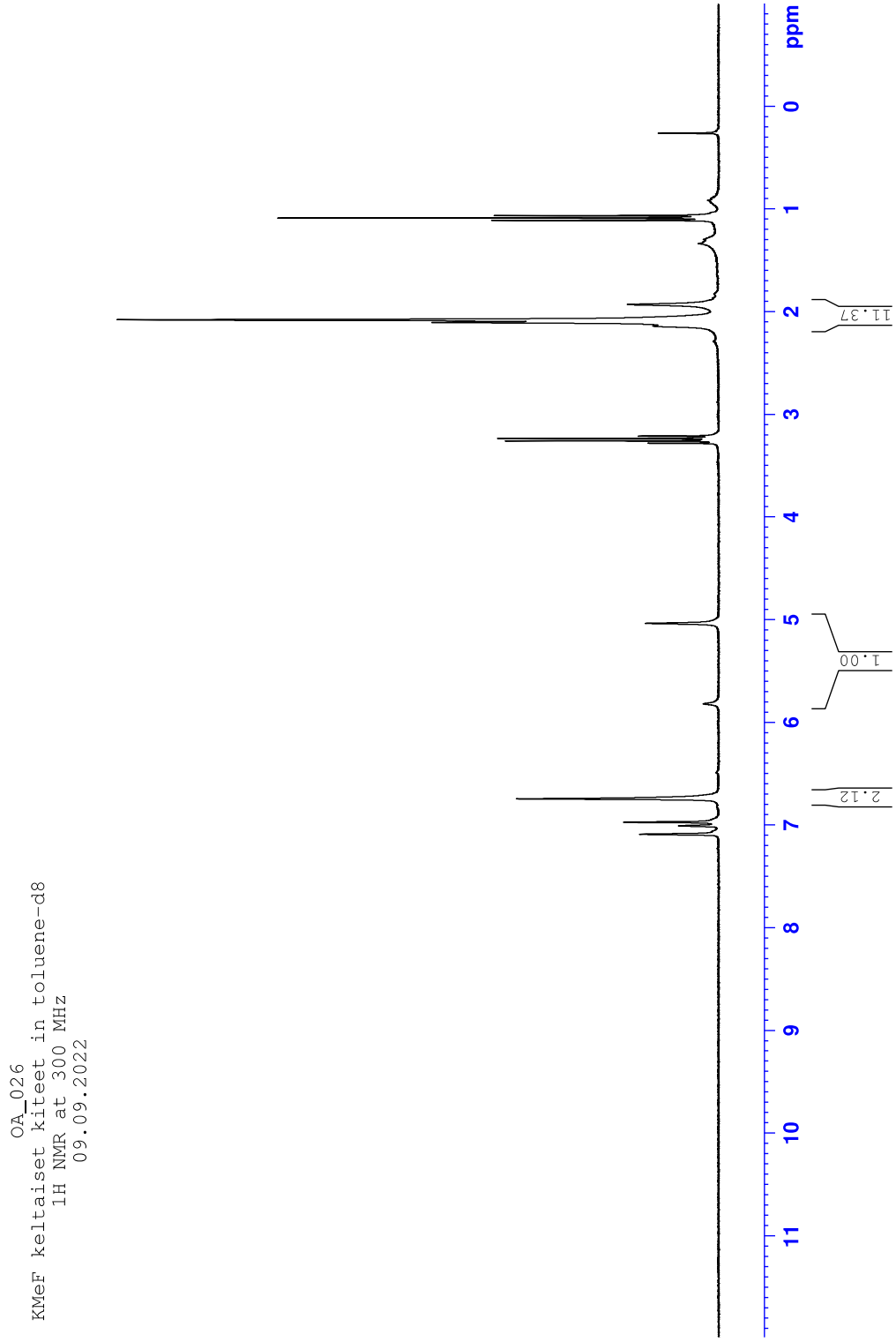

APPENDIX 8. The ^{19}F NMR spectrum of **31** in toluene

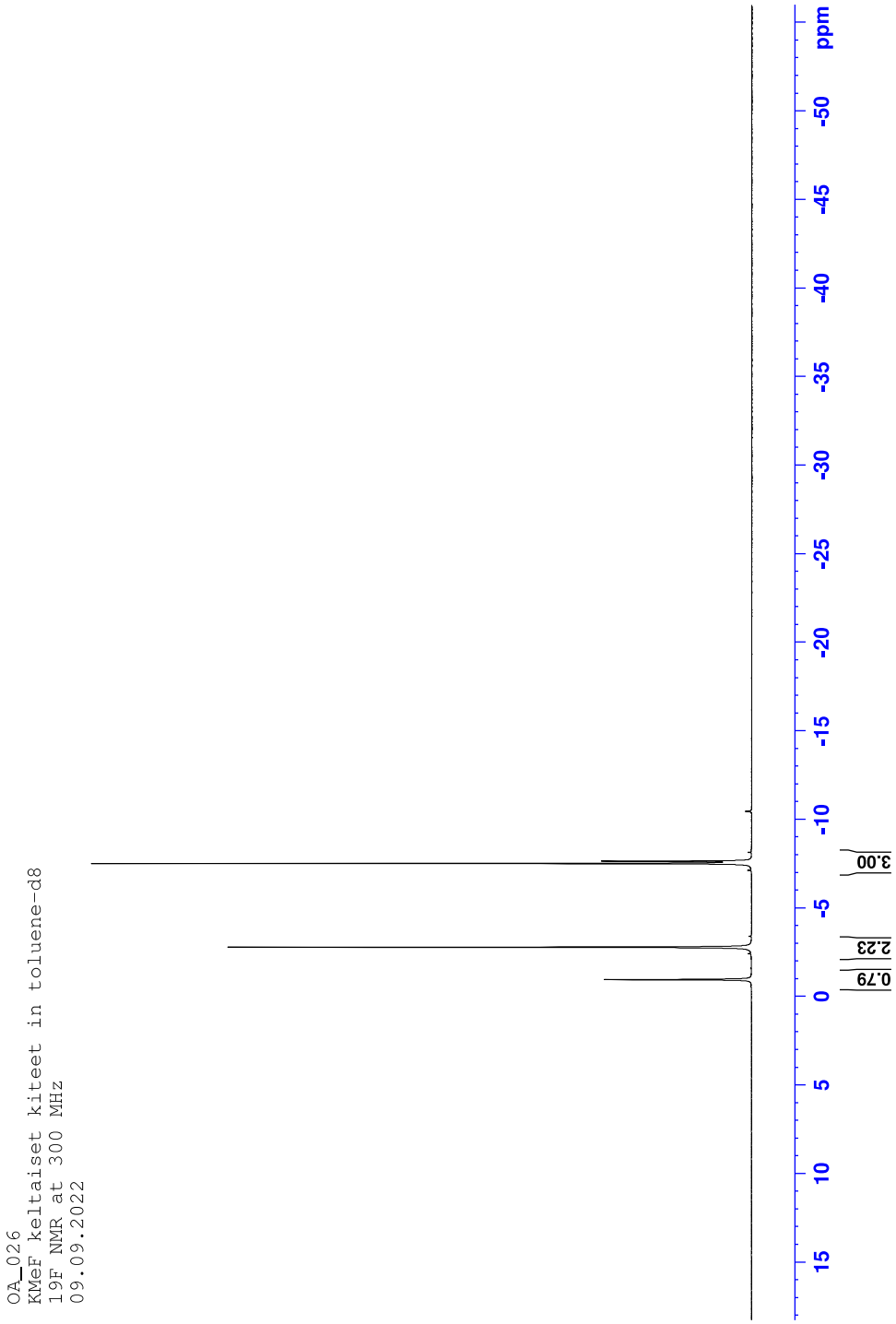

APPENDIX 9. The ^{1}H NMR spectrum of **31** in benzene

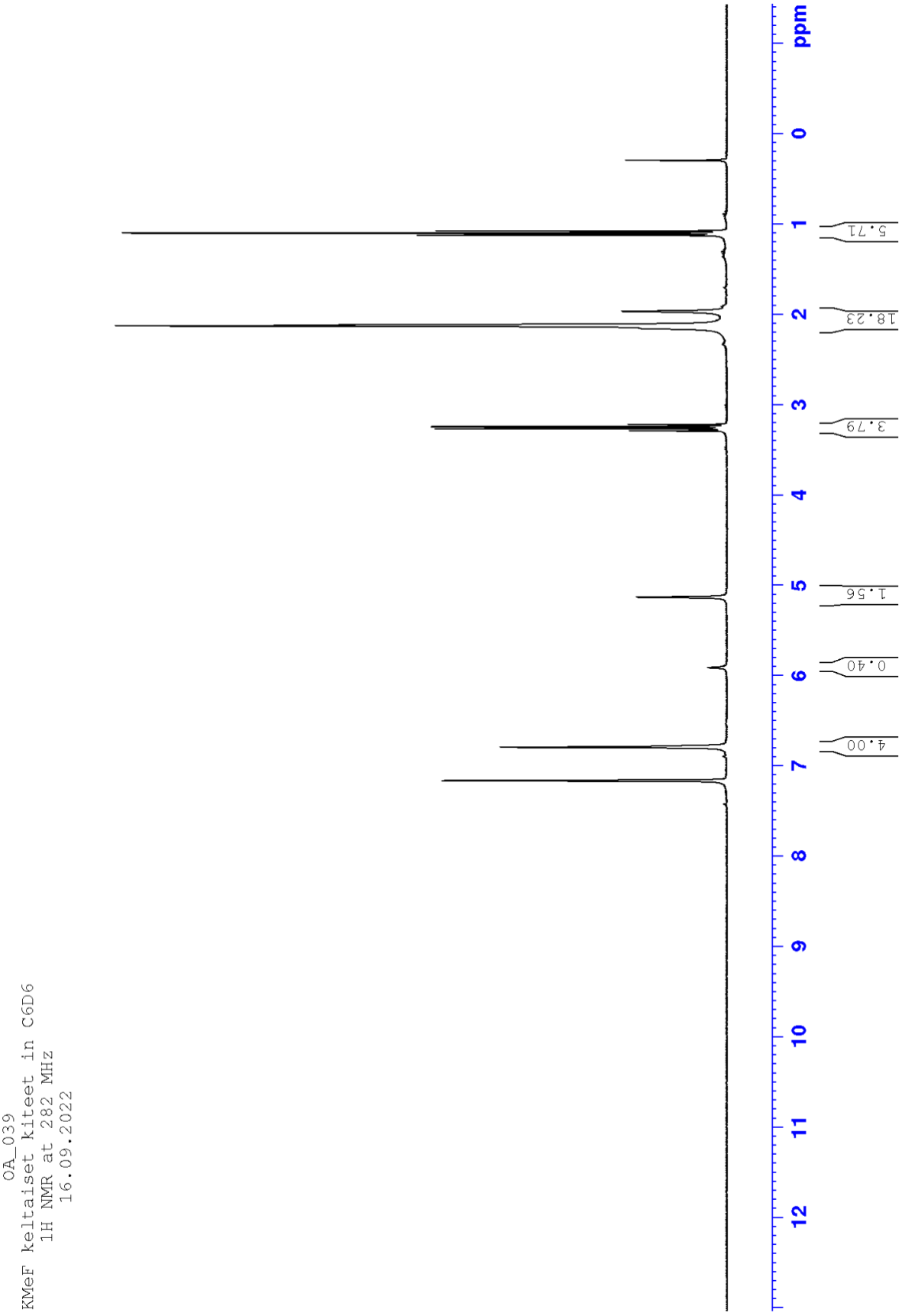

APPENDIX 10. The ^{19}F NMR spectrum of **31** in benzene

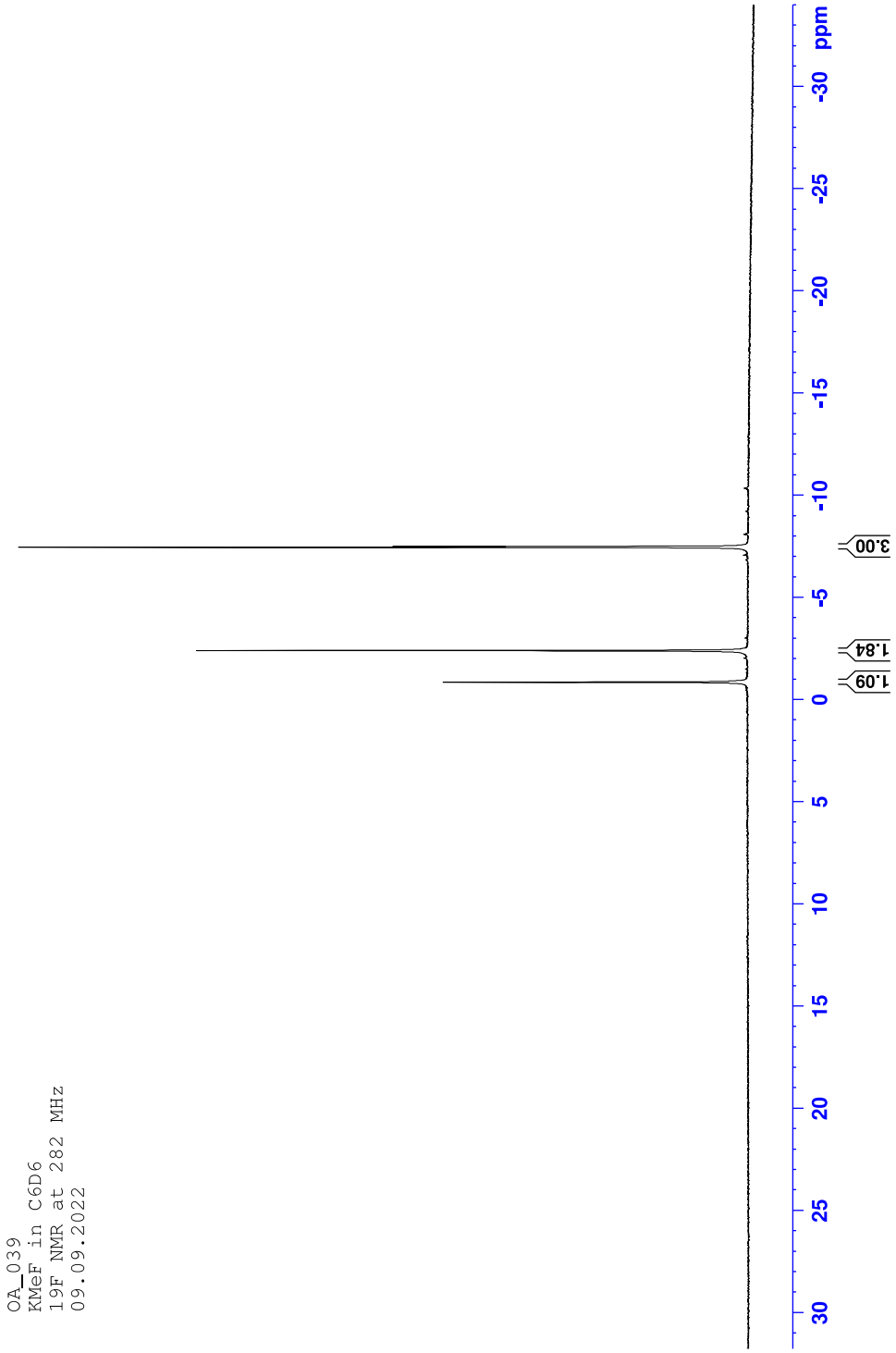

APPENDIX 11. The ^{13}C NMR spectrum of **31** in benzene

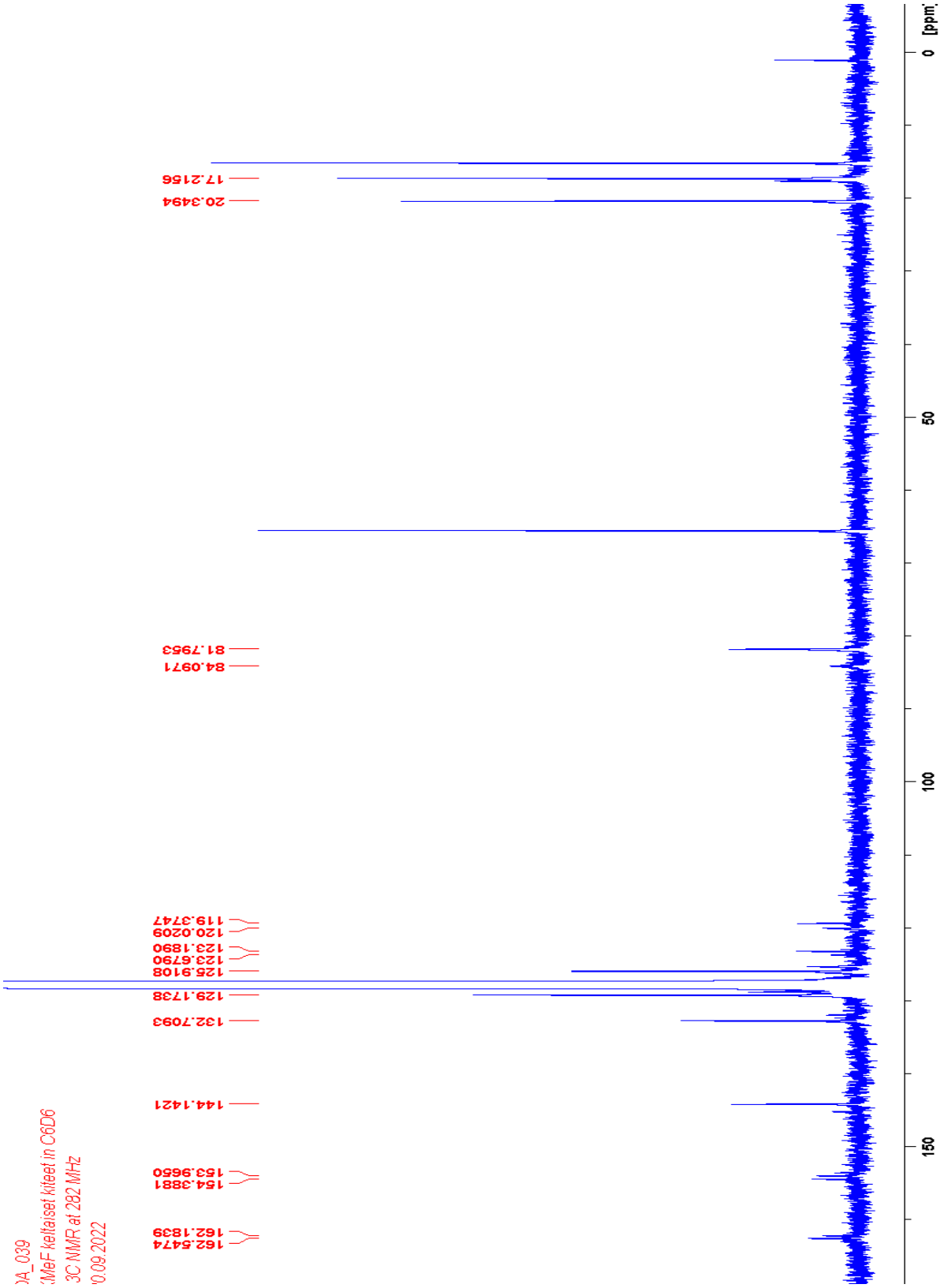

APPENDIX 12. The ^{1}H NMR spectrum of **32** reaction with 0.7 M KHMDS solution

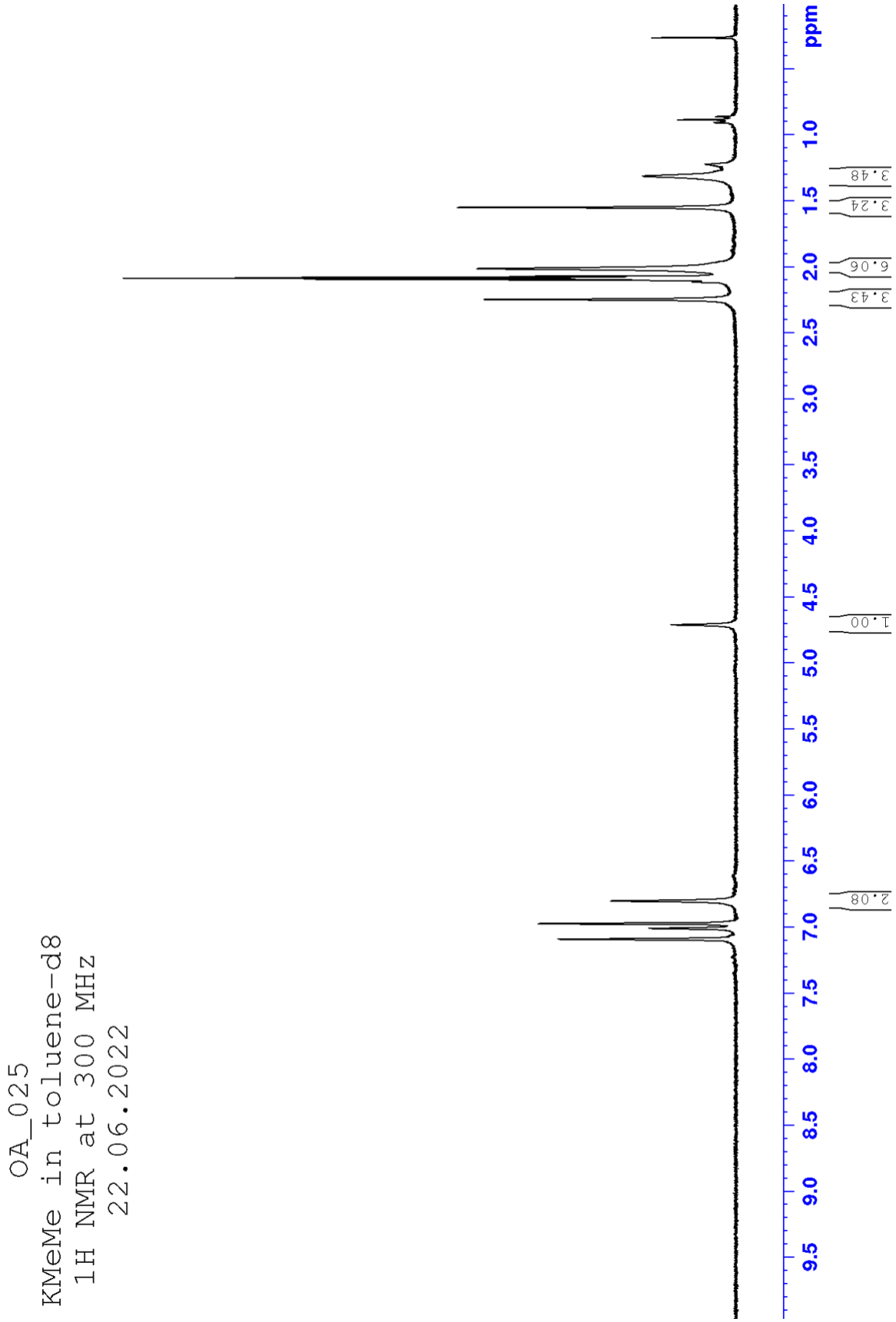

APPENDIX 13. The ^{1}H NMR spectrum of **32** reaction with solid KHMDS

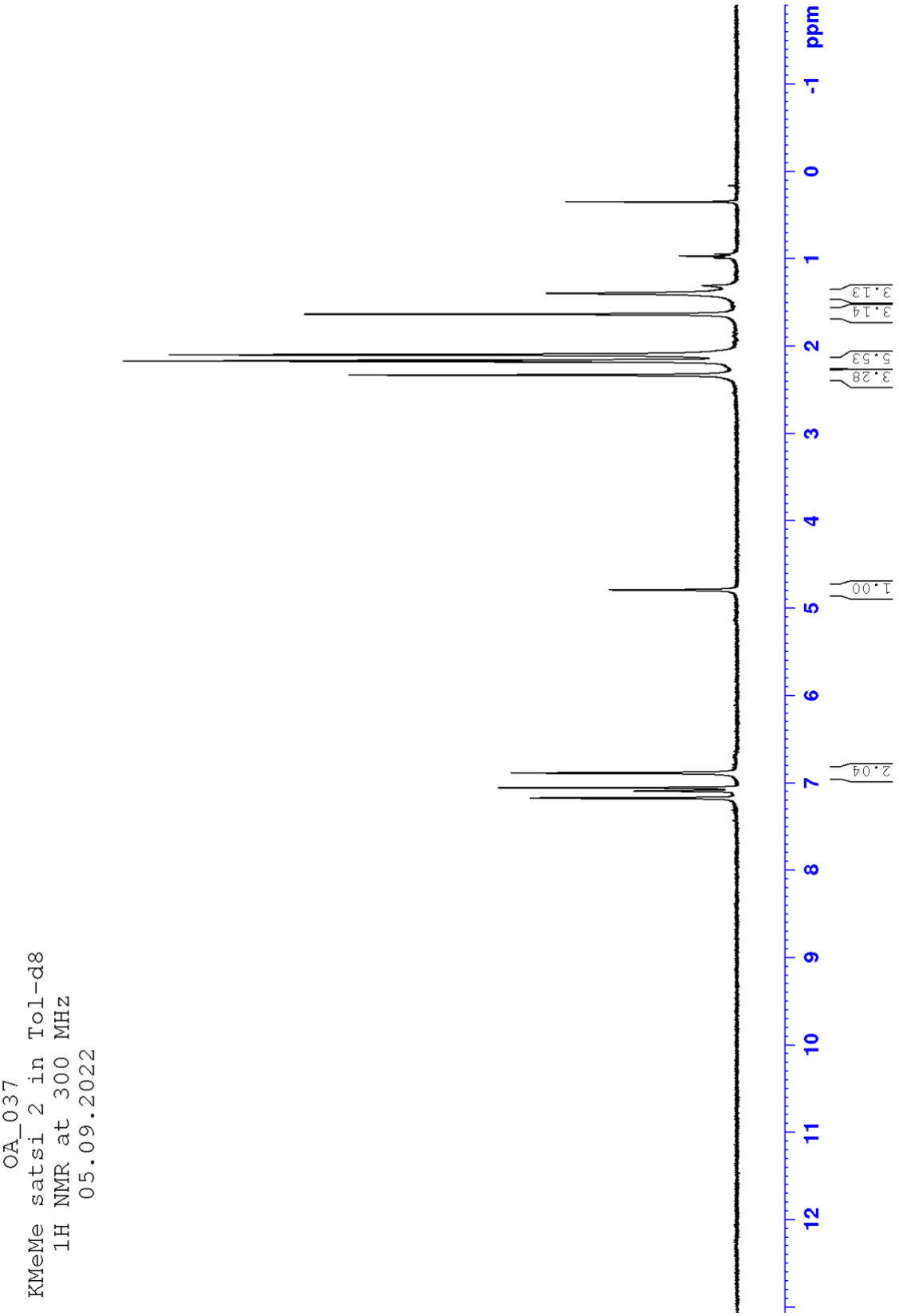

APPENDIX 14. The ^{13}C NMR spectrum of **32**

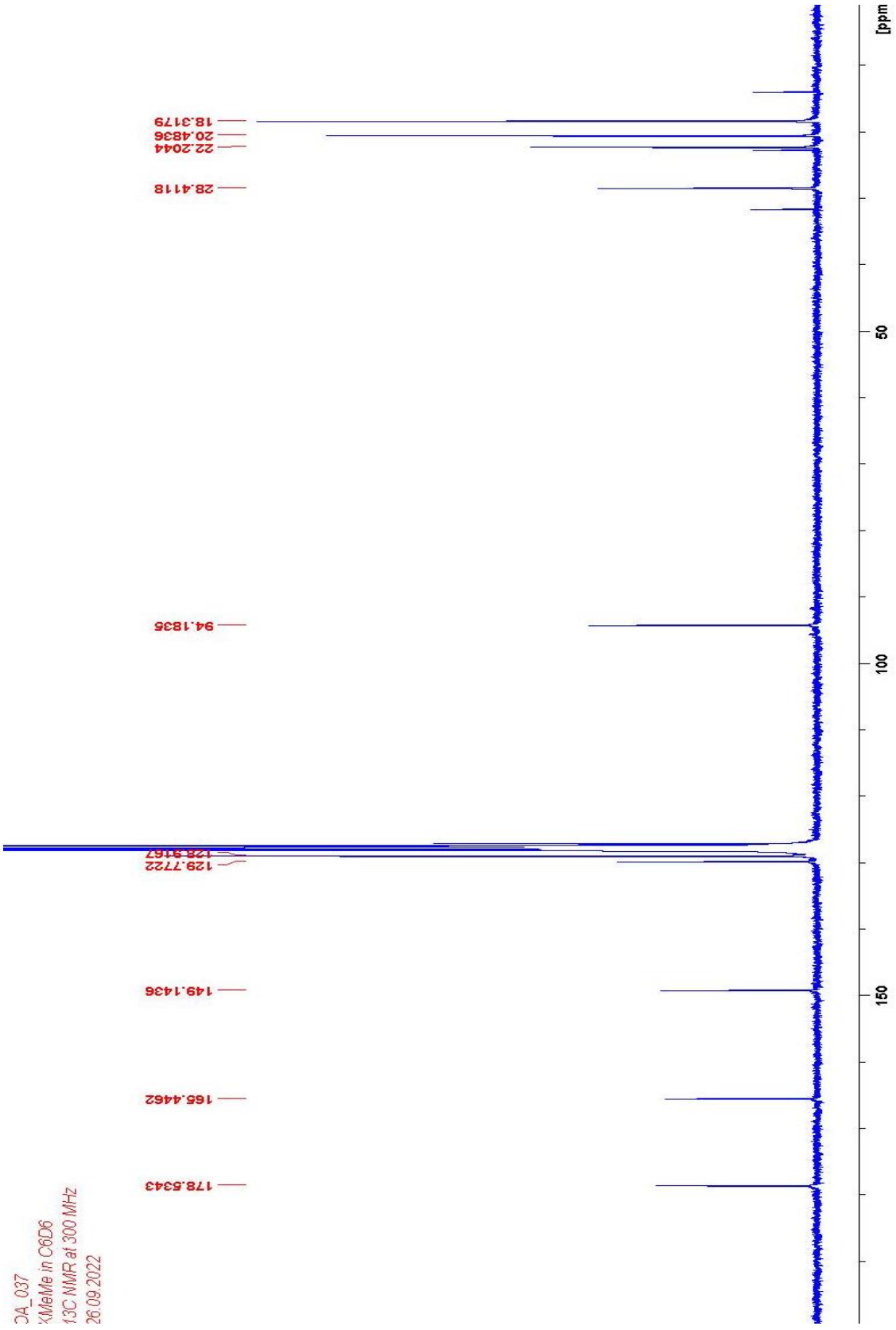

APPENDIX 15. The ^{1}H NMR spectrum of **33**

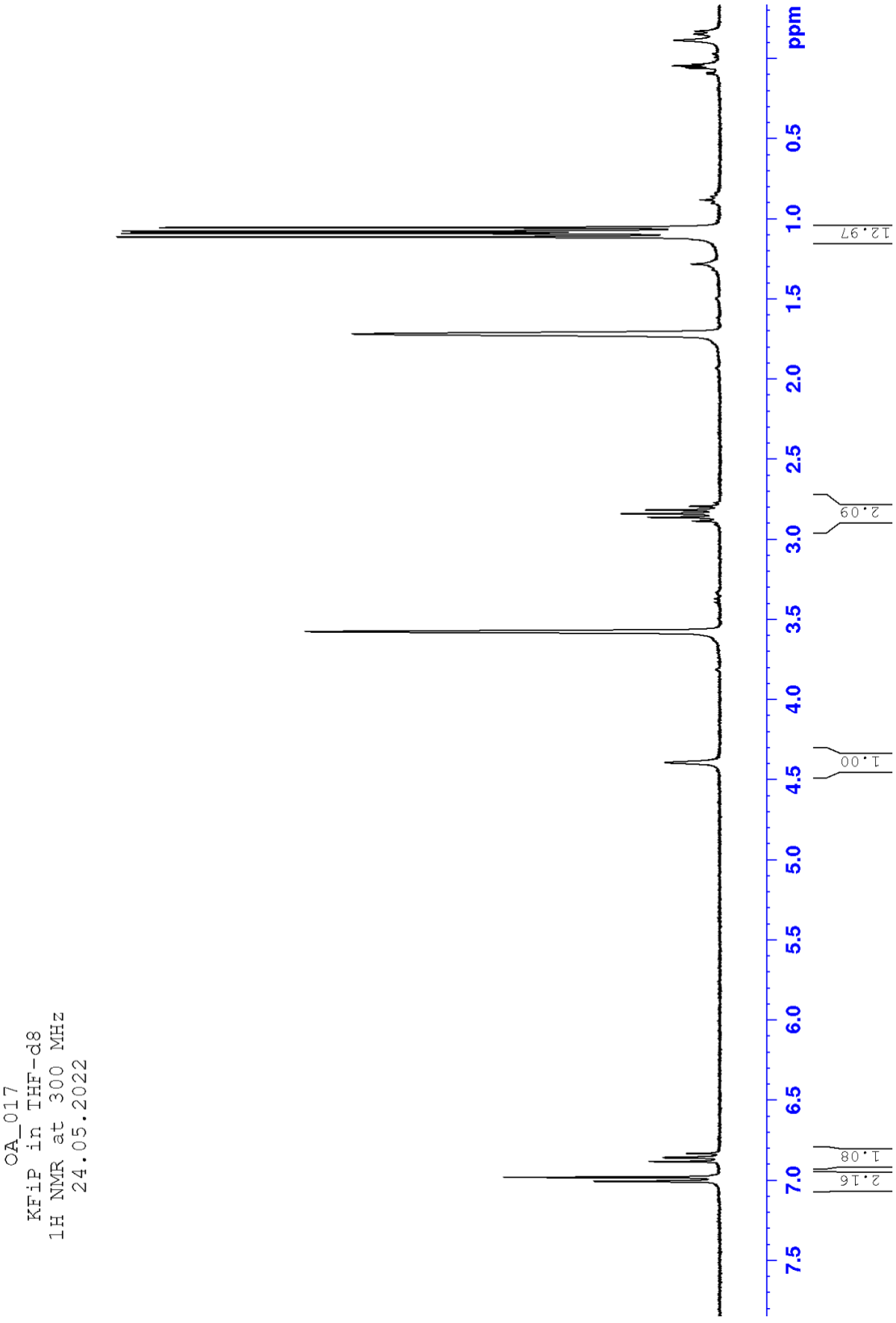

APPENDIX 16. The ^{19}F NMR spectrum of **33**

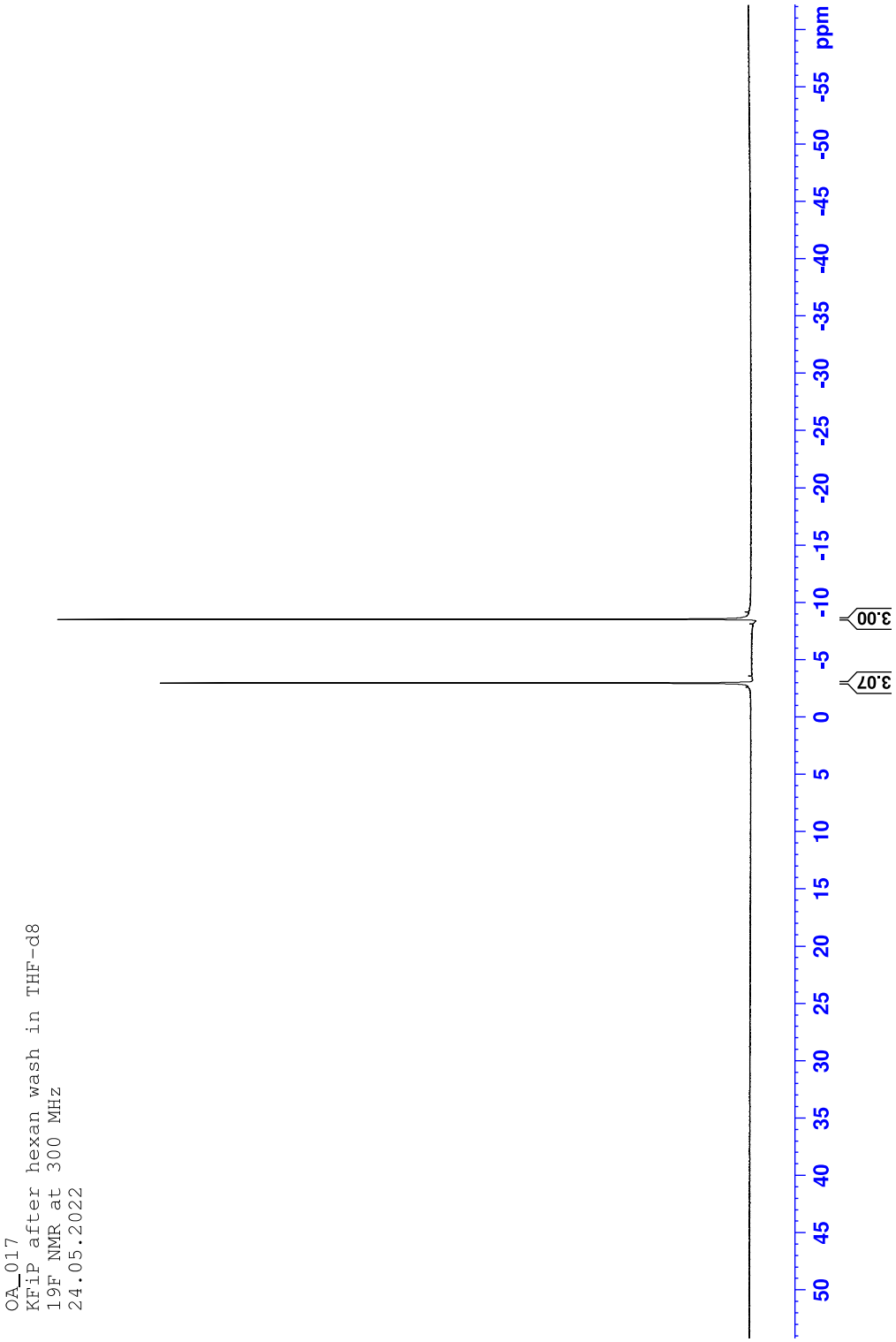

APPENDIX 17. The ^{1}H NMR spectrum of **33** large scale reaction

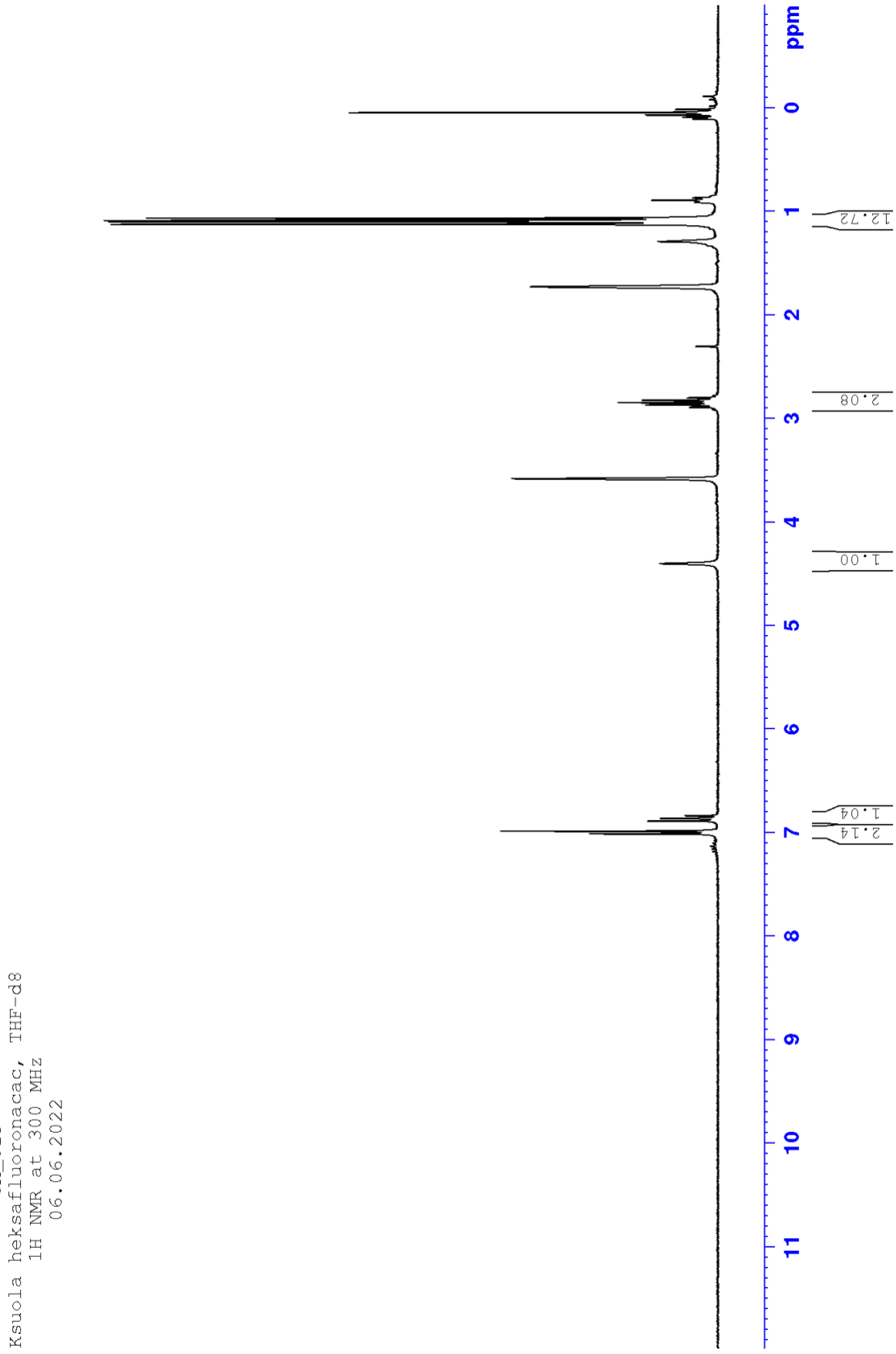

APPENDIX 18. The ^{19}F NMR spectrum of **33** large scale reaction

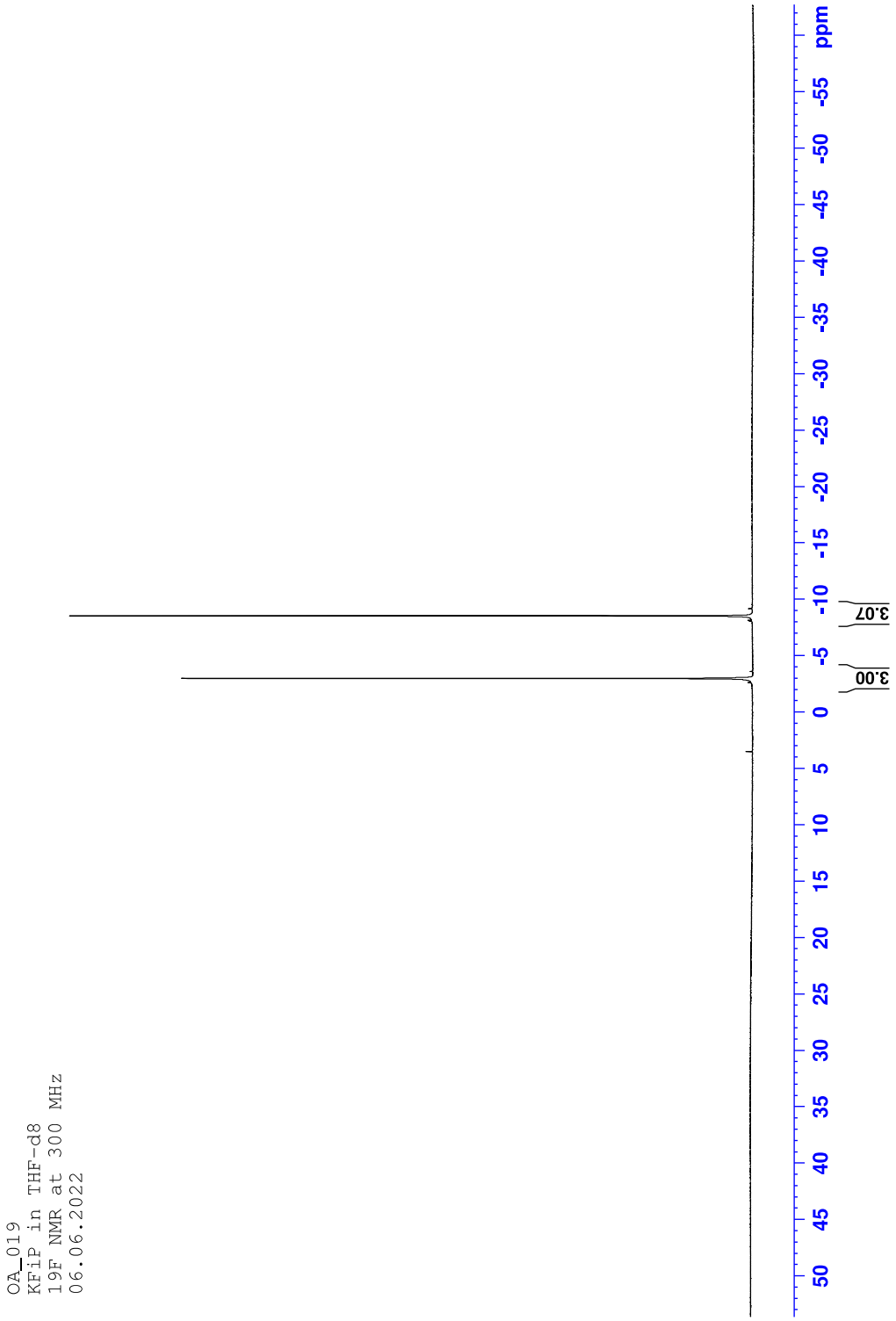

APPENDIX 19. The ^{1}H NMR spectrum of **34**

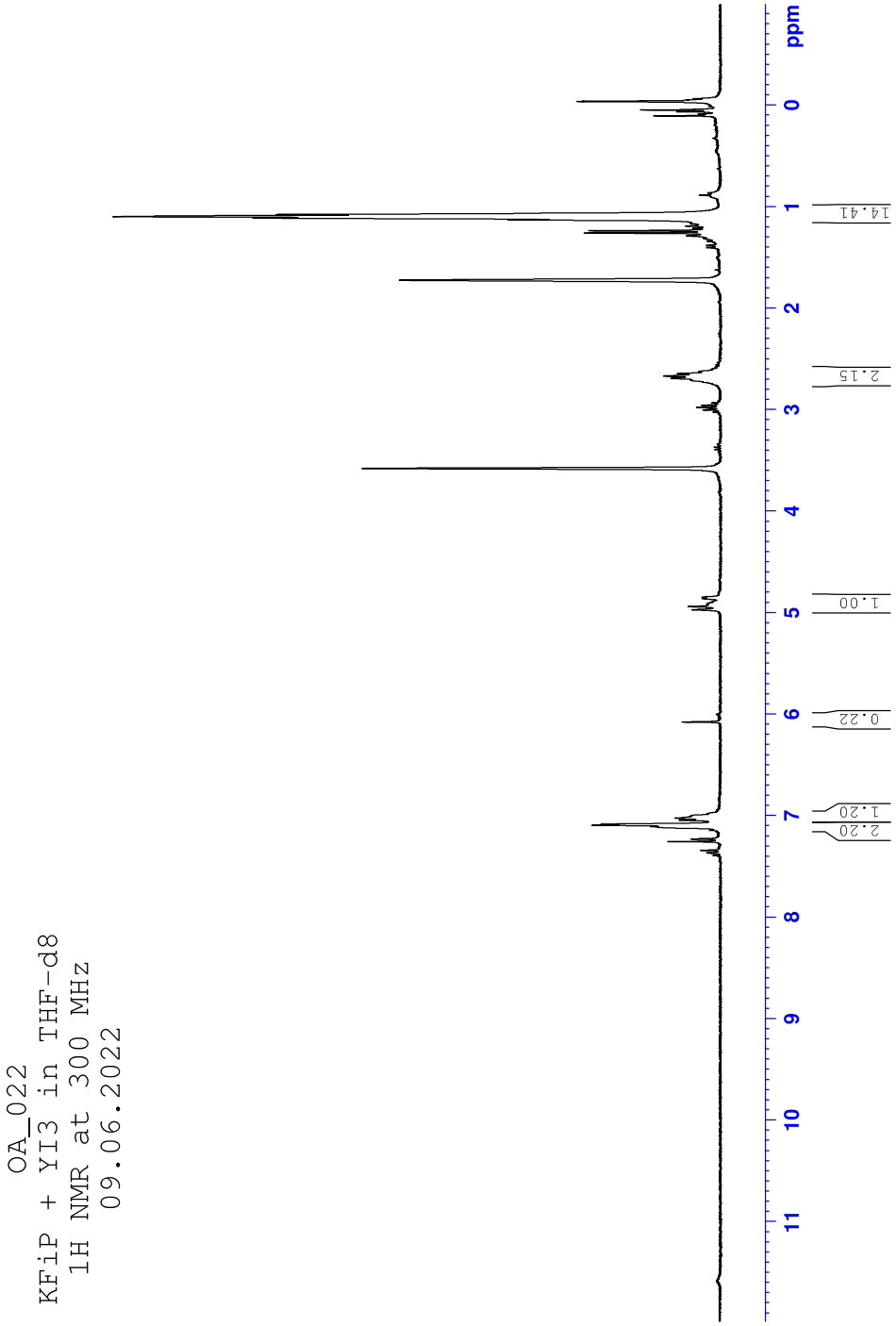

APPENDIX 20. The ^{19}F NMR spectrum of **34**

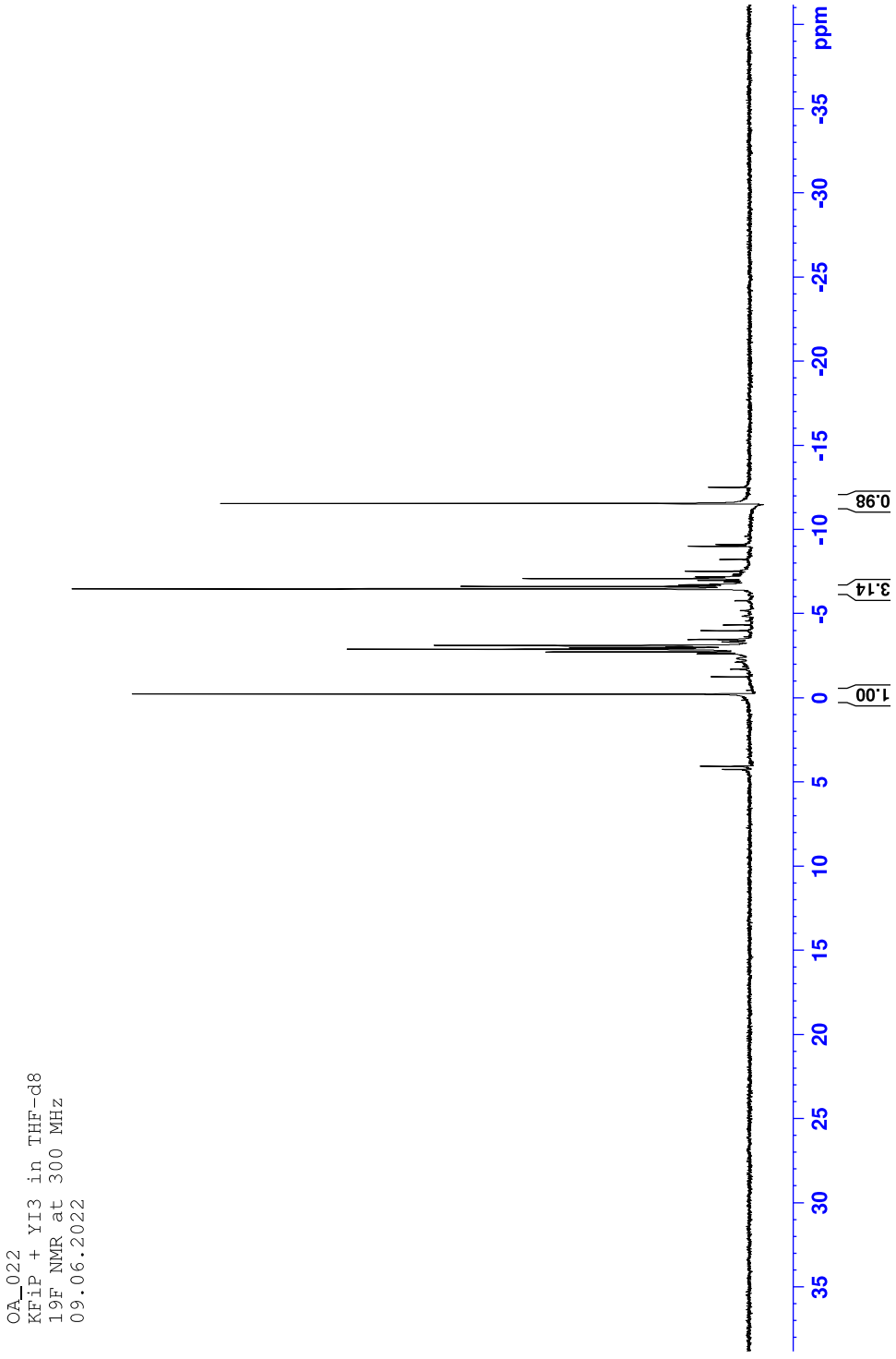

APPENDIX 21. The ^{1}H NMR spectrum of **35** 3:1 complex

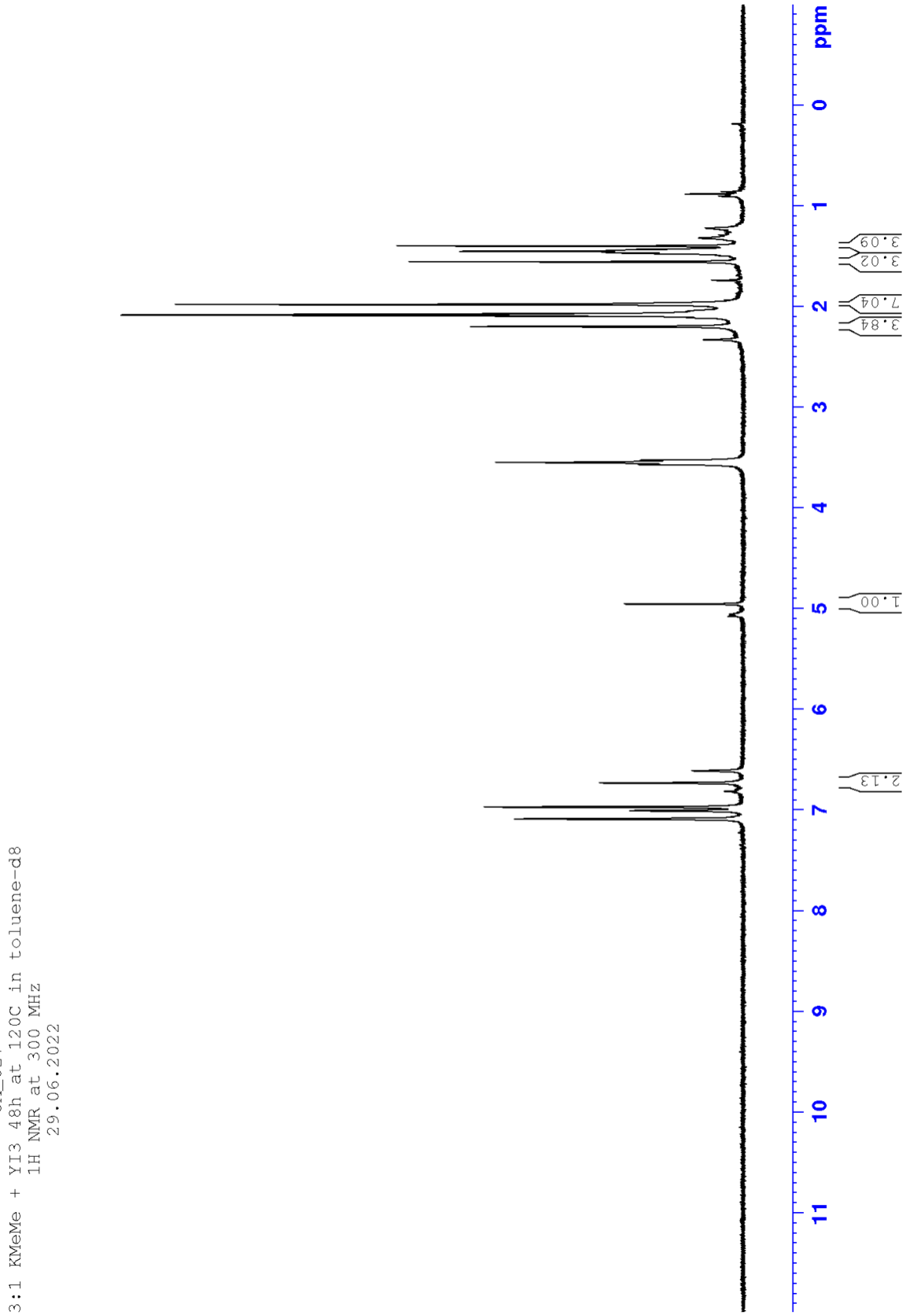

APPENDIX 22. The ^{1}H NMR spectrum of **35** NMR scale 3:1, 2:1 and 1:1 reactions

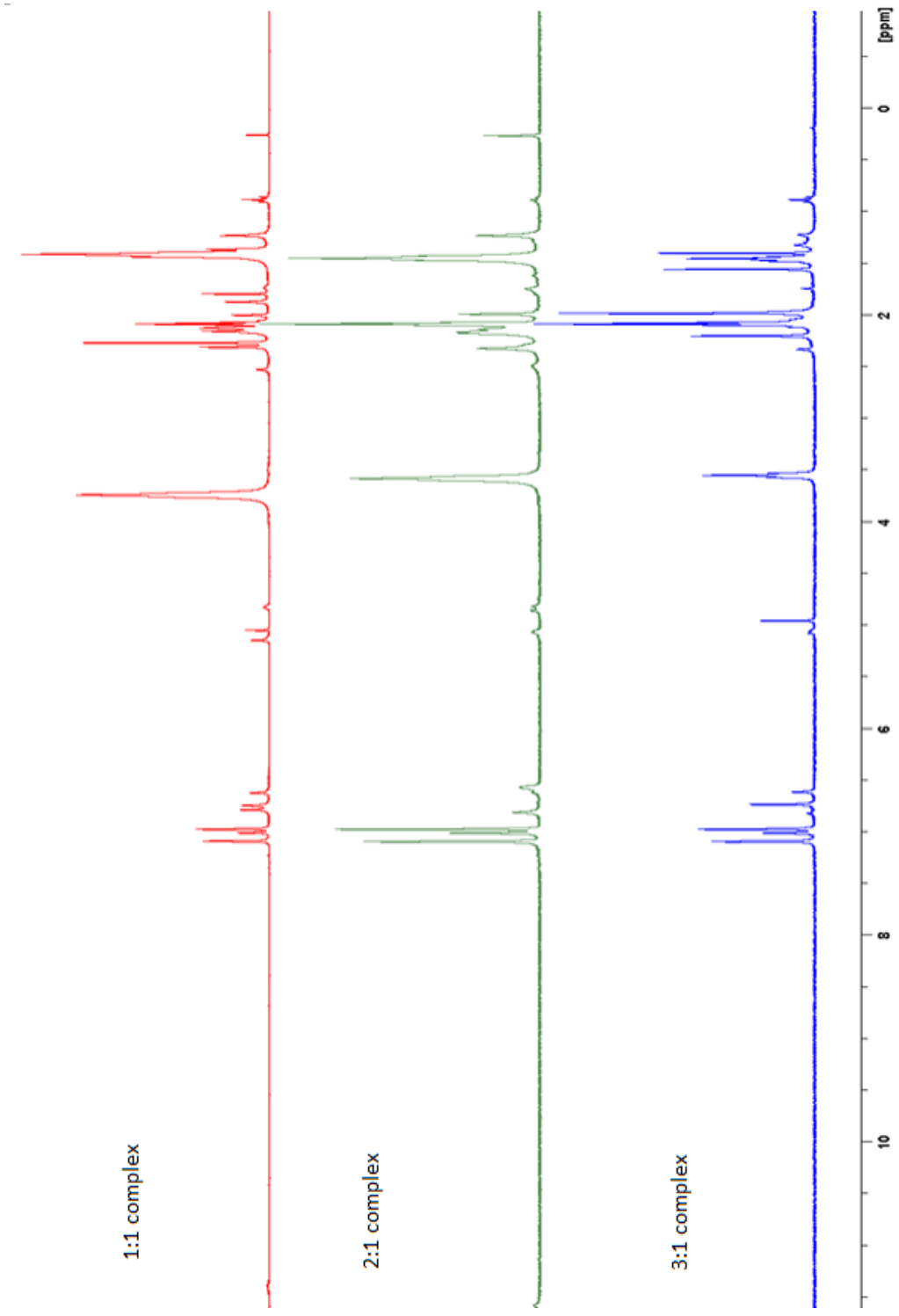

APPENDIX 23. The ^{1}H NMR spectrum of **35** large scale reaction of 3:1 complex

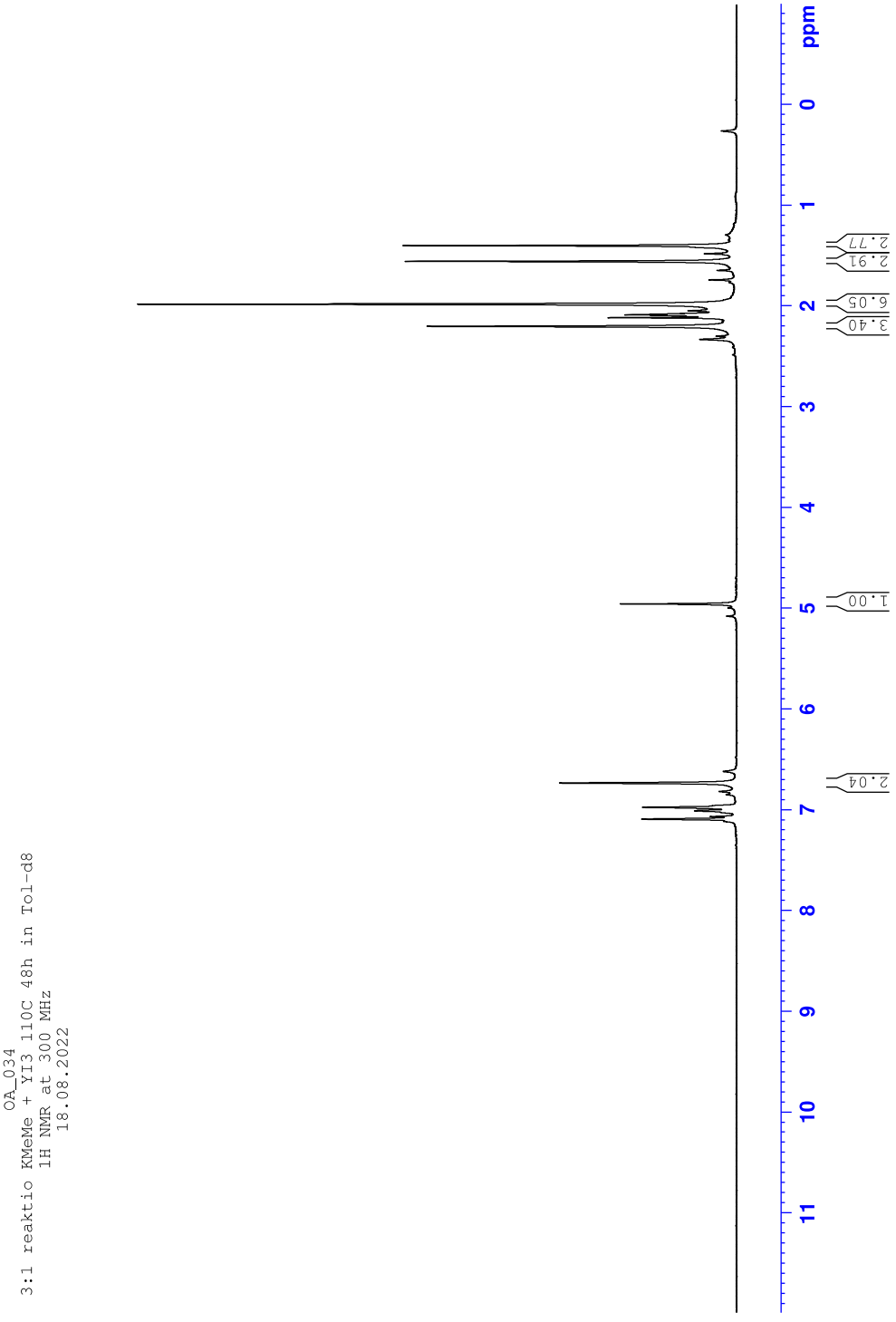

APPENDIX 24. The ^{1}H NMR spectrum of **36** synthesized in NMR scale in benzene

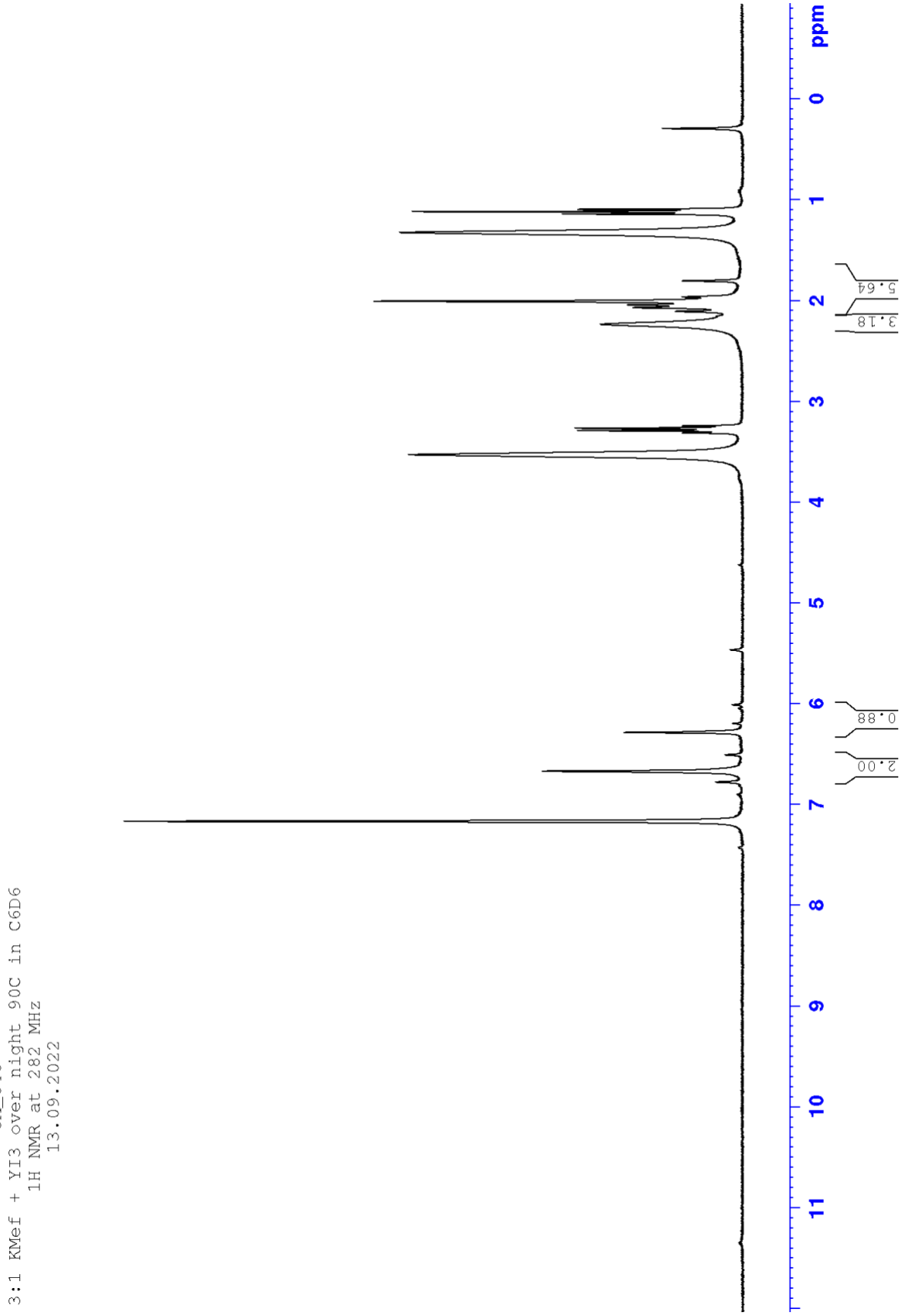

APPENDIX 25. The ^{19}F NMR spectrum of **36** synthesized in NMR scale in benzene

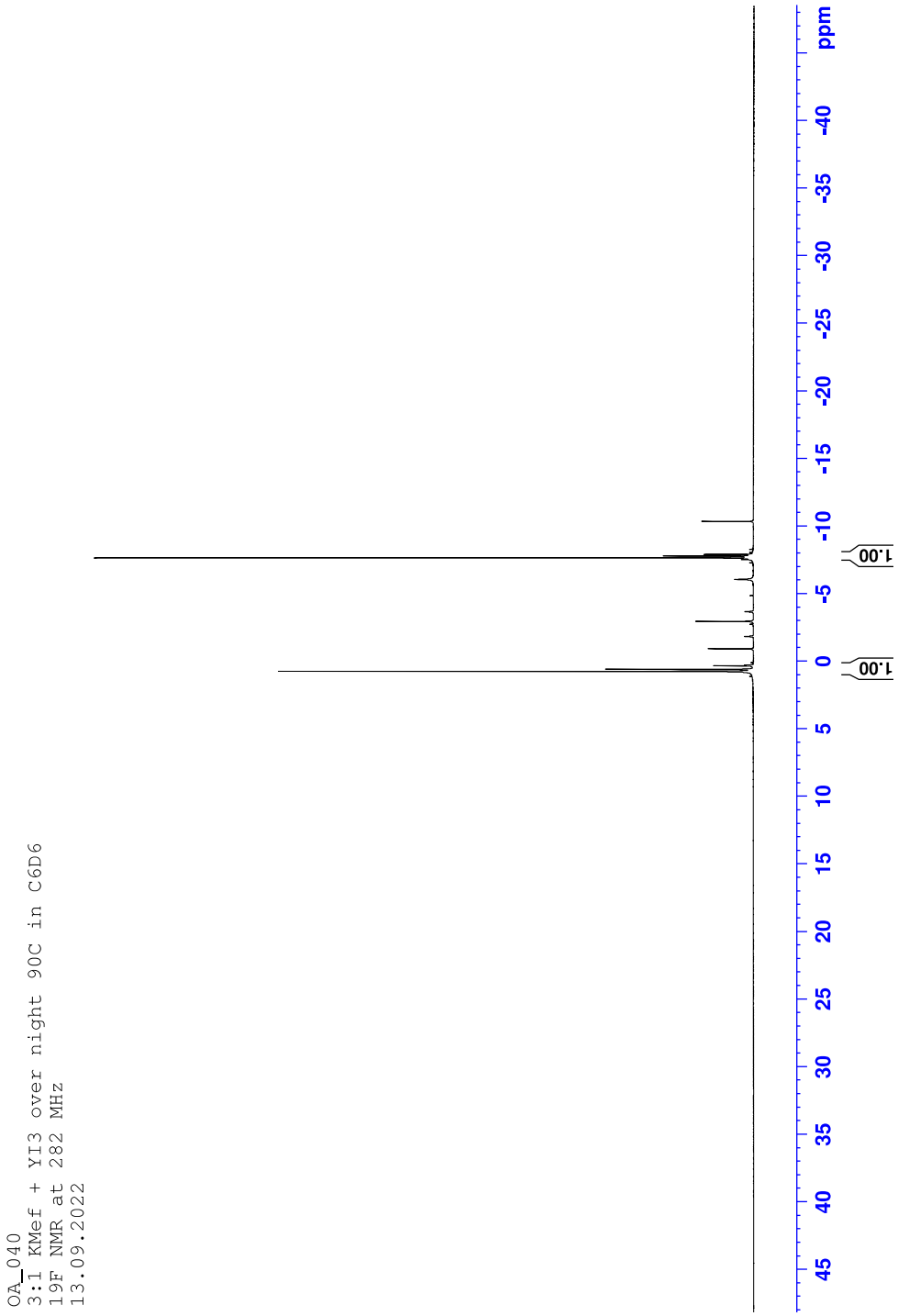

APPENDIX 26. The ^{1}H NMR spectrum of **37** synthesized in large scale in diethyl ether in cold

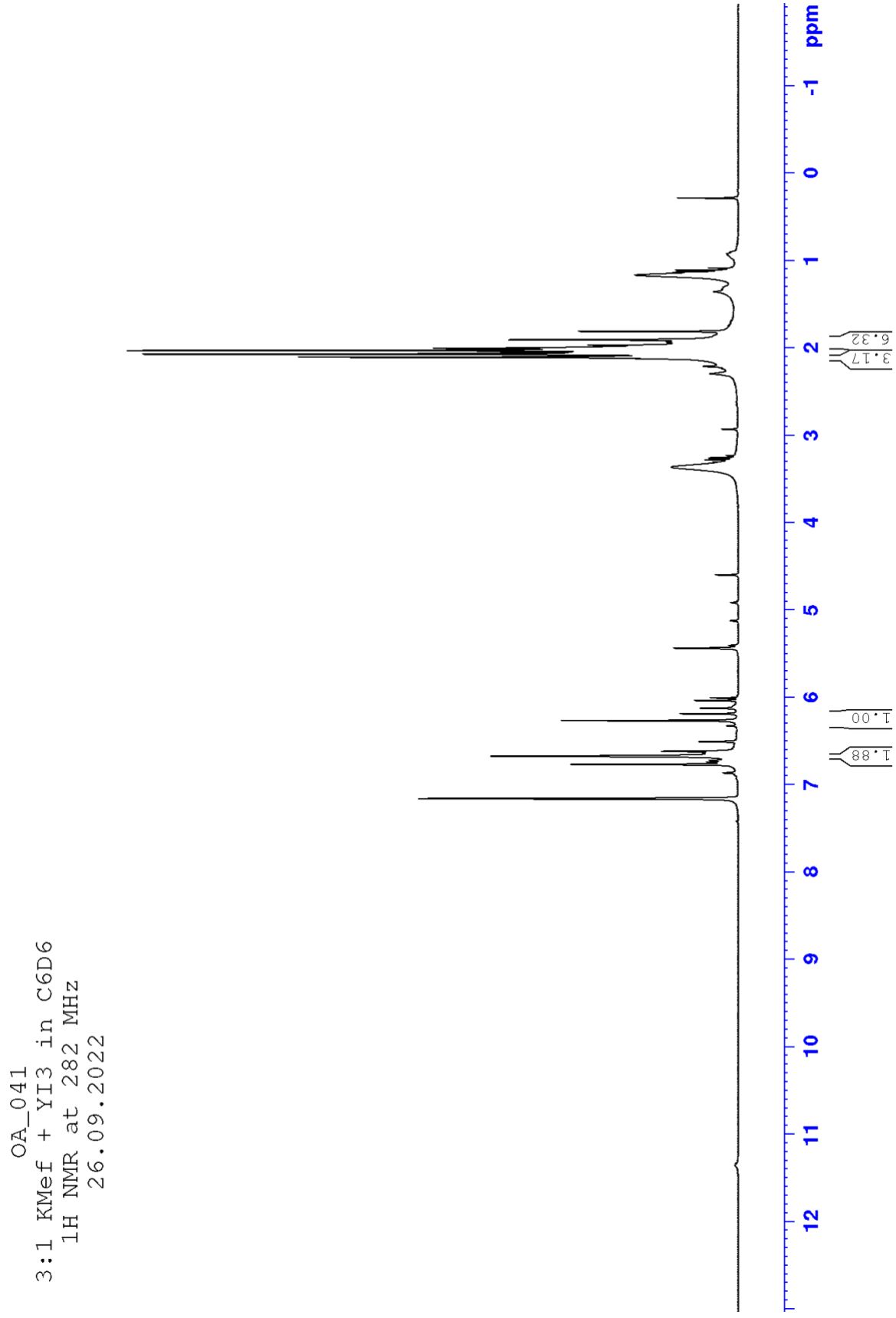

APPENDIX 27. The ^{19}F NMR spectrum of **37** synthesized in large scale in diethyl ether in cold

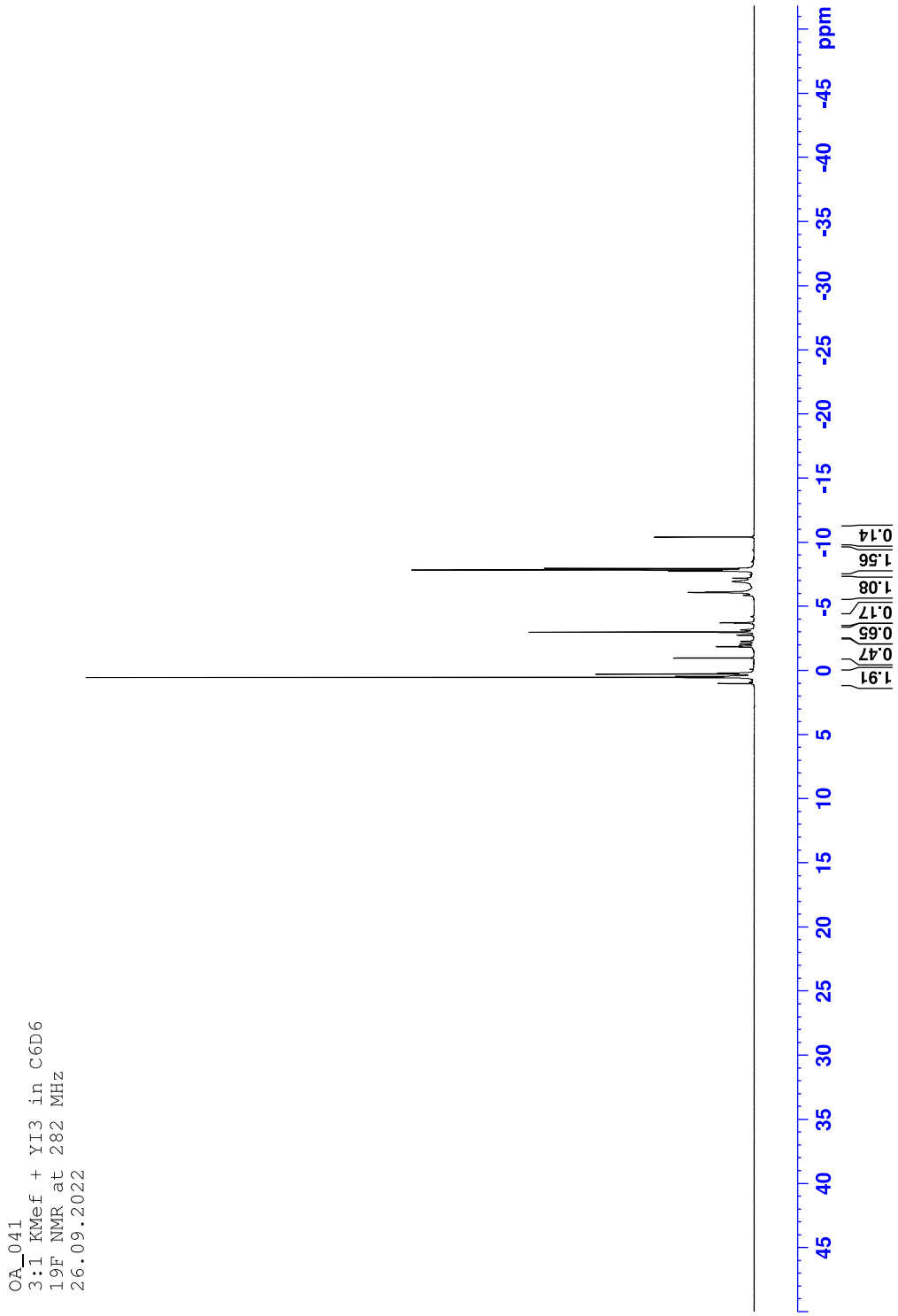

APPENDIX 28. The crystal data and structure refinement for **29**

Identification code	OA-023-R1
Empirical formula	$C_{14}H_{12}NOF_6$
Formula weight/ g mol^{-1}	324.25
Temperature/K	120.01(10)
Crystal system	monoclinic
Space group	$P2_1/n$
a/Å	10.18543(18)
b/Å	10.88503(16)
c/Å	12.77055(17)
α/°	90
β/°	97.1093(14)
γ/°	90
Volume/Å^3	1404.97(4)
Z	4
ρ_{calc}g/cm^3	1.533
μ/mm^{-1}	1.347
F(000)	660.0
Crystal size/mm^3	0.333 × 0.251 × 0.104
Radiation	CuKα (λ = 1.54184)
2Θ range for data collection/°	10.498 to 153.358
Reflections collected	14905
Independent reflections	2928 [R_{int} = 0.0222, R_{sigma} = 0.0137]
Data/restraints/parameters	2928/0/251
Goodness-of-fit on F^2	1.053
Final R indexes [I>=2σ (I)]	R_1 = 0.0312, wR_2 = 0.0827
Final R indexes [all data]	R_1 = 0.0345, wR_2 = 0.0861
Largest diff. peak/hole / e Å^{-3}	0.29/-0.32

APPENDIX 29. The crystal data and structure refinement for **31**

Identification code	OA-026_R1
Empirical formula	$C_{32}H_{34}N_2O_3F_{12}K_2$
Formula weight/ g mol^{-1}	800.81
Temperature/K	120.01(10)
Crystal system	triclinic
Space group	P-1
a/Å	7.9588(5)
b/Å	9.1306(8)
c/Å	27.9099(19)
α/°	80.794(7)
β/°	84.397(6)
γ/°	65.056(8)
Volume/Å^3	1814.3(3)
Z	2
ρ_{calc}g/cm^3	1.466
μ/mm^{-1}	3.190
F(000)	820.0
Crystal size/mm^3	0.125 × 0.047 × 0.038
Radiation	CuKα (λ = 1.54184)
2Θ range for data collection/°	6.42 to 153.196
Reflections collected	13968
Independent reflections	7432 [R_{int} = 0.0671, R_{sigma} = 0.1012]
Data/restraints/parameters	7432/0/467
Goodness-of-fit on F^2	1.049
Final R indexes [I>=2σ (I)]	R_1 = 0.0919, wR_2 = 0.2523
Final R indexes [all data]	R_1 = 0.1137, wR_2 = 0.2715
Largest diff. peak/hole / e Å^{-3}	1.58/-0.68